REPORT DOCUMENTATION PAGE	Form Approved OMB No. 0704-0188

1. AGENCY USE ONLY *(Leave blank)*	2. REPORT DATE	3. REPORT TYPE AND DATES COVERED
	30.Oct.00	DISSERTATION

4. TITLE AND SUBTITLE
VARIABLE STRATEGY MODEL OF THE HUMAN OPERATOR

5. FUNDING NUMBERS

6. AUTHOR(S)
MAJ PHILLIPS JOHN M

7. PERFORMING ORGANIZATION NAME(S) AND ADDRESS(ES)
VIRGINIA POLYTECHNICAL INSTITUTE

8. PERFORMING ORGANIZATION REPORT NUMBER
CY00396

9. SPONSORING/MONITORING AGENCY NAME(S) AND ADDRESS(ES)
THE DEPARTMENT OF THE AIR FORCE
AFIT/CIA, BLDG 125
2950 P STREET
WPAFB OH 45433

10. SPONSORING/MONITORING AGENCY REPORT NUMBER

11. SUPPLEMENTARY NOTES

12a. DISTRIBUTION AVAILABILITY STATEMENT
Unlimited distribution
In Accordance With AFI 35-205/AFIT Sup 1

12b. DISTRIBUTION CODE

13. ABSTRACT *(Maximum 200 words)*

14. SUBJECT TERMS	15. NUMBER OF PAGES
	121
	16. PRICE CODE

17. SECURITY CLASSIFICATION OF REPORT	18. SECURITY CLASSIFICATION OF THIS PAGE	19. SECURITY CLASSIFICATION OF ABSTRACT	20. LIMITATION OF ABSTRACT

Variable Strategy Model of the Human Operator

John Michael Phillips

Dissertation submitted to the Faculty of the
Virginia Polytechnic Institute and State University
in partial fulfillment of the requirements for the degree of

Doctor of Philosophy
in
Aerospace Engineering

Mark R. Anderson, Chair
Eugene M. Cliff
Wayne C. Durham
Christopher D. Hall
Frederick H. Lutze

July 27, 2000
Blacksburg, Virginia

Keywords: Man-Machine Systems, Human Operator Modeling, Pilot Modeling, Variable Structure Control, Sliding Mode Control

Variable Strategy Model of the Human Operator

John Michael Phillips

(ABSTRACT)

Human operators often employ discontinuous or "bang-bang" control strategies when performing large-amplitude acquisition tasks. The current study applies Variable Structure Control (VSC) techniques to model human operator behavior during acquisition tasks. The result is a coupled, multi-input model replicating the discontinuous control strategy. In the VSC formulation, a switching surface is the mathematical representation of the operator's control strategy. The performance of the Variable Strategy Model (VSM) is evaluated by considering several examples, including the longitudinal control of an aircraft during the visual landing task. The aircraft landing task becomes an acquisition maneuver whenever large initial offsets occur. Several different strategies are explored in the VSM formulation for the aircraft landing task. First, a switching surface is constructed from literal interpretations of pilot training literature. This approach yields a mathematical representation of how a pilot is trained to fly a generic aircraft. This switching surface is shown to bound the trajectory response of a group of pilots performing an offset landing task in an aircraft simulator study. Next, front-side and back-side landing strategies are compared. A back-side landing strategy is found to be capable of landing an aircraft flying on either the front side or back side of the power curve. However, the front-side landing strategy is found to be insufficient for landing an aircraft flying on the back side. Finally, a more refined landing strategy is developed that takes into the account the specific aircraft's dynamic characteristics. The refined strategy is translated back into terminology similar to the existing pilot training literature.

Dedication

To Betsy and Meghan,

Thanks for always reminding me of what is really important in life...

Acknowledgments

So much learning goes into the graduate student experience that never gets into a thesis. All of those dead-end ideas that produce no results but insight. All of those insightful discussions about other students research that produce a wealth of experience. For this reason, I thank Professor Mark Anderson for teaching me two things. First, the academic experience is about learning. Second, learning new things is fun.

I thank three professors for teaching excellent courses here at Virginia Tech. First, Professor Mark Anderson for teaching me linear multivariable control. Second, Professor Chris Beattie for teaching me matrix theory. His course was the most useful math class I have taken for understanding linear control theory. And third, Professor Scott Hendricks for teaching me dynamics.

I acknowledge Professors Eugene M. Cliff, Wayne C. Durham, Christopher D. Hall, and Frederick H. Lutze for the guidance and support they provided during my doctoral program.

This degree would not have been possible without the financial support of the US Air Force through the Air Force Institute of Technology Civilian Institution Program.

Contents

List of Figures

List of Tables

Chapter 1

Introduction

The motivation behind mathematically modeling the human operator is to help explain the response characteristics of the dynamic system including the manual controller. In the case of manual control of a vehicle, this modeling yields the "closed-loop" or "operator-vehicle" dynamics. A quantitative explanation of this closed-loop behavior is necessary to summarize operator behavioral data, to understand operator control actions, and to predict the operator-vehicle dynamic characteristics. For these reasons, control engineering methodologies are applied to modeling human operators. These "control theoretic" models primarily attempt to represent the operator's control behavior, not the physiological and psychological structure of the operator. As McRuer states, these models "gain in acceptability" if they can identify features of these structures, "although they cannot be rejected" for failing to do so. [1]

One broad division of human operator models is whether they simulated a continuous or discontinuous operator control strategy. Significant success has been achieved in modeling human operators performing compensatory and pursuit tracking tasks by employing continuous, quasi-linear operator models. Examples of these include the crossover model and the Optimal Control Model. [2, 3]

Discontinuous input behavior is often observed during manual control of large amplitude

and acquisition tasks. [2, 4, 5, 6] These discontinuous human operator responses are usually associated with precognitive human control behavior. [2, 7] Discontinuous control strategies have been previously described by "bang-bang" or relay control techniques. Young and Meiry highlighted operator's preference for this type of relay control strategy in a study that compared controlling high-order system plants with a proportional verses a relay control stick. By allowing the operator to generate a sharper step input, the relay control stick improved the operators' performance by up to 50 percent. Young and Meiry hypothesized that when a human controls a high-order plant, the operator must consider the error of the system to be dependent upon the integral of the control input. Pulse and step inputs would reduce the integration requirements on the operator and should make the system error response more predictable to the operator. [8]

Although operator's may employ a bang-bang control strategy, they often impose an internal limit on the magnitude of control inputs. This internal limit is typically less than the full control authority available. [2] Pew hypothesized that this behavior is due to the operator's recognition of their own reaction time delay. The operator must tradeoff the cost of a switching time error with the cost of limiting the velocity of the output to a value less than the maximum. [9]

A significant amount of research during the 1960's and 1970's examined discontinuous input behavior by human operators and developed models to emulate it. [7, 10, 11, 12, 13, 14, 15, 16, 17] Good summaries of these efforts can be found in Costello [18], Sheridan [4], and McRuer. [2] All of these efforts employed some type of relay element to model the discontinuous input behavior. During the 1980's and 1990's, Andrisani [19], Heffley [20], Hess [21], Innocenti [5, 6], and Moorehouse [22] developed pilot models that included switching or discrete changes in pilot behavior.

To summarize these past research efforts, existing human operator models can be divided into four domains based on the operator control strategy and the complexity of the dynamic system. This division is summarized in Table 1.1. Several different models successfully

Table 1.1: Existing Human Operator Models.

System Complexity	Continuous Strategy	Discontinuous Strategy
Single Input	Crossover Model	Multiple Models
Multi-Input	Optimal Control Model	No Existing Models

replicated discontinuous operator control behavior for single input dynamic systems. [2, 5, 6, 7, 11, 12, 13, 15, 16, 17, 19] However, no models have been developed for multi-input dynamic systems. The proposed Variable Strategy Model for the human operator attempts to fill this void.

The ability of the Variable Strategy Model to model a multi-input, discontinuous control strategy is a benefit of the application of variable structure control (VSC) techniques. Variable structure controllers easily blend discontinuous and linear control strategies for multi-input dynamic systems. A review of VSC techniques is provided in Chapter 2. The application VSC techniques to a human operator model is explored by the development of the Variable Strategy Model (VSM) in Chapter 3. To apply the multi-input VSM, Chapter 4 examines the longitudinal control of an aircraft during the visual landing task. Due to the possibility of a large initial error in distance to the runway, the visual landing task is an acquisition task. The response of the VSM for the landing task is compared to a flight simulator study of pilots response to vertical navigation error. The VSM trajectory response is shown to bound the piloted simulator data set.

In the VSM, the switching surface formulation allows for easy mathematical representation of various piloting strategies. Chapters 5 compares front-side and back-side landing strategies constructed from a literal interpretation of pilot training literature. Although representative of the data set, neither of these generic strategies are representative of the coupled strategy implemented by an experienced pilot. A more refined acquisition strategy is developed in Chapter 6 by analyzing the dynamics of an idealized point mass representation of an aircraft.

The dynamics of this idealized system are produced by the control technique of eigenstructure assignment. This technique allows for inclusion of parameters representative of the dynamics of the aircraft being controlled. As a result, a switching surface is developed that is specific to the aircraft flown and allows for interpretation of a landing strategy to achieve the desired dynamics in terms similar to the pilot training literature.

Chapter 2

Variable Structure Control Theory

Variable structure control evolved from the 1960's work of the Russian researchers Emel'yanov and Barbashin. [23] The first introduction of this work in the West was a survey paper by Utkin published in 1977. [24] A good tutorial for this control technique can be found in an article by DeCarlo. [25] Whereas a linear control law uses constant parameters to implement a control law (i.e. $u = kx$), a variable structure controller allows the structure of the control law (such as k above) to switch at any instant from one to another member in a finite set of continuous control laws. [24] This switching behavior results in a discontinuous control time history.

2.1 Sliding Mode Control

A subset of variable structure control techniques is called "sliding mode" control. This control strategy attempts to drive the system state variables to, and maintain them on, a hyperplane in the state space. Consider the linear time invariant system given by

$$\dot{x} = Ax + Bu \tag{2.1}$$

where $A \in \Re^{n\times n}$, $x(t) \in \Re^n$, $B \in \Re^{n\times m}$ and $u(t) \in \Re^m$. The plant matrix A can be thought of as a linear mapping of $\Re^n$ onto $\Re^n$, (or $A \in L(\Re^n, \Re^n)$). Similarly, the input matrix B can be thought of as a linear mapping of $\Re^m$ onto $\Re^n$, (or $B \in L(\Re^m, \Re^n)$).

For a state regulation task, define a switching surface through the origin of the form

$$\sigma(x) = 0 \tag{2.2}$$

where $\sigma \in \Re^m$. For simplicity, the switching surface is usually chosen to be a time-invariant, linear function of the state vector

$$\sigma(x) = Sx \tag{2.3}$$

with $S \in \Re^{m\times n}$ representing a matrix of constants resulting in a hyperplane passing through the origin in the state space. When the system response is restricted to the switching surface defined by equation (2.3), this condition can be expressed as

$$\dot{\sigma} = 0 = SAx + SBu \tag{2.4}$$

Restricting the system response to the switching surface is referred to as "sliding mode." Since S is a design choice, one requirement is that it should be chosen such that the inverse of SB exists. Solving equation (2.4) for the linear control needed to maintain the system response on the switching surface (σ is constant) gives the "equivalent control" (u_{eq}).

$$u_{eq} = -\left(SB\right)^{-1} SAx \tag{2.5}$$

Substituting this control law into the system equation (2.1) gives the closed-loop system dynamics when the system states are constrained to be on the switching surface,

$$\dot{x} = \left[I_n - B(SB)^{-1}S\right] Ax \tag{2.6}$$

The eigenvalues ($\lambda_i \in \mathcal{C}^1$) and eigenvectors ($v_i \in \mathcal{C}^n$) of this system are defined by

$$\left[\lambda_i I_n - \left(I_n - B(SB)^{-1}S\right) A\right] v_i = 0 \tag{2.7}$$

where $i = 1, 2, \cdots, n$. This constrained dynamic system, equation (2.6), has m zero eigenvalues resulting from the constraint equations (2.3). The other $(n - m)$ eigenvalues represent

the dynamics of the constrained system. [23] They are insured to be stable by the appropriate choice of S. The constrained dynamic system defined by these $(n-m)$ dynamic modes is referred to in variable structure control literature as the "reduced-order system." The reduced-order system or null space dynamics of S can be designed with any desired properties, such as system stabilization, tracking, or regulation.

If the linear system defined by equations (2.1) and (2.3) is a minimal (or least order) system, then the transmission zeros, defined by the matrix triple (S, A, B), are not elements of the spectrum of the plant matrix. [26] And the eigenvalues of the reduced-order system are equivalent to the transmission zeros [27] of the unconstrained dynamic system. Therefore, the eigenvalues of the reduced-order system (λ_j) are defined as the roots of

$$\det\left[S\left(\lambda_j I_n - A\right)^{-1} B\right] = 0 \tag{2.8}$$

where $j = 1, 2, \cdots, n-m$.

Because the system is minimal, the reduced-order system eigenvalues (i.e. the open-loop transmission zeros) are not elements of the spectrum of the plant matrix A and $(\lambda_j I_n - A)^{-1}$ exists. [26] Appendix A provides further details regarding the equivalence of transmission zeros and the reduced-order system eigenvalues.

If the system is not minimal order, but employs the same system matrix, the additional eigenvalues of the reduced-order system are the decoupling zeros of the system. [26] The decoupling zeros are elements of the spectrum of A and are responsible for pole/zero cancellations in the system dynamics. [26]

El-Ghezawi showed how the zero input directions are related to the reduced-order system eigenvectors. [28] The zero input direction vectors $(\alpha_j, j = 1, 2, \cdots, n-m)$ are defined by

$$S\left(z_j I_n - A\right)^{-1} B\alpha_j = 0 \tag{2.9}$$

This definition can be reformulated as

$$\left[I_n - B\left(SB\right)^{-1} S\right] A\left(N\alpha_j\right) = z_j\left(N\alpha_j\right) \tag{2.10}$$

where N is a matrix whose columns are a set of basis vectors for $\ker(S)$. As already noted, the transmission zeros (z_j) are equivalent to the reduced-order system eigenvalues (λ_j). Comparison of equation (2.10) with equation (2.7) also reveals that the reduced-order system eigenvectors (v_j) are related to the zero input directions (α_j) by

$$v_j = N\alpha_j \tag{2.11}$$

Since N is a matrix whose columns are a set of basis vectors for $\ker(S)$,

$$v_j \in \ker(S) \tag{2.12}$$

The design of a sliding mode control system can be broken into two parts: design of the switching surface and design of the control law.

2.1.1 Switching Surface

The switching surface plays the major role in defining the reduced-order system dynamics. Many techniques have been devised for designing the switching surface. These techniques include: Filoppov's method, Utkin's equivalent control method, pole placement, eigenstructure assignment, and quadratic minimization methods. [25, 29, 30]

One classical means of designing control systems is by pole placement. Not surprisingly, this method is often used to design the switching surface for sliding mode control systems. Examples can be found in Edwards and Utkin. [23, 29] Pole placement of the reduced-order system eigenvalues is accomplished using the so-called "regular form." Consider the linear time invariant system given in equation (2.1). It is desired to transform this system into the variable structure regular form,

$$\begin{pmatrix} \dot{x}_1 \\ \dot{x}_2 \end{pmatrix} = \begin{bmatrix} A_{11} & A_{12} \\ A_{21} & A_{22} \end{bmatrix} \begin{pmatrix} x_1 \\ x_2 \end{pmatrix} + \begin{bmatrix} 0 \\ B_2 \end{bmatrix} u \tag{2.13}$$

where $x_1 \in \Re^{n-m}$, $x_2 \in \Re^m$, and $u \in \Re^m$. In general, the aircraft system equations examined in this dissertation are already in this form. For more general applications, Edwards outlines

a transformation method to generate this regular form. [23] On the sliding surface, this dynamic system is constrained by equation (2.3). This constraint can be expressed as

$$0 = S_1 x_1 + S_2 x_2 \tag{2.14}$$

where $S_1 \in \Re^{m\times(n-m)}$ and $S_2 \in \Re^{m\times m}$. Since S_2 is full rank for $(SB)^{-1}$ to exist, solving for x_2 gives

$$x_2 = -S_2^{-1} S_1 x_1 \tag{2.15}$$

If a matrix $M \in \Re^{m\times(n-m)}$ is defined as

$$M = S_2^{-1} S_1 \tag{2.16}$$

then substituting this definition into equations (2.15) and (2.13) gives the reduced-order dynamic system

$$\dot{x}_1 = (A_{11} - A_{12} M)\, x_1 \tag{2.17}$$

This form of the reduced-order system dynamics is very similar to the form that results when the state feedback control is applied to a general linear time invarinat state-space model.

$$\dot{x} = (A - BK)\, x \tag{2.18}$$

where $K \in \Re^{m\times n}$ is the state feedback gain matrix. Comparing (2.17) to (2.18), A_{11} could be considered the plant matrix A; A_{12} the input matrix B; and M the gain matrix K. Traditional pole placement algorithms can therefore be used to achieve the desired dynamics for (2.17). For a scalar control ($u \in \Re^1$), sufficient information is given to specify all $n-1$ reduced-order system eigenvalues.

For a multi-input system, additional degrees of freedom exist, namely $(n-m)m$ degrees of freedom. This situation allows for specification of all $n-m$ eigenvalues and portions of the eigenvector structure. [23] The technique applied to multi-input systems is referred to as multi-input pole placement or eigenstructure assignment. [30, 31, 32] Wonham and Morse developed a geometric, vector-space approach to this problem in the 1970's. [33, 34, 35, 36] This method consists of determining a state feedback gain matrix and cross-control gain

matrix. The gain matrices are determined from an analysis of the system's invariant and controllablity subspaces. The gain matrices are usually chosen to decouple the system's output response and place the poles at desired locations. Although the geometric decoupling method can be used to create desired mode shapes, instead of decoupling the modes, the eigenstructure method is a more straight forward presentation of this concept. The following description of the eigenstructure technique closely parallels the notation provided by Brogan adapted for the reduced-order system. [31]

The eigenvalues (λ_j, $j = 1, 2, \cdots, n-m$) and associated eigenvectors ($w_j \in \mathcal{C}^{(n-m)}$) of the null space or reduced-order dynamics given by equation (2.17) are defined by

$$\left(\lambda_j I_{(n-m)} - A_{11} + A_{12}M\right) w_j = 0 \tag{2.19}$$

This expression can be rearranged into a partitioned matrix of the form

$$\left[\begin{array}{cc} \left(\lambda_j I_{(n-m)} - A_{11}\right) & A_{12} \end{array} \right] \left[\begin{array}{c} w_j \\ M w_j \end{array} \right] = 0 \tag{2.20}$$

so

$$\left[\begin{array}{c} w_j \\ M w_j \end{array} \right] \in \ker\left(\left[\begin{array}{cc} \left(\lambda_j I_{(n-m)} - A_{11}\right) & A_{12} \end{array} \right] \right) \tag{2.21}$$

Let N_j be a matrix whose columns are a set of basis vectors for the null space of $\left[\left(\lambda_j I_{(n-m)} - A_{11}\right) \; A_{12}\right]$. Since λ_j is not in the spectrum of A, it is not in the spectrum of A_{11}. [23] So the dimension of N_j is $(n-m) \times m$. Let $\xi_j \in \mathcal{C}^n$ be partitioned in accordance with (2.13),

$$\xi_j = \left(\begin{array}{c} \xi_1 \\ \xi_2 \end{array} \right)_j \tag{2.22}$$

where $\xi_1 \in \mathcal{C}^{n-m}$ and $\xi_2 \in \mathcal{C}^m$. The vector $(\xi_1)_j$ is the best representation of the null space eigenvector w_j in the m dimensional subspace N_j. The "best representation" terminology is used since there are insufficient degrees of freedom in the problem to specify all $(n-m)$ components of all $(n-m)$ eigenvectors w_j. As a result, some judgement must be used in

selecting the desirable structure of the vector v_j. The selection usually consists of attempting to place 1's and 0's in certain components of w_j to decouple mode responses.

After all $n-m$ vectors ξ_j are found, define a matrix $\Psi \in \mathcal{C}^{n\times(n-m)}$ of the form

$$\Psi = \begin{bmatrix} \xi_1 & \cdots & \xi_{n-m} \end{bmatrix} \tag{2.23}$$

that can be partitioned as

$$\Psi = \begin{bmatrix} \Psi_1 \\ \Psi_2 \end{bmatrix} = \begin{bmatrix} \begin{pmatrix} \xi_1 \\ \xi_2 \end{pmatrix}_1 & \cdots & \begin{pmatrix} \xi_1 \\ \xi_2 \end{pmatrix}_{n-m} \end{bmatrix} \tag{2.24}$$

where $\Psi_1 \in \mathcal{C}^{(n-m)\times(n-m)}$ and $\Psi_2 \in \mathcal{C}^{m\times(n-m)}$. Since each column of Ψ is in the null space of $\left[\left(\lambda_j I_{(n-m)} - A_{11}\right) \; A_{12}\right]$, it must satisfy equation (2.20). So,

$$\begin{bmatrix} \Psi_1 \\ \Psi_2 \end{bmatrix} = \begin{bmatrix} \Psi_1 \\ M\Psi_1 \end{bmatrix} \tag{2.25}$$

then

$$M = \Psi_2 \Psi_1^{-1} \tag{2.26}$$

Given the definition of M in equation (2.16) and letting $S_2 = I_m$, the switching surface to achieve the desired null space dynamics is

$$S = \begin{bmatrix} \Psi_2\Psi_1^{-1} & I_m \end{bmatrix} \tag{2.27}$$

2.1.2 Control Law

A discontinuous control input is used to drive the state variables to the switching surface (called the "reaching phase") and maintain them there if they are perturbed off the surface. Since the system state variables are not on the switching surface ($\sigma \neq 0$), attempting to drive them onto the switching surface can be expressed as a "reachability condition." The general multivariable form of this condition is

$$\sigma^T \dot{\sigma} < 0 \tag{2.28}$$

where $\sigma \in \Re^m$. Sometimes a more restrictive reachability condition is imposed that requires each reaching dynamic mode to individually satisfy this condition

$$\sigma_i \dot{\sigma}_i < 0 \quad \text{for} \quad i = 1, 2, \cdots, m \tag{2.29}$$

There are many possible choices for the control elements needed to achieve this goal. [25, 37] A simple form is a unit vector non-linearity

$$u = -\rho(SB)^{-1} \frac{\sigma}{\|\sigma\|} \tag{2.30}$$

where ρ is a positive scalar and $\|\cdot\|$ is the Euclidean norm. A slight modification of this control law includes a matrix P such that

$$u = -\rho(SB)^{-1} \frac{P\sigma}{\|P\sigma\|} \tag{2.31}$$

where $P \in \Re^{m \times m}$ is a solution to the Lyapunov equation

$$P\Phi + \Phi^T P = -I_m \tag{2.32}$$

and $\Phi \in \Re^{m \times m}$ is a stable design matrix intended to specify the dynamics of the switching variables in the following form,

$$\dot{\sigma} = \Phi\sigma \tag{2.33}$$

Another simple choice is a multi-variable constant gain relay. [25] If a vector signum function "sign" is defined as

$$\text{sign}(\sigma) = \begin{bmatrix} \text{sign}(\sigma_1) & \text{sign}(\sigma_2) & \cdots & \text{sign}(\sigma_m) \end{bmatrix}^T \tag{2.34}$$

and the symmetric control limits for each relay are defined as a diagonal matrix U_{max}

$$U_{max} = \text{diag}\left[u_{max_1}, u_{max_2}, \cdots, u_{max_m}\right] \tag{2.35}$$

then the relay control law can be expressed as

$$u = -U_{max} \, \text{sign}(\sigma) \tag{2.36}$$

In the scalar control case ($m = 1$), all of these control laws reduce to a simple relay.

In general, the relay element can be allowed to chatter during the "sliding phase" ($\sigma = 0$) to approximate the equivalent control given by equation (2.5). However, often the non-linear relay is combined with a linear control law. The most common form is to include the equivalent control as a linear portion of the control law, such as

$$u = -(SB)^{-1}\left[SAx + \rho\frac{\sigma}{\|\sigma\|}\right] \tag{2.37}$$

The advantage of this form is that if the controls are not saturated, the control law in equation (2.37) satisfies the reachability condition (2.28) globally, since

$$\sigma^T\dot{\sigma} = -\rho\|\sigma\| < 0 \tag{2.38}$$

Consequently, the state trajectories are always driven to and captured by the switching surface.

Unlike linear control techniques, the relay element of sliding mode control laws in equations (2.30) and (2.37) allow more control power to be used in maintaining the desired state trajectory while moving towards the switching surface. As a result, once the sliding mode is achieved, the system behavior is independent of matched external disturbances and internal uncertainties. This characteristic is referred to as the invariance property of sliding mode control. [38]

Whereas most sliding mode control techniques concentrate on designing the reduced-order dynamics, Gao proposed a method that also considers requirements on the reaching mode dynamics. [37] In this method, the designer specifies the type of desired reaching mode characteristics and solves for the required control law. For example, if it is desired that the system maintain a constant reaching rate,

$$\dot{\sigma} = SAx + SBu = -G\,\mathrm{sign}\,(\sigma) \tag{2.39}$$

where $\mathrm{sign}\,(\sigma)$ is the vector sign function defined in equation (2.34) and

$$G = \mathrm{diag}\,[g_1, g_2, \cdots, g_m] \tag{2.40}$$

Then the desired control law becomes

$$u = -(SB)^{-1}\left[SAx + G\,\mathrm{sign}(\sigma)\right] \tag{2.41}$$

If the desired reaching dynamics are a constant plus proportional rate,

$$\dot{\sigma} = -G\,\mathrm{sign}(\sigma) - H\sigma \tag{2.42}$$

where H is an m by m matrix of constants. In this case, the desired control law is

$$u = -(SB)^{-1}\left[SAx + G\,\mathrm{sign}(\sigma) + H\sigma\right] \tag{2.43}$$

In general, since the inverse of the matrix (SB) exists by the design requirement of the switching surface S, any form of desired reaching dynamics can be used to define the sliding mode control law.

2.1.3 Example

A simple, second-order example highlights some of the VSC design aspects. Consider the linear-time invariant system

$$\begin{bmatrix} \dot{x}_1 \\ \dot{x}_2 \end{bmatrix} = \begin{bmatrix} 0 & 25 \\ 0 & 0 \end{bmatrix} \begin{bmatrix} x_1 \\ x_2 \end{bmatrix} + \begin{bmatrix} 0 \\ 1 \end{bmatrix} u \tag{2.44}$$

and the switching surface

$$0 = \begin{bmatrix} s_1 & s_2 \end{bmatrix} \begin{bmatrix} x_1 \\ x_2 \end{bmatrix} \tag{2.45}$$

The reduced-order system dynamics, given by (2.17), are

$$\dot{x}_1 = -25\frac{s_1}{s_2}x_1 \tag{2.46}$$

Using the pole placement design method for the switching surface, a selection of $\lambda = -1$ results in the relationship

$$-1 = -25\frac{s_1}{s_2} \tag{2.47}$$

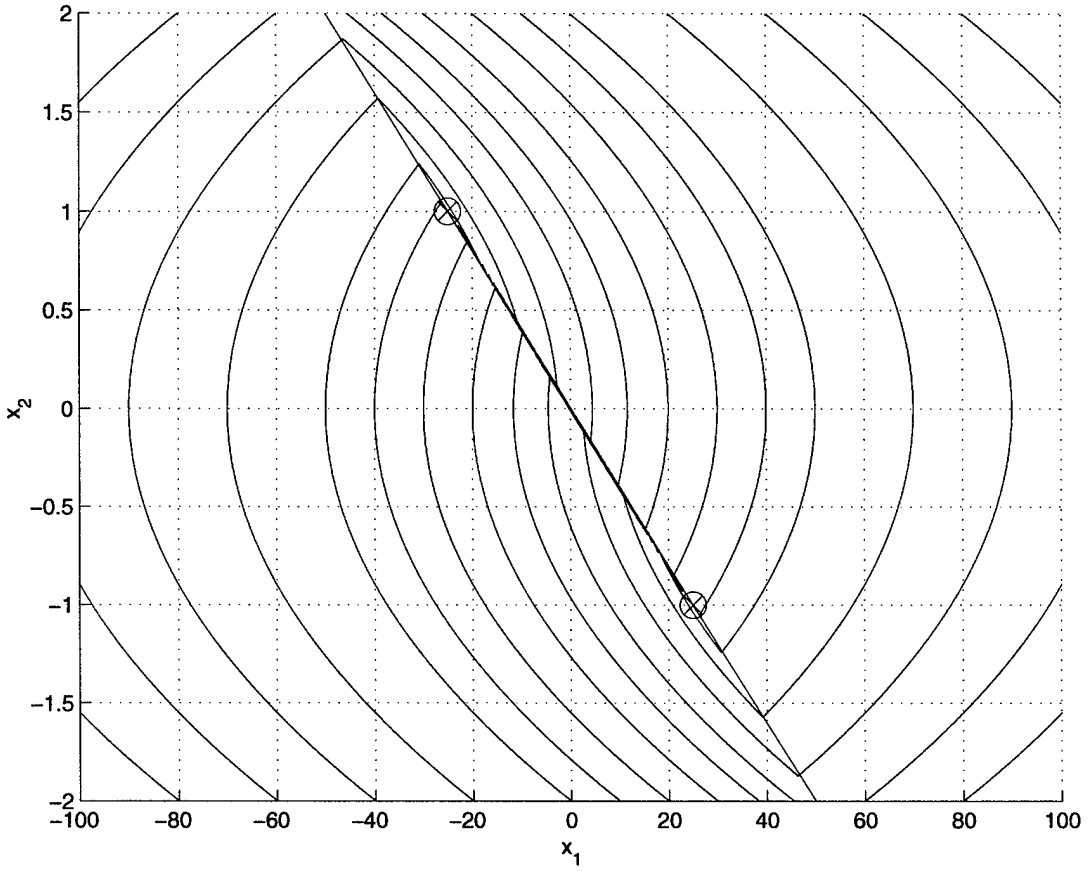

Figure 2.1: Second Order System Sliding Mode Example

giving the switching surface

$$S = \begin{bmatrix} \frac{1}{25} & 1 \end{bmatrix} \tag{2.48}$$

Figure 2.1 illustrates the state trajectories for the dynamic system in equation (2.48) using a control law of the from

$$u = -1 \operatorname{sign}(Sx) \tag{2.49}$$

The straight red line in the Figure 2.1 is the switching surface (2.48) and the curved blue lines are the state trajectories.

The control law in (2.49) generates a locally stable sliding mode. This stable region is

determined from examining the reachability condition (2.28). For this example

$$\sigma\dot{\sigma} = \sigma\left[x_2 - 1\,\mathrm{sign}\left(\sigma\right)\right] < 0 \tag{2.50}$$

Dividing by the positive scalar $\sigma\,\mathrm{sign}\left(\sigma\right)$ gives

$$\frac{x_2}{\mathrm{sign}\left(\frac{1}{25}x_1 + x_2\right)} - 1 < 0 \tag{2.51}$$

Examine a point (x_{1o}, x_{2o}) on $\sigma = 0$; so,

$$x_{1o} = -25x_{2o} \tag{2.52}$$

and consider a slight perturbation in the direction (δx_1) from this point

$$\begin{aligned} x_1 &= x_{1o} + \delta x_1 \\ x_2 &= x_{2o} \end{aligned} \tag{2.53}$$

So (2.51) becomes

$$\frac{x_{2o}}{\mathrm{sign}\left(\delta x_1\right)} - 1 < 0 \tag{2.54}$$

Equation (2.54) implies that the sliding mode is bounded by

$$\begin{aligned} x_{2o} &= 1 \quad \text{and} \quad \delta x_1 < 0 \\ x_{2o} &= -1 \quad \text{and} \quad \delta x_1 > 0 \end{aligned} \tag{2.55}$$

or on the sliding surface $(\sigma = 0)$ within the bounds

$$\begin{aligned} -1 < x_2 < 1 \\ x_1 = -25x_2 \end{aligned} \tag{2.56}$$

The limits of the stable portion of the sliding mode are denoted in Figure 2.1 by the red x's surrounded by circles. Inside of this region the sliding mode is stable on the switching surface. Outside of this region, there is insufficient control power to maintain a sliding mode; so, state trajectories are not captured but overshoot the switching surface.

2.2 Comparison of VSC to other Control Techniques

Variable structure control and sliding mode control have similarities with many more familiar control techniques. Buffington has illustrated the similarities between sliding mode control and feedback linearization. [39] In addition, sliding mode control is similar to many high-gain, output control techniques with bounded control inputs. The two primary reasons for this connection are: the structure of the sliding mode dynamics is determined by the transmission zeros and zero directions of the open-loop system just like a high-gain controller; and the relay-like, non-linear behavior of the sliding mode control law is similar to the control saturation non-linearity encountered with high gain controllers.

The next section highlights the similarities between sliding mode control and three more familiar control techniques: bang-bang control, Lyapunov control, and the asymptotic linear quadratic regulator. The shape of the control saturation for a multi-input control problem significantly affects the control law response. As a result, the following section only considers a maximum allowable control input of one. The control laws are then typical of the unit vector form of

$$u = -\frac{\sigma}{\|\sigma\|} \tag{2.57}$$

where $\|\cdot\|$ is the Euclidean norm and σ is a switching surface.

2.2.1 Bang-Bang Control

Due to its relay-like usage of the control, it would appear that VSC should have many similarities with "bang-bang" control. In fact, if a time-varying switching surface is employed, the control techniques are very similar. The following development is based on material presented by Lewis. [40] Let the dynamic system under consideration be a linear-time invariant system of the form

$$\dot{x} = Ax + Bu \tag{2.58}$$

where $x \in \Re^n$, $u \in \Re^m$, $A \in \Re^{n \times n}$, and $B \in \Re^{n \times m}$. The control is bounded in the form of

$$\|u\| \leq 1 \tag{2.59}$$

where $\|\cdot\|$ is the Euclidean norm.

Consider the minimum time control strategy. The cost function to minimize the transient time is

$$J = \int_0^{t_f} 1 \, dt \tag{2.60}$$

This optimal control problem is solved by minimizing the Hamiltonian

$$H = 1 + \lambda^T (Ax + Bu) \tag{2.61}$$

where $\lambda \in \Re^n$ are the co-state variables. Since the dynamics are linear in the control vector, the stationarity condition gives

$$0 = \frac{dH}{du} = B^T \lambda(t) \tag{2.62}$$

but is not explicitly solvable for the control, u. Therefore, to minimize H, u would be selected to make H as negative as possible (usually $u = +\infty$ or $-\infty$). However, since the controls are bounded, Pontryagin's Minimum Principle is applied to make H as negative as possible within the control bounds

$$H(x^*, u^*, \lambda^*, t) \leq H(x^*, u, \lambda^*, t) \tag{2.63}$$

where $\|u\| \leq 1$. This consideration gives an optimal control of

$$u^* = -\frac{B^T \lambda(t)}{\|B^T \lambda(t)\|} \tag{2.64}$$

where the co-state variables are determined by the dynamic system

$$\dot{\lambda}(t) = -A^T \lambda(t) \tag{2.65}$$

Evaluating the Hamiltonian for the terminal conditions gives

$$0 = 1 + \lambda^T(t_f) \left[Ax(t_f) + Bu(t_f) \right] \tag{2.66}$$

In variable structure control terms, the switching surface σ could be thought of as a time varying function of the co-state variables

$$\sigma(t) = B^T \lambda(t) \tag{2.67}$$

So the bang-bang control is

$$u^* = -\frac{\sigma(t)}{\|\sigma(t)\|} \tag{2.68}$$

Example

As a comparison to sliding mode structure controller, consider the same second-order system used in the previous VSC design example in section 2.1.3.

$$\begin{bmatrix} \dot{x}_1 \\ \dot{x}_2 \end{bmatrix} = \begin{bmatrix} 0 & 25 \\ 0 & 0 \end{bmatrix} \begin{bmatrix} x_1 \\ x_2 \end{bmatrix} + \begin{bmatrix} 0 \\ 1 \end{bmatrix} u \tag{2.69}$$

For a second-order system with a scalar control, the known minimum time control strategy employs one switch (or two bangs). As a result, the time varying switching surface given in equation (2.64) is a composite of the positive and negative control input state trajectories that go to the origin. For both of these trajectories, the state values at the final time (t_f) are zero.

$$x_1(t_f) = x_2(t_f) = 0 \tag{2.70}$$

Consider the $u = +1$ (or $x_2 < 0$) trajectory to the origin. From the state space model (2.69)

$$\dot{x_2} = +1 \tag{2.71}$$

Integrating back from the final time (t_f) to any other time (t) gives

$$x_2 = t - t_f \tag{2.72}$$

Next integrating the other state space equation in (2.69) back in time from t_f to t gives

$$x_1 = \frac{25}{2}(t - t_f)^2 = \frac{25}{2}x_2^2 \tag{2.73}$$

So the $x_2 < 0$ branch of the switching surface is

$$\sigma(x) = x_1 - \tfrac{25}{2}x_2^2 \quad \text{for} \quad x_2 < 0 \tag{2.74}$$

Repeating the same analysis for the $u = -1$ (or $x_2 > 0$) trajectory to the origin gives

$$\sigma(x) = x_1 + \tfrac{25}{2}x_2^2 \quad \text{for} \quad x_2 > 0 \tag{2.75}$$

Equations (2.74) and (2.74) can be combined into a single equation defining the non-linear, bang-bang switching surface of the form

$$\sigma(x) = x_1 + \frac{25}{2}x_2|x_2| \tag{2.76}$$

The control law would be of the form

$$u = -\operatorname{sign}[\sigma(x)] = -\frac{\sigma(x)}{|\sigma(x)|} \tag{2.77}$$

Figure 2.2 illustrates the state trajectories for this bang-bang control in the state space. The red line in the Figure 2.2 is the non-linear, switching surface and the blue lines are the state trajectories.

The sliding mode example derived earlier could be thought of as a linear approximation to the time optimal bang-bang solution, see Figure 2.1. In fact, for the two sets of initial conditions whose state trajectories go through the intersection of the linear and parabolic switching surfaces but are beyond the range of a stable sliding mode, the solutions are the same.

2.2.2 Lyapunov Control

Brogan gives an example of a control-constrained quadratic Lyapunov controller that illustrates the similarities between this type of controller and a unit-vector, sliding mode controller. [31] Consider the LTI state space dynamic system defined in equation (2.58). Let the control vector be constrained to a unit-magnitude,

$$\|u(t)\| \leq 1 \tag{2.78}$$

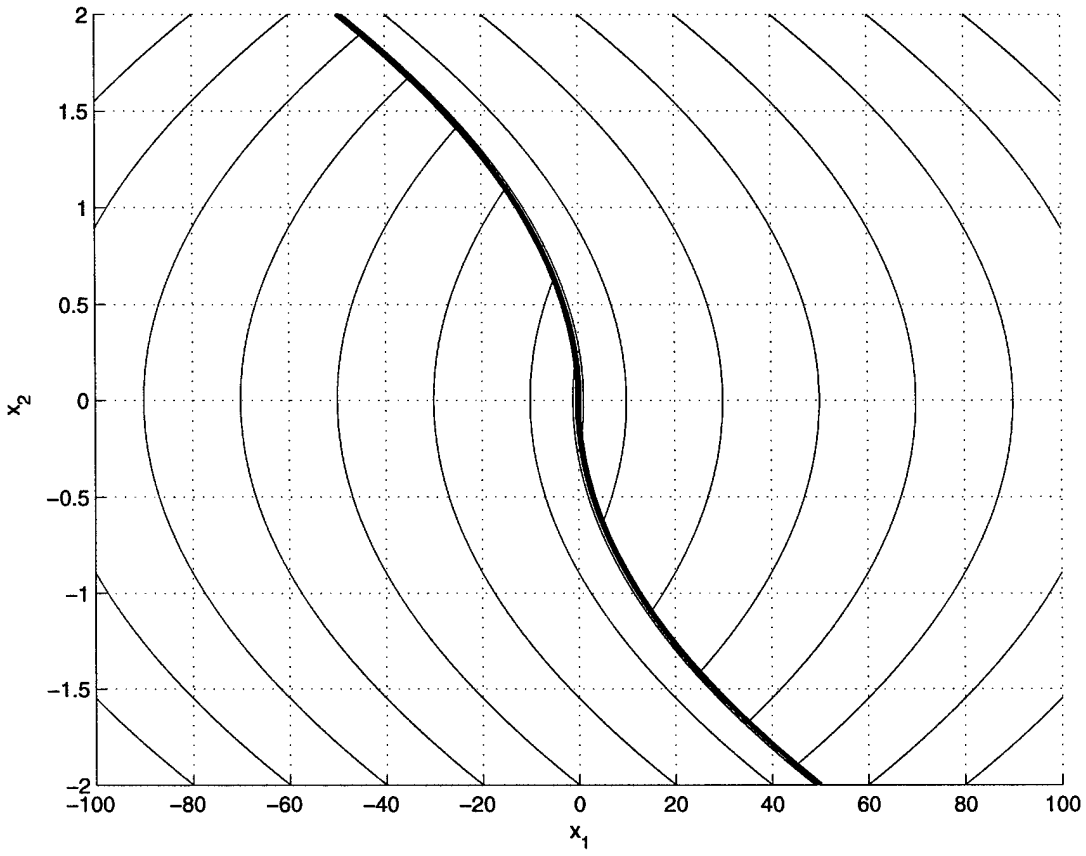

Figure 2.2: Second Order System Bang-Bang Example

where $\|\cdot\|$ is the Euclidean norm. Define the Lyapunov function

$$V(x) = x^T P x \tag{2.79}$$

with $P \in \Re^{n \times n}$ symmetric and positive definite. Then

$$\begin{aligned} \dot{V}(x) &= \dot{x}^T P x + x^T P \dot{x} \\ &= x^T \left(A^T P + P A \right) x + 2 u^T B^T P x \end{aligned} \tag{2.80}$$

The desired result of

$$\dot{V}(x) < 0 \tag{2.81}$$

can be achieved if P is defined in terms of the Lyapunov equation

$$A^T P + P A = -Q \tag{2.82}$$

where Q is a positive definite matrix, and if u is parallel but opposite in sign to $B^T P x$. In addition, for a minimum time solution given the control constraint in equation (2.78), u should be always be maximum in magnitude. This consideration gives a control law of the form

$$u = -\frac{B^T P x}{\|B^T P x\|} \tag{2.83}$$

This expression is the same as a unit vector, variable structure control law of the form

$$u = -\frac{S x}{\|S x\|} \tag{2.84}$$

where the switching surface is defined by

$$S = B^T P \tag{2.85}$$

So the choice of the Lyapunov function (P) could be considered a design method for determining the sliding mode switching surface (S). This design method would ensure a stable set of sliding or reduced-order system dynamics.

2.2.3 Asymptotic LQR

In the late 1970's, Stein and others examined the asymptotic properties of the linear quadratic regulator (LQR) to gain insights in the proper selection of weighting matrices. [41, 42, 43, 44] Consider the LTI state space dynamic system defined in equation (2.58) and the LQR cost function

$$J = \int_0^\infty x^T Q x + \rho u^T R u \, dt \tag{2.86}$$

where $Q \in \Re^{n \times n}$, $\rho \in \Re^1$, and $R \in \Re^{m \times m}$, consider a matrix C to be the full rank factorization of the symmetric state weighting matrix Q

$$Q = C^T C \tag{2.87}$$

where $C \in \Re^{p \times n}$ and $p = \text{rank}(Q) \leq n$. If C is considered as the output matrix of the system in equation (2.58)

$$y = Cx \tag{2.88}$$

where $y \in \Re^p$, then the LQR cost function in equation (2.86) can be formulated as an output cost function of the form

$$J = \int_0^\infty y^T y + \rho u^T R u \, dt \tag{2.89}$$

The optimal solution for this formulation is

$$u^* = -\frac{1}{\rho} R^{-1} B^T P x \tag{2.90}$$

where P is the solution to the matrix Riccati equation

$$0 = PA + A^T P + C^T C - \frac{1}{\rho} P B R^{-1} B^T P \tag{2.91}$$

Examining the control law in equation (2.90), as $\rho \to 0$, the magnitude of any vector $u^* \in \text{Ran}(B^T P)$ is very large. In the case of a physical system, the control law in equation (2.90) would define a direction in the control space ($\Re^{m \times m}$) and the magnitude of the control vector would be limited by the physical bounds on the control. The control law in equation (2.90) would also exhibit discontinuous inputs based on $\ker\left(B^T P\right)$. If the control were limited in

magnitude to one, then an equivalent variable structure control law would be a unit vector non-linearity of the form

$$u = -\frac{R^{-1}B^T Px}{\|R^{-1}B^T Px\|} \tag{2.92}$$

or considering $B^T P$ as the switching surface S

$$u = -\frac{R^{-1}Sx}{\|R^{-1}Sx\|} \tag{2.93}$$

The control weight matrix R affects the direction of the control vector by assigning different relative costs to the various controls. For $R = I_m$, the controls are equally weighted, equation (2.93) is similar to the Lyapunov control example in equation (2.83).

Kawkernaak [44, 45] shows that for square, minimum phase plants, the solution the Riccati equation (2.91) in the limit as $\rho \to 0$ approaches the zero matrix

$$\lim_{\rho \to 0} P = [0] \tag{2.94}$$

and that the matrix Riccati equation (2.91) can be reposed as

$$0 = \lim_{\rho \to 0} \left[C^T C - \frac{1}{\rho} PBR^{-1}B^T P \right] \tag{2.95}$$

Defining the optimal control gain matrix K^* as

$$K^* = \frac{1}{\rho} R^{-1}B^T P \tag{2.96}$$

equation (2.95) can be rearranged to show

$$\lim_{\rho \to 0} (K^*)^T \rho R K^* = C^T C \tag{2.97}$$

Equation (2.97) reveals that the state feedback gain matrix K approaches $R^{-1/2}C$ as the control weighing approaches zero. Therefore, the output matrix C of the asymptotic LQR control law can be thought of as a switching surface S in a VSC law. A unit vector VSC law equivalent to the asymptotic LQR control law in equation (2.90) is

$$u = -\frac{R^{-1/2}Cx}{\|R^{-1/2}Cx\|} \tag{2.98}$$

Chapter 3

Variable Strategy Pilot Model

A simple definition of strategy is "a plan of action." [46] In control applications, the most straight forward example of a plan of action is the if-antecedent-then-consequent rules frequently found in fuzzy logic and expert system control techniques. Similarly, it should be evident from the examples in Chapter 2 that the switching surface (S) is the VSC plan of action for accomplishing a control task. In the scalar VSC examples, it is a simple plan. If the VSC reaching variable (σ) is positive, a predetermined negative control action is used. If σ is negative, a predetermined positive control action is used. In multi-input cases, the predetermined inputs are based on the direction of the reaching vector σ. Like fuzzy logic and expert systems, the VSC switching surface can be used to mathematically interpret literal if-then rules.

The instructions used to train human operators performing a control task are often in the form of if-then rules. As a result, all three of these control techniques can be useful in modeling human operator precognitive behavior. [5, 6, 47, 48, 49] However, fuzzy logic and expert systems usually require "training" of some kind. Whereas, the VSC switching surface is derived from the dynamics. It is chosen to achieve a desired set of reduced-order or null-space dynamics. In this sense, the switching surface is considered a mathematical representation of a control strategy for accomplishing a specific task.

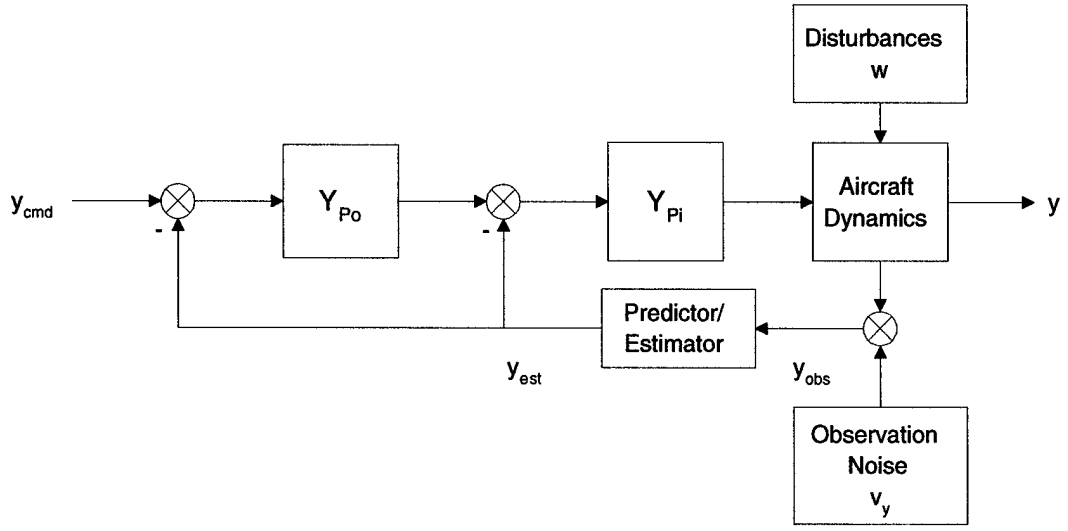

Figure 3.1: Inner/Outer Loop VSM

Consider now the specific task of piloting an aircraft. The pilot's goal is to safely control the aircraft's trajectory relative to the ground. The primary technique pilots are taught to accomplish this goal is "attitude flying" or using the aircraft's attitude to control the trajectory. In this method of flying, the pilot uses the aircraft's pitch, bank, and power to control the trajectory. [50, 51] To represent this pilot control strategy, the variable strategy pilot model is constructed in a classic inner and outer loop configuration, as shown in Figure 3.1. The outer loop (Y_{Po}) translates the guidance and navigation commands into aircraft attitude and power commands. It is where the pilot's acquisition strategy is implemented. The inner loop (Y_{Pi}) translates the attitude and power commands into stick, throttle, and peddle commands. The inner loop is also where the pilot augments the basic aircraft's dynamics to achieve better overall task performance.

3.1 Pilot Acquisition Strategy

The outer loop translates the guidance and navigation commands into aircraft attitude and power commands. In the variable strategy pilot model, it is a manifestation of the pilot's

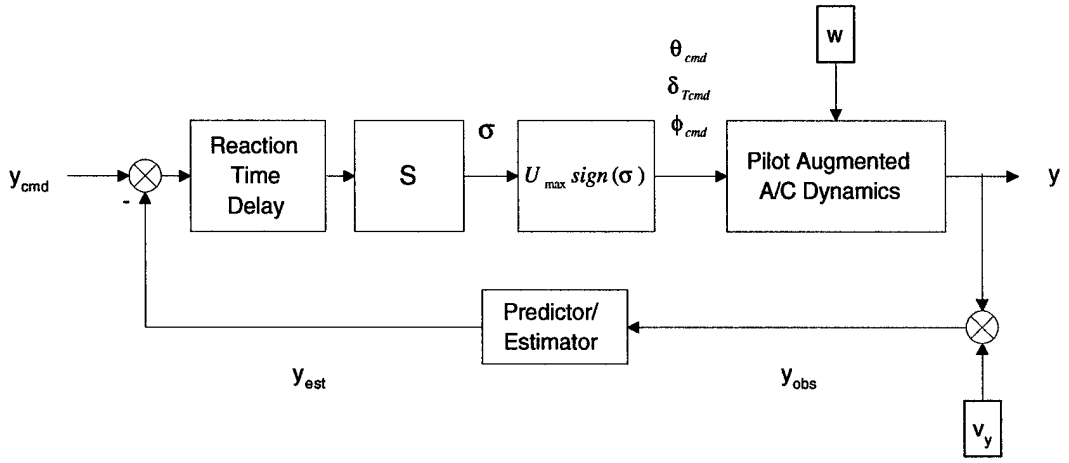

Figure 3.2: VSM Outer Acquisition Loop

acquisition strategy and is the primary focus of this research effort. As discussed earlier, human operator's often employ discontinuous control strategies in accomplishing acquisition tasks. This discontinuous control strategy is modeled with a variable structure control technique.

Figure 3.2 illustrates the proposed variable structure control representation of the pilot's control strategy. The switching surface (S) is the mathematical representation of the acquisition strategy. The switching surface is determined by the physical geometry of the task to be accomplished and general piloting techniques. As Heffley has shown, these piloting techniques can be drawn from existing pilot training and flight manual literature. [52] The simple non-linear element sign(σ) is the vector signum function defined by (2.34) and used to generate the discontinuous pilot commands. The diagonal gain matrix U_{max} (2.35) is a manifestation of the maximum control amplitudes that the pilot uses for accomplishing the acquisition task.

While executing an acquisition task, the pilot is attempting to perform large amplitude maneuvers to quickly reduce the system output errors and error rates. So, the objective of the acquisition control law is to drive the system state variables to the switching surface in the minimum time. A time optimal solution to this problem would be a full authority

bang-bang solution and U_{max} would represent the maximum control available in each axis. However, as Pew noted, the pilot must tradeoff the cost of a switching time error with the cost of limiting the velocity of the output to a value less than the time optimal value. [9] As a result, the pilot typically uses control inputs that are less than the maximum amount available. An estimate for a reasonable range of these maximum control inputs can be based on piloting procedures and techniques, similar to Heffley's approach. [52]

Since the instrument flight rules environment is a more structured flight environment, the military and civilian instrument flight procedures are used to estimate both the pilot's switching surface and controller gain matrices. [50, 51] Although instrument procedures are more restrictive than visual procedures, they are representative of the "smooth" piloting and "stabilized" flight characteristics desired for commercial aviation. However, an individual pilot's gain within this feasible range is determined by the individual's aggressiveness in performing the task.

Decision and reaction time delays are critical elements in realistically modeling human operator performance during an acquisition task. The decision time delay is the time needed for a pilot to assess the situation and decide upon a course of action. Depending on the task and the available cues, this time delay is typically greater than one second. The reaction time delay is the time needed to physically respond to any stimuli. For a task where the pilot perceives rates and accelerations, the pilot has a certain amount of predictive capability to overcome reaction time delay.

3.2 Pilot Augmented Aircraft Dynamics

The inner loop of the variable strategy model translates the pilot's attitude and power commands into stick, throttle, and peddle movements. In accomplishing this objective, the pilot augments the basic aircraft's dynamics to achieve better task performance. The inner loop is also where the pilot's tracking strategy is implemented. Figure 3.3 illustrates a block

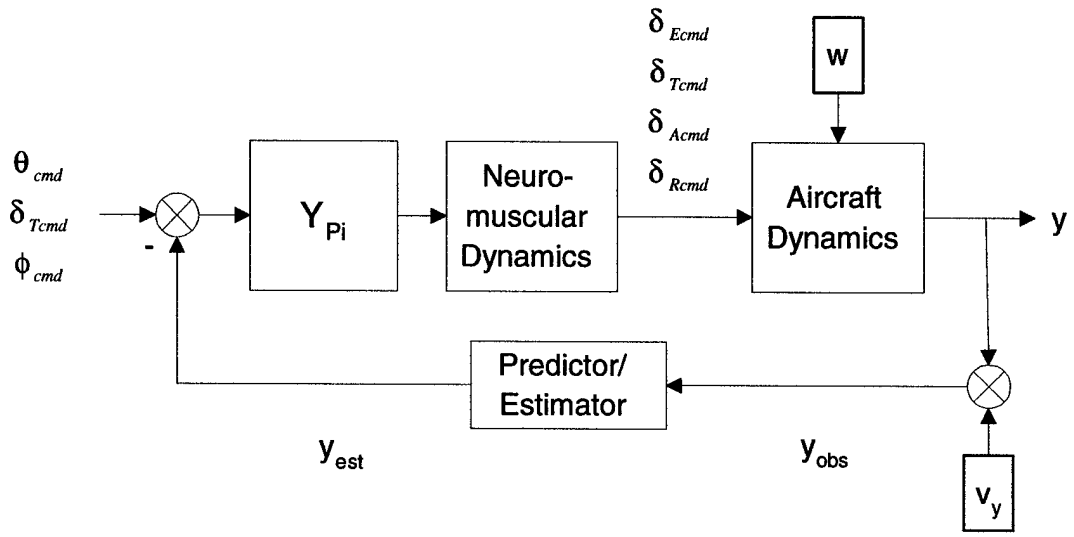

Figure 3.3: VSM Inner Pilot Augmented Loop

diagram layout of this control structure.

Two aspects of human operator dynamics included in this control structure are the operator's neuromuscular dynamics and the ability of the operator to generate accurate state estimates. The need for accurate estimates arises from insufficient information in the observation vector, inaccuracies in human perception (usually modeled as observation noise), and the need to anticipate the system's output due to internal human delays and lags.

The inner loop structure shown in Figure 3.3 has many similarities to previous pilot models such as the crossover model, the optimal control model (OCM), and the modified optimal control model (MOCM). [2, 3, 53] These models (or non-linear derivatives based on them) could be used as a basis for modeling the human operator from first principles. [54, 55]

Another method for determining the pilot augmented dynamics of the system is by interpreting data from experimental studies. A 1983 study by Heffley used this method for an analysis of landing flare data. Heffley found that the altitude dynamics of the closed-loop pilot-vehicle system exhibited characteristics similar to a well-damped, second-order system. The natural frequency and damping of the closed-loop system could be considered represen-

tative of the pilot's aggressiveness in performing the task. Using the assumed closed-loop dynamics and the known open-loop aircraft dynamics, Heffley was able to solve for the inner loop pilot control law (Y_{Pi}). [56]

3.3 Example

To illustrate the application of variable structure control techniques to pilot modeling, the single-input, single-output task of regulating lateral course error is modeled. This task becomes an acquisition task when a large initial lateral course error is given to the system. In this example, the aircraft dynamics are approximated by a first order roll lag. The inner loop dynamics consist of the pilot's neuromuscular dynamics and reaction time delay appended to the open-loop aircraft dynamics. Since the pilot began the task from a frozen time condition, with the initial course error visually displayed, no decision time delay was used. The pilot's outer-loop, acquisition strategy is based on a literal interpretation of pilot training literature. The input/output characteristics of this strategy are compared to the input/output results of a piloted simulation experiment.

3.3.1 Task Description

The manual control task is the regulation of lateral course error in level, constant airspeed flight. For this task, aircraft bank angle (ϕ) is considered representative of the pilot's input to control the lateral trajectory. The lateral track error (y_t) is the aircraft output response. To better understand the task, a simple experiment was conducted using the flight simulator at Virginia Tech. [57] The simulator hardware is a former US Navy 2F122A operational flight trainer for the A-6E. The cockpit consists of A-6E flight hardware, except for the stick feel system. The stick is driven by a programmable control loader capable of simulating various stick dynamics. The visual scene is produced by an Evans and Sutherland night-time visual computer. It is displayed on pilot front and side calligraphic display monitors. The visual

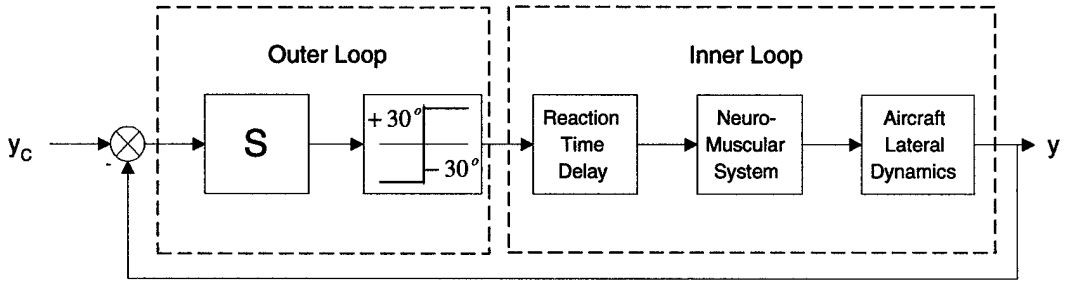

Figure 3.4: Lateral Course Regulation VSM Structure

update rate is on the order of 60 hertz. The simulator software has been re-hosted on a Silicon Graphics Origin 2000^{TM} Deskside computer system. This allows the hardware to simulate a variety of different aircraft dynamics.

A retired US Navy fighter/test pilot flew a model representative of a modern jet fighter in the approach configuration. The task was to regulate lateral track error based on the localizer signal and visual references to runway centerline. The visual scene was a fully-lighted night airport environment, with unlimited visibility and no clouds. The initial conditions were established at three miles from the threshold with initial lateral course offset of 1000 feet.

3.3.2 Model Structure

The proposed variable strategy model (VSM) for this task closely parallels the modified optimal control model (MOCM) developed by Davidson and Schmidt. [53] The VSM is shown in block diagram form in Figure 3.4. The switching surface matrix S is the mathematical representation of the pilot's acquisition strategy. A scalar relay element is used to model the pilot's discontinuous control inputs. Referring to pilot training literature, typically bank angles above thirty degrees are considered large in the instrument and approach environments. [50, 51] Therefore, the acquisition control is a simple relay employing this maximum input.

As in the MOCM development, the pilot's reaction time delay and neuromuscular characteristics are appended to the aircraft's dynamic response to form an augmented dynamic

system. For an aircraft at constant altitude and airspeed (V), a state space representation of the lateral course dynamics is

$$\begin{aligned} \dot{y}_t &= -V \sin\psi \\ \dot{\psi} &= \tfrac{g}{V} \tan\phi \end{aligned} \tag{3.1}$$

where the dynamic state variables are: lateral track error (y_t, in feet) and heading angle (ψ in radians). The input to the system is aircraft bank angle (ϕ, in radians). The aircraft dynamics are approximated by a first order lag of the form

$$\tau_R \dot{\phi} + \phi = \phi_c \tag{3.2}$$

where τ_R is the roll mode time constant (in seconds) and ϕ_c is the commanded bank angle (in radians). In this analysis, no display dynamics or simulator delays are considered. The pilot's reaction time delay is represented by a second-order Padé approximation,

$$\frac{\phi_c(s)}{u_p(s)} = \frac{1 - \frac{1}{2}(\tau_d s) + \frac{1}{8}(\tau_d s)^2}{1 + \frac{1}{2}(\tau_d s) + \frac{1}{8}(\tau_d s)^2} \tag{3.3}$$

where τ_d is the pilot's time delay (in seconds). The commands u_p and ϕ_c are the command signals before and after the time delay, respectively. The pilot's neuromuscular system dynamics are represented by a first-order lag with time constant τ_n.

$$\tau_n \dot{u}_p + u_p = u_c \tag{3.4}$$

where u_c and u_p are the command signals before and after the neuromuscular time lag, respectively.

Equations (3.1), (3.2), (3.3), and (3.4) are combined to form an augmented system including the basic aircraft dynamics and the pilot's human dynamics. A non-linear, state-space

Table 3.1: Lateral Course VSM Parameters

Airspeed (V)	253 ft/sec
Roll Mode Time Constant (τ_R)	1.4 sec
Pilot Time Delay (τ_d)	0.15 sec
Neuromuscular Time Lag (τ_n)	0.13 sec

representation of this system is

$$\begin{aligned} \dot{y}_t &= -V \sin\psi \\ \dot{\psi} &= \tfrac{g}{V} \tan\phi \\ \dot{\phi} &= -\tfrac{1}{\tau_R}\phi - \tfrac{8}{\tau_R \tau_d} x_1 + \tfrac{1}{\tau_R} u_p \\ \dot{x}_1 &= -\tfrac{4}{\tau_d} x_1 - \tfrac{8}{\tau_d^2} x_2 + u_p \\ \dot{x}_2 &= x_1 \\ \dot{u}_p &= -\tfrac{1}{\tau_n} u_p + \tfrac{1}{\tau_n} u_c \end{aligned} \tag{3.5}$$

where x_1 and x_2 are two state variables for the Padé approximation of the operator time delay. The numerical values for the state space model in (3.5) are summarized in Table 3.1. The observable outputs are

$$y_{obs} = \begin{bmatrix} y_t & \psi & \phi \end{bmatrix}^T \tag{3.6}$$

For this example, no observation noise is injected into the output signal, and only the output signals are used in the acquisition strategy. So, an estimator is not needed for state reconstruction is needed.

3.3.3 Acquisition Strategy

Since the pilot's switching surface (S) is a mathematical representation of the acquisition strategy, it is based upon how the pilot would mentally plan a course intercept maneuver. As Heffley proposed, the required strategy is extracted from pilot training rules. [52] Both the military and civil instrument flight training manuals outline simple procedures for lateral

course intercepts. [50, 51] First, a lead point to initiate a turn can be computed based on the time needed to complete the final heading change with a commanded rate of turn. And second, for small heading corrections (usually defined as less than thirty degrees) a bank angle equal to the heading error should be used. This information can be used to construct an acquisition switching surface.

When estimating a course intercept, it is assumed that the pilot uses a simple point mass representation of the aircraft to form the strategy for controlling the aircraft's trajectory. A linearized form of (3.1) is the state space model

$$\begin{pmatrix} \dot{y}_t \\ \dot{\psi} \end{pmatrix} = \begin{bmatrix} 0 & -V \\ 0 & 0 \end{bmatrix} \begin{pmatrix} y_t \\ \psi \end{pmatrix} + \begin{bmatrix} 0 \\ g/V \end{bmatrix} \phi \tag{3.7}$$

The lead point (y_l) to initiate the lateral course intercept maneuver is defined by the course closure rate ($\dot{y}_t$) and the time to complete the turn ($\frac{\psi}{\dot{\psi}}$). Putting this information together gives

$$y_l = \dot{y}_t \frac{\psi}{\dot{\psi}} \tag{3.8}$$

Using a linearized form of $\dot{y}_t$ and $\dot{\psi}$ and employing the rule that the bank angle should equal the heading error ($\phi = -\psi$) gives

$$y_l = \frac{V^2}{g}\psi \tag{3.9}$$

Since the lead point (y_l) is the switch point, it must be on the switching surface (S). This gives a potential pilot switching strategy of

$$\sigma = \psi - \frac{g}{V^2} y_t \tag{3.10}$$

or a switching surface referenced to the full state space model in (3.5) of the form

$$S = \begin{bmatrix} -\frac{g}{V^2} & 1 & 0 & 0 & 0 & 0 \end{bmatrix} \tag{3.11}$$

Putting this switching surface together with $\pm 30^o$ relay element gives a pilot control law of the form

$$u_c = -\left(\frac{\pi}{6}\right) \text{sign}\left(\psi - \frac{g}{V^2} y_t\right) \tag{3.12}$$

The following simulation results were obtained by numerically integrating the non-linear state space system of equations (3.5) with the VSM acquisition control law in equation (3.12) using a Runge-Kutta algorithm and a numerical time step of 0.01 seconds. The assumed parameters of the state space model are given in Table 3.1. The initial conditions were set for a 1000 feet lateral offset with a heading angle of zero degrees (parallel to the desired course).

Figure 3.5 illustrates the input/output time history of the VSM acquisition control using these model parameters. The green line tagged with o's is VSM's commanded bank angle, after the taking into account the neuromuscular and Padé time lags (ϕ_c). The blue line tagged with x's is the simulated aircraft's actual bank angle (ϕ). The bang-bang nature of the control strategy is quite evident in the input time history.

Figure 3.6 illustrates an example of the recorded input/output time history of the piloted simulation. This time history is from one of the early runs when the pilot was exhibiting significant discontinuous or bang-bang control behavior. There is an initial, near-constant amplitude input of -30^o bank angle followed by near-constant amplitude inputs of $+20^o$ and -10^o bank angle.

Comparing the two figures, one can see that the VSM commands are very step-like but the aircraft's bank angle is more like a sawtooth response (Figure 3.5); whereas, the piloted simulation results in Figure 3.6 show a more step-like response in bank angle. This characteristic is probably due to the pilot augmenting the basic aircraft roll dynamics with some additional command shaping. In addition, the VSM begins a limit cycle response by continuing to command the maximum allowable back angles. Whereas, the piloted simulation results show a switch to a smaller amplitude and even continuous control inputs later in the simulation run. These can be associated with a change in pilot strategy from an acquisition strategy to a tracking strategy. This transition was explored in more detail in a paper by Phillips and Anderson. [58]

A more revealing comparison of these strategies is found in the state space trajectories.

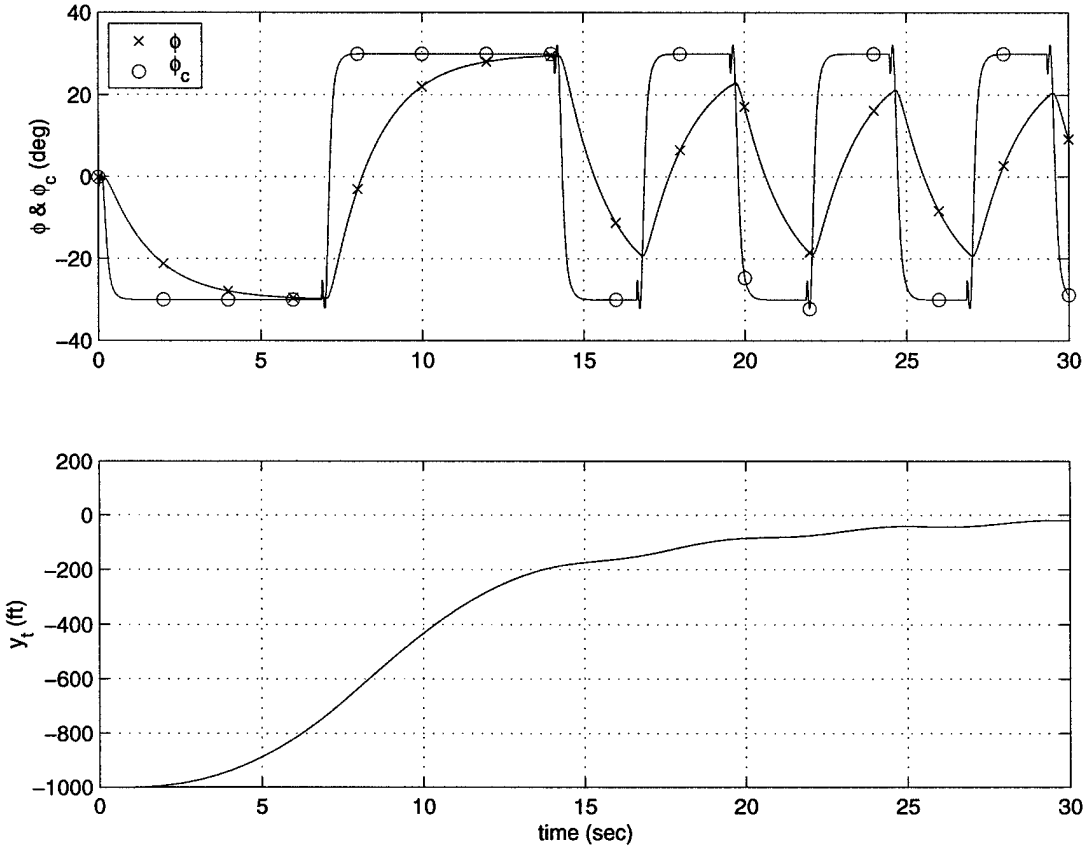

Figure 3.5: Acquisition VSM Time Response

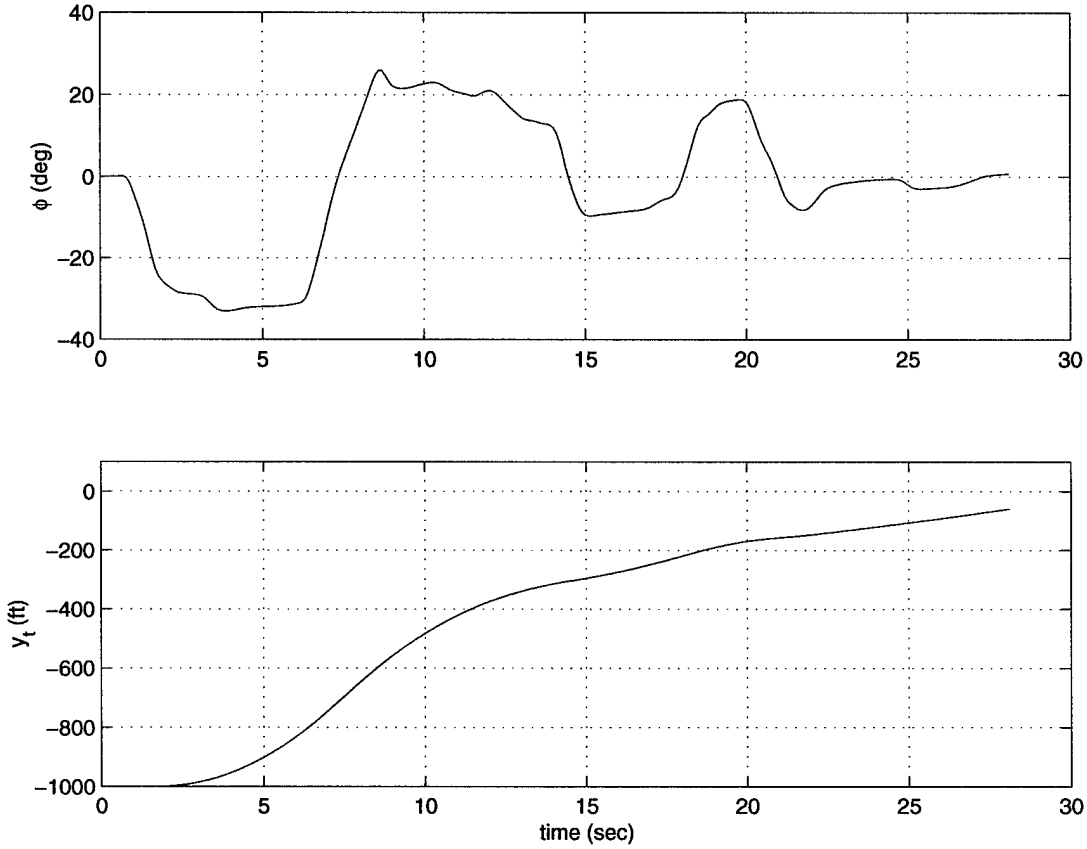

Figure 3.6: Pilot Input/Output Time History

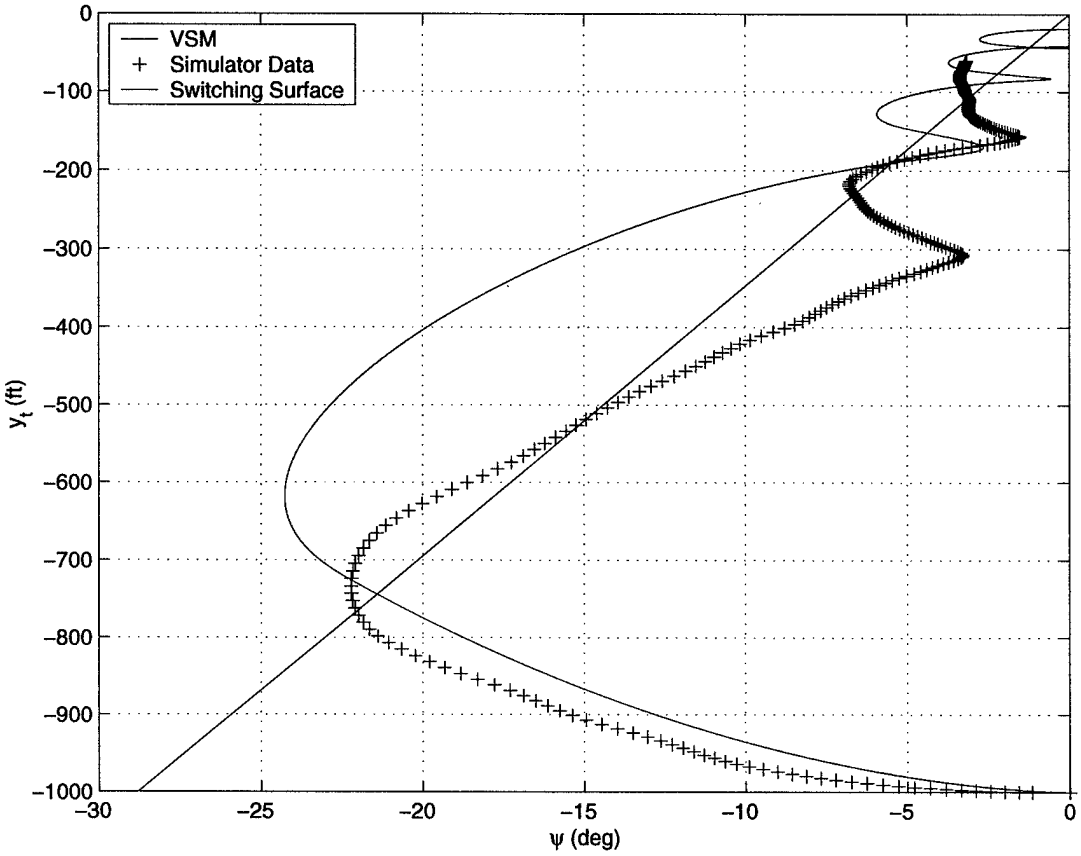

Figure 3.7: Acquisition VSM State Space

Figure 3.7 illustrates the state space trajectory projected onto the (ψ, y_t) plane for both the VSM simulation and the flight simulator results from Figure 3.6. The straight red line is the switching surface (S), the curved blue line is the state trajectory, and the black +'s are the piloted flight simulator results. In general, the VSM predictions and the piloted flight simulator results are very similar in structure. In both, there is an obvious oscillatory response around the switching surface. The primary difference is that the human pilot appears to be using a slightly different lead point than the one specified in equation (3.9). In fact a lead point of $y_l = \frac{V^2}{1.3g}\psi$ gives a better fit for this particular simulator test run.

Chapter 4

Transport Aircraft Visual Landing

For a multi-input, multi-output dynamic system example, the longitudinal control of a transport aircraft during the visual landing task is examined. Of interest is the closed-loop, pilot/aircraft response due to an incorrect initial condition at the precision approach decision height. The pilot's goal is to safely maneuver the aircraft from this incorrect position to a satisfactory position and energy state before executing a flare. Due to the large initial spatial error, this task is an acquisition task wherein the pilot is likely exhibit a non-linear, discontinuous control strategy.

In the VSM, pilot strategies are expressed in the form of a switching surface. These strategies are constructed by a literal interpretation of pilot training literature as proposed by Heffley. [20, 52] The closed-loop trajectory responses of the aircraft with these landing strategies are compared to a set of experimental data generated in a simulator study of pilot response to vertical navigation errors. [62] Through variation of a simple lead term in the switching surface, the predicted closed-loop response is shown to bound the experimental data set.

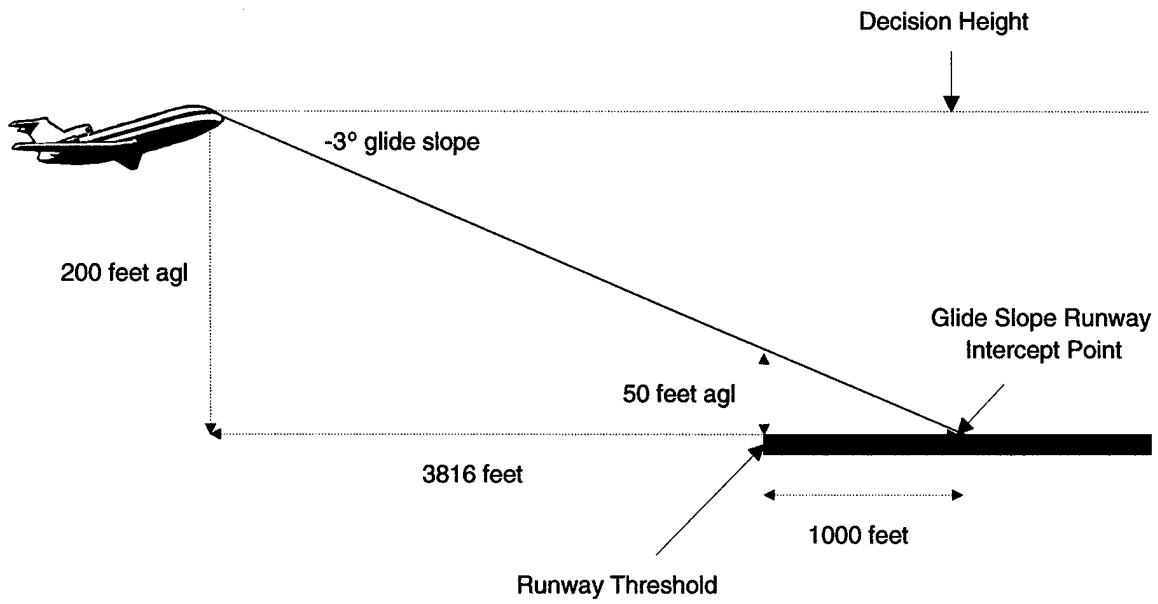

Figure 4.1: Nominal Precision Approach Geometry

4.1 Task Description

A typical precision approach consists of a lateral ground track along the runaway extended center line and a vertical track that is nominally a -3^o glide slope. The glide slope nominally intersects the runway surface 1000 feet beyond the runway threshold. As a result of this geometry, the desired flight path crosses the runway threshold at approximately 50 feet. [59] Figure 4.1 illustrates the nominal precision approach geometry. The pilot tracks this desired path by instrument navigation cues to an altitude called the decision height. The pilot can only continue the flight below the decision height if: the aircraft is continuously in a position to land on the intended runway with normal maneuvering, the flight visibility is not less than that prescribed for the approach, and the necessary visual reference requirements are meet. [60]

The visual landing task consists of maneuvering an aircraft from the decision height to satisfactory landing using visual references. For Category I precision approaches, the decision

height is normally 200 feet above the threshold. [59] For this study, it is assumed that the pilot breaks out of the clouds at 200 feet above ground level (agl) with unlimited visibility. The specific initial conditions of interest are the ones due to a vertical navigation error in the precision approach glide slope. Any vertical navigation error in the glide slope guidance results in the aircraft breaking out of the clouds at 200 feet agl and being either farther away from or closer to the runway than intended. For a negative (low) vertical navigation error, the aircraft is farther away from the runway than intended. For a positive (high) vertical navigation error, the aircraft is closer to the runway than intended. [61]

For the current instrument landing system (ILS), this vertical navigation error is an angular error. If the pilot maintains the indicated ILS glide slope, the aircraft breaks out of the clouds in an incorrect location, but the flight path is pointed at the intended glide slope runway intercept point. For a global positioning system (GPS) precision approach, this vertical navigation error is a linear one. If the pilot maintains the indicated GPS glide slope, the aircraft not only breaks out of the clouds in an incorrect location, but the flight path is parallel to the nominal glide slope and pointed either long or short of the intended point on the runway.

To better understand pilot capabilities to overcome these linear navigation errors, the US Federal Aviation Administration (FAA) funded a flight simulator study managed by NAV CANADA. [62] The study employed a Canadian Airlines Boeing 767 simulator and nine Canadian Airlines B-767 flight crews. The crews flew a total of 117 simulated GPS precision approaches with vertical navigation errors between -15 and $+15$ meters. They were given a candidate GPS landing criteria and were instructed to go-around if the criteria was not met or if they ever felt they were not in a safe position to land. Due to a data system failure, the only data recorded was the aircraft trajectory data at a sample rate of 1 hertz and with an airspeed resolution of one knot. However, this data can be used as a basis of comparison for trends in the output response of various pilot landing strategies. Additionally, after each approach the pilots completed a questionnaire specific to the approach just completed. At the end of each crew's simulator session, a 30 minute debrief was conducted and another

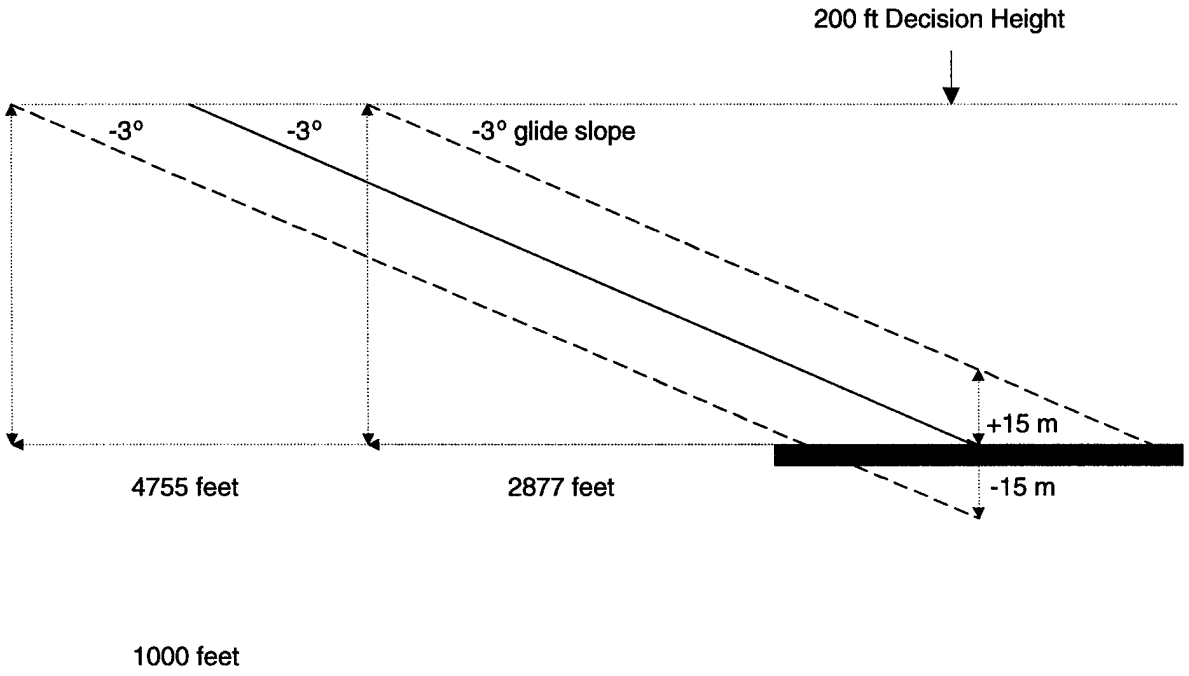

Figure 4.2: Precision Approach Geometry with Vertical Error

questionnaire was completed.

Figure 4.2 illustrates the precision approach geometry with a vertical navigation error. At 200 feet agl, the nominal -3^o glide slope places the aircraft 3816 feet from the desired glide slope runway intercept point. A -15 meter vertical navigation error places the aircraft at 4755 feet with its glide slope runaway intercept point "short" of the desired location. A $+15$ meter vertical navigation error places the aircraft at 2877 feet with its glide slope runaway intercept point "long" of the desired location. Therefore, the ± 15 meter vertical navigation error results in a ± 939 feet error in the longitudinal position of the aircraft.

4.2 Model Details

In this section, a Variable Strategy Model for the visual landing task is developed along the lines described in Chapter 3. First, a structure for the inner loop or pilot augmented dynamics is defined. Then the variable structure control law for the outer or acquisition loop is developed. This control law is a simple relay with a switching surface. Both the magnitudes of relay control inputs and the switching surface are based on a literal interpretation of pilot training literature. Finally, since the visual landing task blends directly into a landing flare maneuver, a simple flare control law is used to complete the landing trajectory.

4.2.1 Pilot Augmented Dynamics

The basic dynamics of interest for this task are the aircraft flight path dynamics. It is assumed that the pilot controls the flight path and velocity of the aircraft using the aircraft's pitch attitude and thrust. Similar to a point mass representation of the aircraft's flight path dynamics, the effect of the elevator deflection on the aircraft's velocity and angle of attack dynamics are ignored. Although the non-linear form of the aircraft's flight path dynamics could be used, the magnitude of the initial errors and the pilot control inputs considered for this study are well within the linear response of the aircraft. Therefore, the linearized form of the flight path dynamics is used.

For an aircraft with zero thrust incidence angle, the linear form of the flight path dynamics is given by

$$\begin{aligned}
\dot{\gamma} &= -\left(\tfrac{L_\alpha+T_o-mg\sin\gamma_o}{mV_o+L_{\dot{\alpha}}}\right)\Delta\gamma + \left(\tfrac{L_\alpha+T_o}{mV_o+L_{\dot{\alpha}}}\right)\Delta\theta + \left(\tfrac{L_V}{mV_o+L_{\dot{\alpha}}}\right)\Delta V + \left(\tfrac{L_q+L_{\dot{\alpha}}}{mV_o+L_{\dot{\alpha}}}\right)q \\
\dot{\theta} &= q \\
\dot{V} &= \left(\tfrac{D_\alpha}{m} - g\cos\gamma_o\right)\Delta\gamma - \left(\tfrac{D_\alpha}{m}\right)\Delta\theta + \left(\tfrac{T_V-D_V}{m}\right)\Delta V + \left(\tfrac{T_{max}}{m}\right)\tfrac{\Delta T}{T_{max}}
\end{aligned} \tag{4.1}$$

where γ_o is the trim flight path angle, $\Delta\gamma$ is the perturbation of the flight path from the trim value, $\Delta\theta$ is the perturbation of the pitch attitude from the trim value, q is the aircraft pitch rate, V_o is the trim airspeed, ΔV is the perturbation of the airspeed from the trim value,

T_o is the trim thrust, ΔT is the perturbation of the thrust from the trim value, T_{max} is the maximum thrust, m is the mass of the aircraft, and $\{L_{x_i}, D_{x_i}, \text{and} T_{x_i}\}$ are the aircraft lift, drag, and thrust dimensional stability derivatives.

It is assumed that the pilot performs an inner-loop stabilization on the basic aircraft dynamics to achieve a set of desired closed-loop pitch dynamics. In an effort to concentrate on the effects of the outer-loop, discontinuous acquisition strategy, a set of well behaved pilot augmented pitch dynamics is defined. This model form allows for analysis of the task and strategy instead of the typical handling qualities issues involved in evaluating a particular aircraft's ability to perform a task. The form of the pilot-augmented pitch dynamics is based on the Neal-Smith criteria. [63, 64]

Examining the Neal-Smith closed-loop pitch criteria, the pitch command (θ_c) to aircraft pitch attitude (θ_c) frequency response is similar to a second order system response of the form

$$\dot{q} + 2\eta_p \omega_p q + \omega_p^2 \theta = \omega_p^2 \theta_c \tag{4.2}$$

If this is taken as an idealized form of the pilot augmented pitch response, then the natural frequency (ω_p) can be equated with the Neal-Smith bandwidth and the damping ratio (η_p) can be correlated with the resonant peak $\left(|\frac{\theta}{\theta_{max}}|\right)$. One desirable characteristic in the closed-loop pitch response is to limit the resonant peak; therefore, a value of $\eta_p = 0.7$ is used in the desired dynamics. There is significant discussion in the flying qualities literature for desirable values of pitch bandwidth. MIL-STD-1797A recommends 2.5 radians/second for the landing phase. [65] Since this value was based on the fighter configurations of the Neal-Smith study, researchers evaluating transport aircraft in the landing phase have found this level of bandwidth to be abrupt. Weingarten found in piloted simulations of very large aircraft (i.e. approximately one million pounds) a pitch bandwidth of 1.5 radians/second was more representative of the data. [66]

A discontinuous input, such as that generated by the outer-loop VSM acquisition strategy, tends to excite high frequency dynamics. To keep the model simple, this VSM does not

model any of the physical pilot/vehicle dynamics which would tend to attenuate these dynamics. These potential attenuating sources include pilot neuromuscular lag, reaction time delays, stick dynamics, actuator dynamics, etc. Also, the NAV CANADA study employed operational flight crews employing operational flight procedures, not test pilots. The operational flight crews are likely to perform the task at a lower bandwidth. In addition, since it simulated an actual landing, the NAV CANADA study was a multi-axis task. It is well-known that the bandwidth of each axis is reduced as the pilot is required to control more degrees of freedom. As a result, an inner loop pitch bandwidth of $\omega_p = 0.5$ radians/second was used and found to generate trajectories representative of the NAV CANADA data set.

It is assumed the pilot does not augment the engine dynamics. As a result, the engine dynamics are modeled as a simple lag with a time constant $\tau_e = 2$ seconds. In terms of the linear perturbation variables this gives

$$\frac{\dot{T}}{T_{max}} = -\frac{1}{\tau_e}\left(\frac{\Delta T}{T_{max}} - \frac{\Delta T_c}{T_{max}}\right) \tag{4.3}$$

where ΔT_c is the pilot's commanded change in thrust from the trim value.

In addition to the aircraft state variables, the navigation error for the landing task is expressed as a glide slope deviation error (d) illustrated in Figure 4.3.

$$d = h - x\tan\gamma_o \tag{4.4}$$

where $\gamma_o = -3^o$. Differentiating (4.4) gives

$$\dot{d} = \dot{h} - \dot{x}\tan\gamma_o \tag{4.5}$$

where

$$\begin{aligned} \dot{h} &= V\sin\gamma \\ \dot{x} &= V\cos\gamma \end{aligned} \tag{4.6}$$

Linearizing about the trim condition V_o and γ_o gives a kinematic relation of the form

$$\dot{d} = \frac{V_o}{\cos\gamma_o}\Delta\gamma \tag{4.7}$$

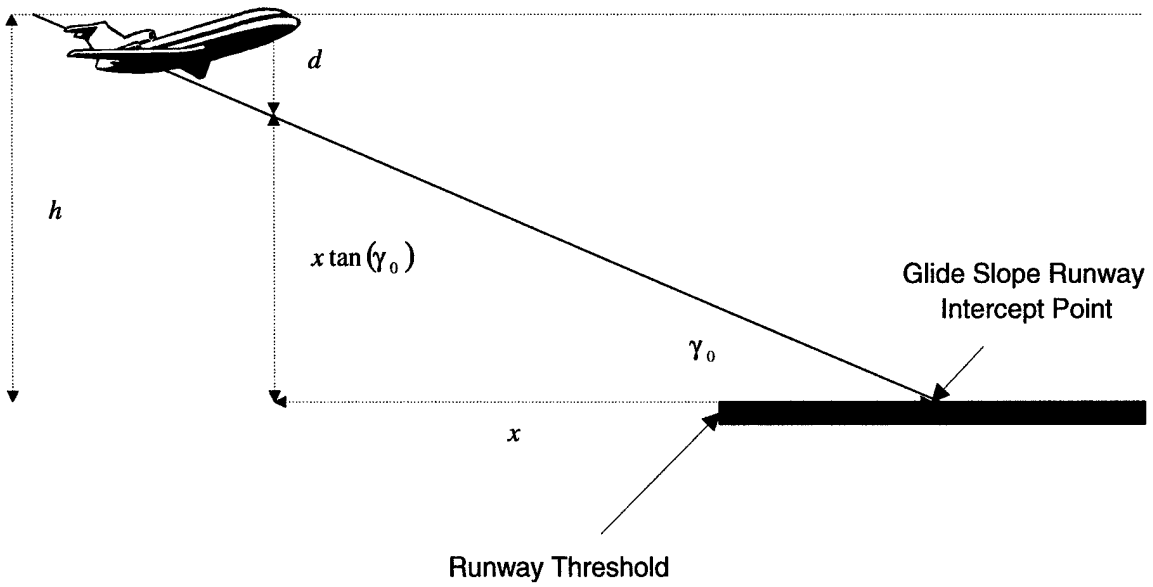

Figure 4.3: Glide Slope Deviation Geometry

Putting equations (4.1), (4.2), (4.3), and (4.7) together gives following the state space representation of the pilot-augmented vehicle dynamics. The state variable vector is represented by

$$x = \begin{bmatrix} d & \Delta\gamma & \Delta\theta & \Delta V & q & \frac{\Delta T}{T_{max}} \end{bmatrix}^T \tag{4.8}$$

and the pilot control vector

$$u = \begin{bmatrix} (\Delta\theta)_c & \left(\frac{\Delta T}{T_{max}}\right)_c \end{bmatrix}^T \tag{4.9}$$

The pilot augmented dynamic system is represented by

$$\dot{x} = Ax + Bu \tag{4.10}$$

where the plant matrix A is

$$A = \begin{bmatrix} 0 & \frac{V_o}{\cos\gamma_o} & 0 & 0 & 0 & 0 \\ 0 & -\left(\frac{L_\alpha + T_o - mg\sin\gamma_o}{mV_o + L_{\dot\alpha}}\right) & \left(\frac{L_\alpha + T_o}{mV_o + L_{\dot\alpha}}\right) & \left(\frac{L_V}{mV_o + L_{\dot\alpha}}\right) & \left(\frac{L_{\dot\alpha} + L_q}{mV_o + L_{\dot\alpha}}\right) & 0 \\ 0 & 0 & 0 & 0 & 1 & 0 \\ 0 & \left(\frac{D_\alpha}{m} - g\cos\gamma_o\right) & -\frac{D_\alpha}{m} & \left(\frac{T_V - D_V}{m}\right) & 0 & \frac{T_{max}}{m} \\ 0 & 0 & -\omega_p^2 & 0 & -2\eta_p\omega_p & 0 \\ 0 & 0 & 0 & 0 & 0 & -\frac{1}{\tau_e} \end{bmatrix} \tag{4.11}$$

and the input matrix B is

$$B = \begin{bmatrix} 0 & 0 & 0 & 0 & 0 & \frac{1}{\tau_e} \\ 0 & 0 & 0 & 0 & \omega_p^2 & 0 \end{bmatrix}^T \tag{4.12}$$

Stability derivatives were not available for a Boeing 767. As a result, the stability derivatives for a Boeing 747 were used to represent a large transport aircraft. [67] Using the B-747 stability derivatives and the parameter values given in Table 4.1, the numerical values used for the linear plant and input matrices were

$$A = \begin{bmatrix} 0 & 221.3 & 0 & 0 & 0 & 0 \\ 0 & -0.4802 & 0.4728 & 0.001269 & 0.06079 & 0 \\ 0 & 0 & 0 & 0 & 1 & 0 \\ 0 & -11.55 & -20.58 & -0.04551 & 0 & 9.927 \\ 0 & 0 & -0.25 & 0 & -0.7 & 0 \\ 0 & 0 & 0 & 0 & 0 & -0.5 \end{bmatrix} \tag{4.13}$$

and

$$B = \begin{bmatrix} 0 & 0 & 0 & 0 & 0 & 0.5 \\ 0 & 0 & 0 & 0 & 0.25 & 0 \end{bmatrix}^T \tag{4.14}$$

The characteristic equation for this system is

$$\Delta_{il}(\lambda) = \lambda\left(\lambda^2 + 0.7\lambda + 0.25\right)(\lambda + 0.5)(\lambda + 0.08235)(\lambda + 0.4434) \tag{4.15}$$

with eigenvalues

$$\lambda_{il} = \{0, -0.35 \pm 0.3571i, -0.5, -0.08235, -0.4434\} \tag{4.16}$$

Table 4.1: Summary of Transport Aircraft Model Parameters.

Parameter	Value	
V_o	221 ft/sec	(or 130 kts)
γ_o	-0.05236 radians	(or -3^o)
m	17530 slugs	(564,000 lbs weight)
T_o	83,900 lbs	
T_{max}	174,000 lbs	
τ_e	2 seconds	
ω_p	0.5 radians/sec	
η_p	0.7	

The zero eigenvalue is from the glide slope kinematics. The complex pair of eigenvalues are from the desired pitch dynamics. And the eigenvalue of -0.5 is from the engine dynamics. The additional pair of real eigenvalues are approximately the numerator zeros from the pitch transfer function of the open-loop aircraft dynamics. [65, 68]

One method of categorizing an aircraft's dynamic response characteristics is whether it operates on the front side or back side of the thrust required curve. MIL-STD-1797A defines an aircraft as operating on the front side if $\frac{\partial \gamma}{\partial u}$ is negative at the trim flight condition. An aircraft is operating on the back side if $\frac{\partial \gamma}{\partial u}$ is positive. [65] This derivative can be estimated from the linearized equation of motion along the velocity axis in equation (4.1). For the unforced response of the aircraft near the trim condition of steady, straight, symmetric, flight

$$\begin{aligned} \dot{V} &= 0 \\ \Delta\theta &= \Delta T = 0 \end{aligned} \tag{4.17}$$

From the remaining terms in the $\dot{V}$ equation (4.1), the derivative $\frac{\partial \gamma}{\partial u}$ is

$$\left(\frac{\partial \gamma}{\partial u}\right)_{V=V_o} \approx \frac{\Delta \gamma}{\Delta V} = \frac{T_V - D_V}{mg\cos\gamma_o - D_\alpha} \tag{4.18}$$

The linearized Boeing 747 model for approach conditions used in (4.13) yields

$$\left(\frac{\partial \gamma}{\partial u}\right)_{V=V_o} \approx -0.134^o/KTAS \tag{4.19}$$

Because $\frac{\partial \gamma}{\partial u}$ is negative, the B-747 model is operating on the front side of the thrust required curve during approach, like most jet transport aircraft.

4.2.2 Acquisition Control Law

The acquisition (outer loop) control law is assumed to be a relay control, generating discontinuous pitch and thrust commands. Since it is assumed that the pilot is attempting to perform a minimum time solution, the form of the control inputs are a "bang-bang" formulation where each individual control is always commanded to its maximum allowable limit. The magnitudes of the pitch inputs are based upon the various sources of pilot training literature that are summarized in Table 4.2. As representative values, nose up commands of $+3^o$ and nose down commands of -2^o were chosen to reflective the tendencies of pilot to use greater nose up pitch authority than nose down when operating close to the ground. The magnitude of the thrust commands were based on thrust settings that achieve vertical velocities of 0 feet per minute (+12%) and -1100 feet per minute (-12%) for the aircraft model being employed. These values are representative of a pilot's preference to at most level off during an approach and to not exceed ground proximity warning system (GPWS) limits.

The acquisition control law can then be expressed as

$$\begin{aligned} (\Delta\theta)_c &= \begin{cases} +3^o & \text{for } \sigma_\theta < 0 \\ -2^o & \text{for } \sigma_\theta > 0 \end{cases} \\ \left(\frac{\Delta T}{T_{max}}\right)_c &= \begin{cases} +12\% & \text{for } \sigma_T < 0 \\ -12\% & \text{for } \sigma_T > 0 \end{cases} \end{aligned} \tag{4.20}$$

Table 4.2: Pilot Training Rules for Pitch Commands during Approach.

Source	Purpose	Pitch Inputs	
US Air Force [50]	ILS	$+2^o$	-2^o
US Air Force [50]	Climb/Descent Level Off	$+3.7^o$	-2.1^o
	$\left(\Delta\theta = \frac{\text{vvi}}{\text{Mach}*1000}\right)$	(0 fpm)	(-1100 fpm)
FAA [51]	ILS	$+2.5^o$	-2.5^o
NAV CANADA [62]	Visual Landing	$+2^o$	-2^o
Delta [69]	Definition Unstable Approach	$+5^o$	-5^o

where σ_θ and σ_T are the switching variables defined by

$$\begin{bmatrix} \sigma_\theta \\ \sigma_T \end{bmatrix} = Sx \tag{4.21}$$

The switching surface S is the mathematical representation of the pilot's acquisition strategy.

As discussed in Chapter 3, an additional part of a human operator model is the operator's predictive capabilities to alleviate the reaction time delay and estimating capabilities to overcome imprecise observations. Although deficiencies in these capabilities can play a significant role in tracking tasks, it is assumed that they are not as significant in an acquisition task. This assumption allows for a clearer comparison of various acquisition strategies.

Although it is assumed that the pilot can counteract the reaction time delay, no amount of predictive capability can be used to alleviate the decision time delay encountered when the pilot first breaks out of the clouds. This delay is the amount of time required for the pilot to reorient from the incorrect instrument navigation cues to the correct visual environment and to decide on a course of action. A study conducted by the US Air Force employing multi-crew, transport aircraft in actual weather concluded that it typically takes a heads down pilot three seconds to transition to the visual flight environment. [70] It was found that lateral guidance cues develop earlier with aim point and flare control developing last.

It has also been generally accepted that pilots make the transition to visual flight cues quicker in a simulator than in actual weather. [56] This result may be due to simulator visual systems that transition from zero visibility to the prescribed flight visibility almost instantaneous at a specified altitude. Whereas, in reality, the flight visibility gradually increases as the clouds gradually thin out. A review of the NAV CANADA simulator data showed that although many pilots reacted faster, a three second decision time delay was representative of the slower pilots response. Therefore, a 3 second delay was used in this study.

4.2.3 Front-Side Landing Strategy

In the VSM, the switching surface S is the mathematical representation of the pilot's acquisition strategy. Heffley explored using pilot training literature to construct switching surfaces for single-input, discrete tasks. These tasks included aircraft flare, heading, altitude, and airspeed changes. [20, 52] Two good references for pilot procedures on these and other tasks are the US Air Force *Flying Operations: Instrument Flight Procedures* [50] and the *FAA Instrument Flying Handbook.* [51] Heffley's approach is adopted for this study and applied to the multi-input visual landing task.

A primary theme in pilot training literature is to describe multi-input tasks as multiple, decoupled single-input tasks and to recommend aircraft attitude commands to achieve the desired task. The pilot is expected to develop more refined control strategies as experience in the aircraft and task is gained. In general, transport aircraft pilots are taught to land an aircraft using a front-side landing technique. A front-side landing technique refers to the dynamics of the aircraft on the front side of the power curve where pitch attitude can be used for flight path control and power for airspeed control. A back-side technique refers to the unstable dynamics of the back side of the power curve where thrust must be used for flight path control and pitch for airspeed control. [65]

A simple mathematical representation of a front-side landing strategy as a decoupled switch-

ing strategy for the control law in equation (4.20) is

$$\begin{aligned} \sigma_\theta &= d \\ \sigma_T &= \Delta V \end{aligned} \tag{4.22}$$

This control law would command a nose-up pitch command for low glide slope deviations, nose-down for high glide slope deviations, increased thrust for slow airspeed deviations, and decreased thrust for fast airspeed deviations.

This strategy represents the simplest front-side control strategy implemented by a beginning pilot. A slight improvement can be made by estimating a lead point for glide slope intercept. Using the kinematic relation given in equation (4.7), a lead term ($k_{\dot{d}}$) can be introduced by adding a flight path error to the pitch strategy to yield

$$\begin{aligned} \sigma_\theta &= d + k_{\dot{d}}\dot{d} = d + k_{\dot{d}}\frac{V_o}{\cos\gamma_o}\Delta\gamma \\ \sigma_T &= \Delta V \end{aligned} \tag{4.23}$$

or in terms of the switching surface

$$S_f = \begin{bmatrix} 1 & k_{\dot{d}}\frac{V_o}{\cos\gamma_o} & 0 & 0 & 0 & 0 \\ 0 & 0 & 0 & 1 & 0 & 0 \end{bmatrix} \tag{4.24}$$

Since various aircraft have substantially different pitch dynamics, a specific value for $k_{\dot{d}}$ is difficult to ascertain from the general pilot training literature. Its value is determined from experience in the aircraft being flown. One method to approximate this lead term is to examine the method pilots are taught to level off from climbs and descents. Pilots are taught to calculate a lead point for leveling off based on 10% of the indicated vertical velocity in feet per minute (fpm). [50, 51, 52] So, for a -700 fpm descent, the pilot should begin commanding a level off 70 feet above the target altitude. Taking into account the conversion from feet per minute to feet per second, this altitude can be expressed as

$$h_l = -6\,\dot{h} \tag{4.25}$$

Using this value as a maximum, a reasonable range for the glide slope lead term of $0 \leq k_{\dot{d}} \leq 6$ seconds was used for this study.

In addition, since the front-side strategy uses thrust for airspeed control, it was not considered reasonable to use the large thrust setting prescribed by equation (4.20) for small airspeed deviations. Therefore, a one-half knot indifference threshold was used for the thrust relay control in equation (4.20) for the front-side strategy only. This threshold significantly reduced thrust command chatter to generate more realistic commands.

4.2.4 Flare Control Law

In addition to the limited time of flight for the visual landing task (typically 15 to 25 seconds), another difficulty in analyzing the pilot's response is ill-defined the terminal conditions of the task. At some point, the acquisition task must end, and the landing flare must begin. A pilot typically makes a judgement of when and how large a flare to perform based on the aircraft's energy state (airspeed, altitude, flight path, and their respective rates of change) and location relative to the runway. Several different pilot flare models have been proposed by various researchers. A good summary can be found in a report by Heffley. [56] In general, the structure preferred by Heffley is a precognitive or discrete maneuver starting at a flare initiation altitude. [20, 52, 56]

A very simple flare model is used based on pilot training literature. Using the level off rule expressed in (4.25), the flare initiation altitude can be approximated by

$$h_{\text{flare}} = -6\,\dot{h} \tag{4.26}$$

It is interesting to note that although Heffley defined a more detailed flare model, using the nominal landing flare data in [56] gives a flare initiation relation of $h_{\text{flare}} \approx -5.7\,\dot{h}$.

For a typical large transport aircraft, the pilot attempts to achieve a 4^o to 5^o pitch attitude and use the throttles as needed during roundout and ground effect. [56] For the aircraft dynamics used for this study (that lacked any ground effects) the following flare commands

were found to be fairly robust and were used for a flare command

$$\begin{aligned} (\Delta\theta)_{\text{flare}} &= +4^o \\ \left(\frac{\Delta T}{T_{max}}\right)_{\text{flare}} &= 0\% \end{aligned} \tag{4.27}$$

4.3 Simulation and Analysis

To simulate the response of these control strategies, the linear system described by equations (4.10), (4.13), and (4.14) with the pilot control law described by equations (4.20) and (4.23) were numerically integrated using a fourth-order Runge-Kutta integration scheme with a time step of 0.05 seconds. During the integration, the relay control inputs were held constant for the entire integration time step. The initial conditions of interest were the "short" longitudinal initial condition due to a -15m vertical navigation error and the "long" longitudinal initial condition due to a +15m vertical navigation error.

Figure 4.4 illustrates the state variable and control trajectories employing a front-side pilot strategy with no glide slope deviation lead term ($k_{\dot{d}} = 0$ seconds) for the short initial condition of 4755 feet from the glide slope intercept point. The x's are the NAV CANADA data set. The red (straight) line in the top (altitude verses distance) graph is the desired -3^o glide slope. The blue lines tagged with squares are the simulated state trajectories using the front-side strategy (4.23) with no lead. The green step inputs in the bottom two ($\Delta\theta$ and $\frac{\Delta T}{T_{max}}$ verses distance) graphs are the discontinuous control inputs. In this simulation, the flare maneuver is begun at approximately 900 feet from the desired glide slope runway intercept point or 100 feet past the runway threshold. In general, this simulation does a fairly good job of reproducing the trajectories of the NAV CANADA pilots responding late to the glide slope acquisition task and overshooting the desired glide slope.

Figure 4.5 illustrates the state variable and control trajectories employing a front-side pilot strategy with $k_{\dot{d}} = 6$ seconds. The blue lines tagged with diamonds are the simulated state trajectories using the front-side strategy (4.23) with lead. In this simulation, the flare

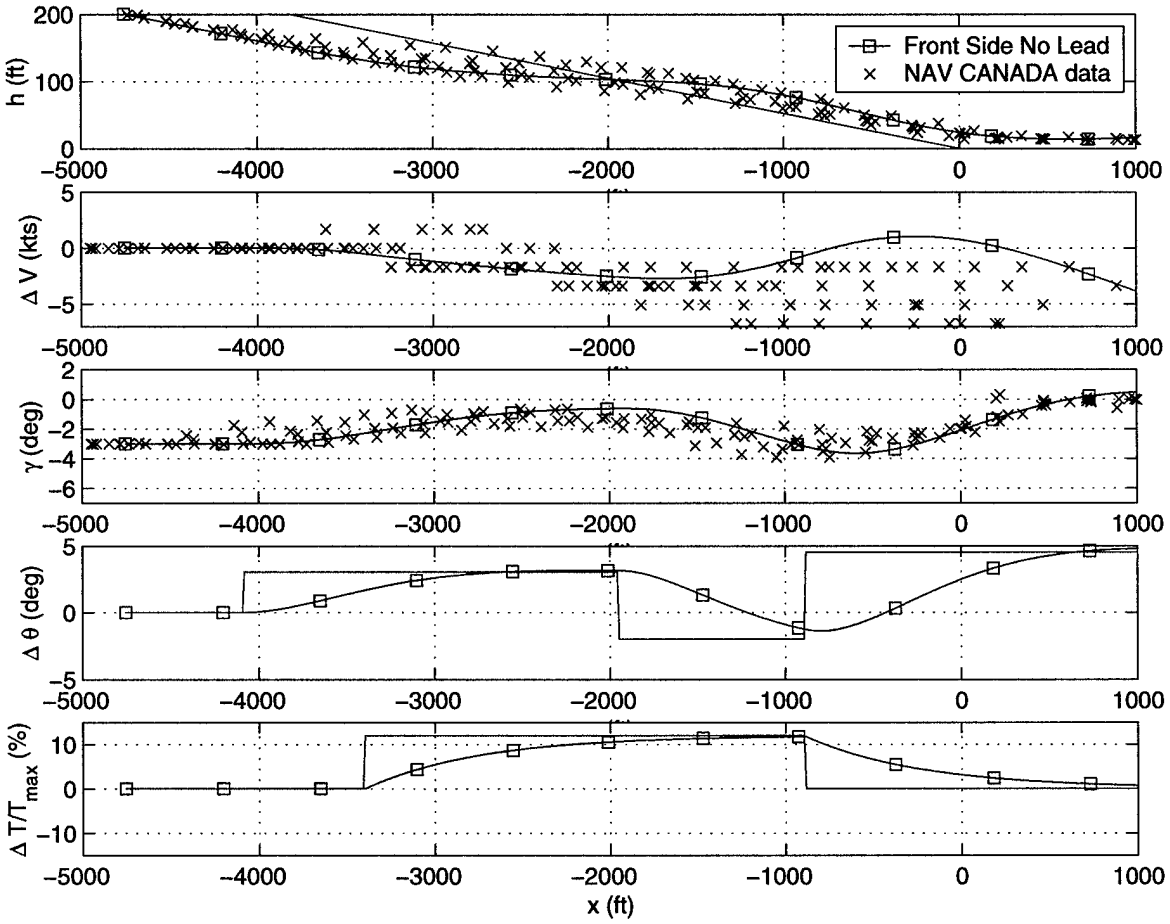

Figure 4.4: Short Initial Condition Response with No Lead

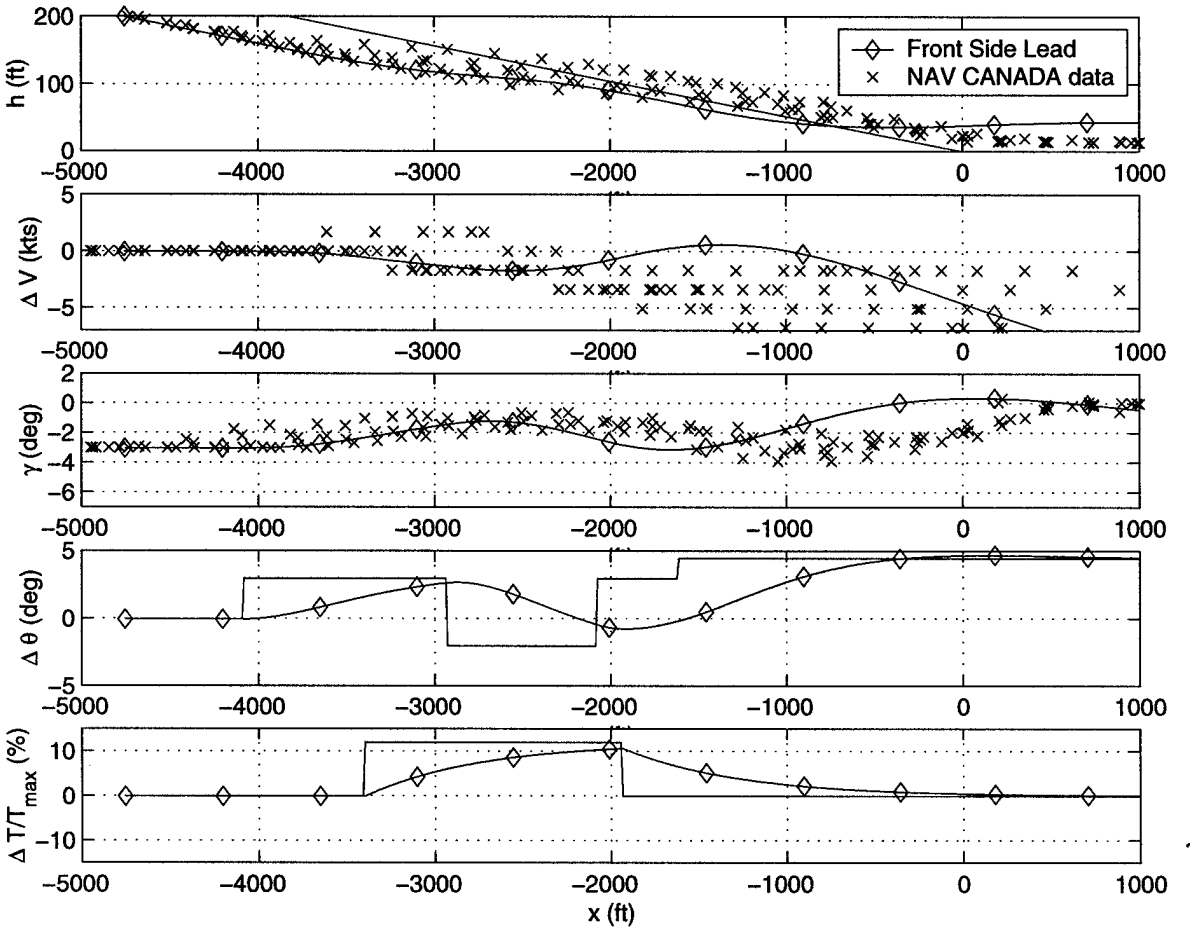

Figure 4.5: Short Initial Condition Response with Lead

maneuver is begun at approximately 1600 feet from the desired glide slope runway intercept point or 800 feet past the runway threshold and at an altitude of approximately 80 feet. This values of lead brackets the lower trajectories in Figure 4.5. The deviation of the VSM simulated trajectory and the NAV CANADA trajectories within 900 feet are due to the flare model and not the acquisition strategy.

Figure 4.6 summarizes the trajectory response of the previous two cases. Except for some variation in decision time delay in the NAV CANADA data set, the model response is representative of the range of responses of the slower reacting pilots in the data set. The

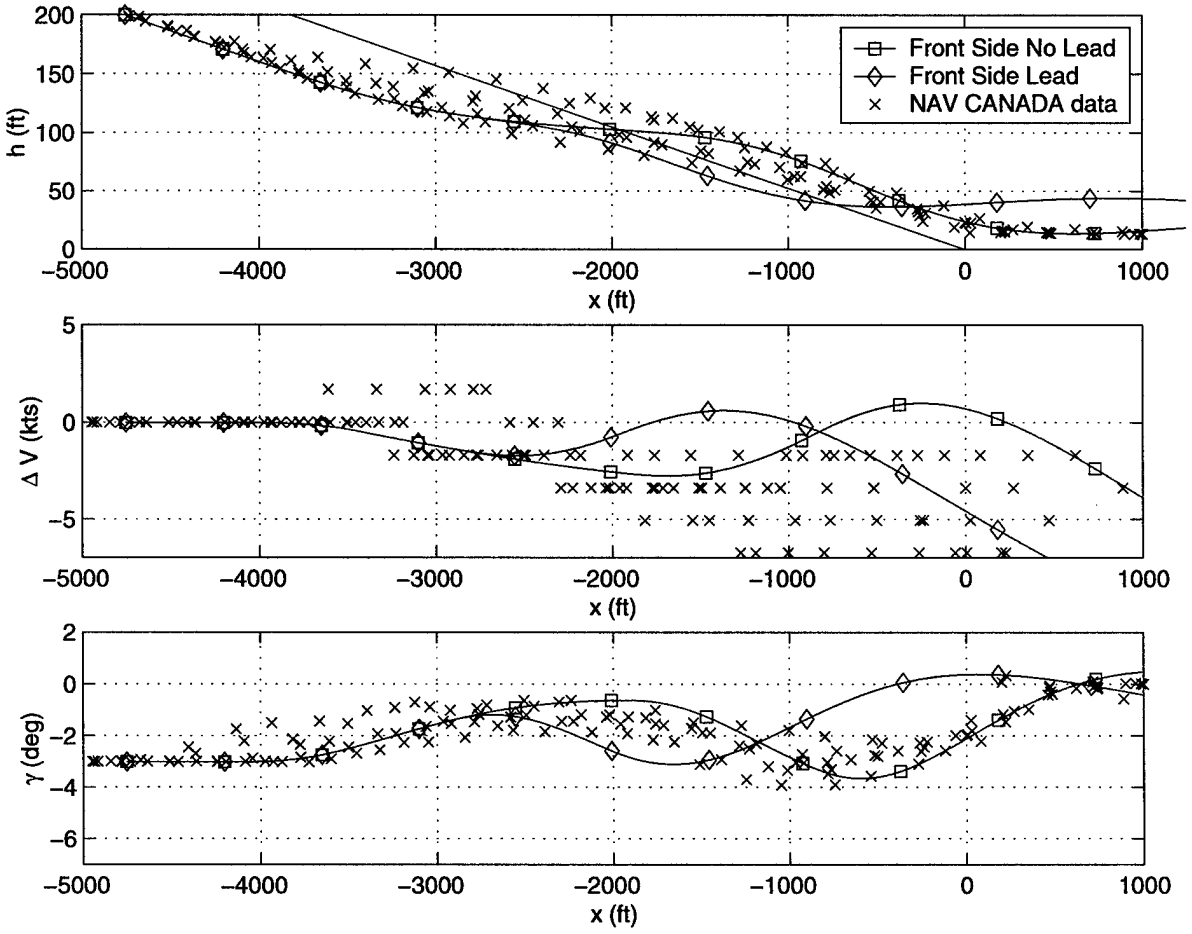

Figure 4.6: Summary Short Initial Condition Response

most significant difference is in the airspeed and flight path of the model and the data set within 1000 feet of the glide slope intercept point. Since this point is over the runway threshold and after the model's flare initiation, this characteristic is due to incomplete flare and ground effect modeling.

In general, varying the lead term ($k_{\dot{d}}$) over the range from 0 to 6 seconds primarily affected the glide slope overshoot characteristics of the closed-loop trajectories and had a negligible effect on the cross over frequency of the closed-loop system. Overall, this range of lead terms appear representative of the varied task performance of the pilots under study.

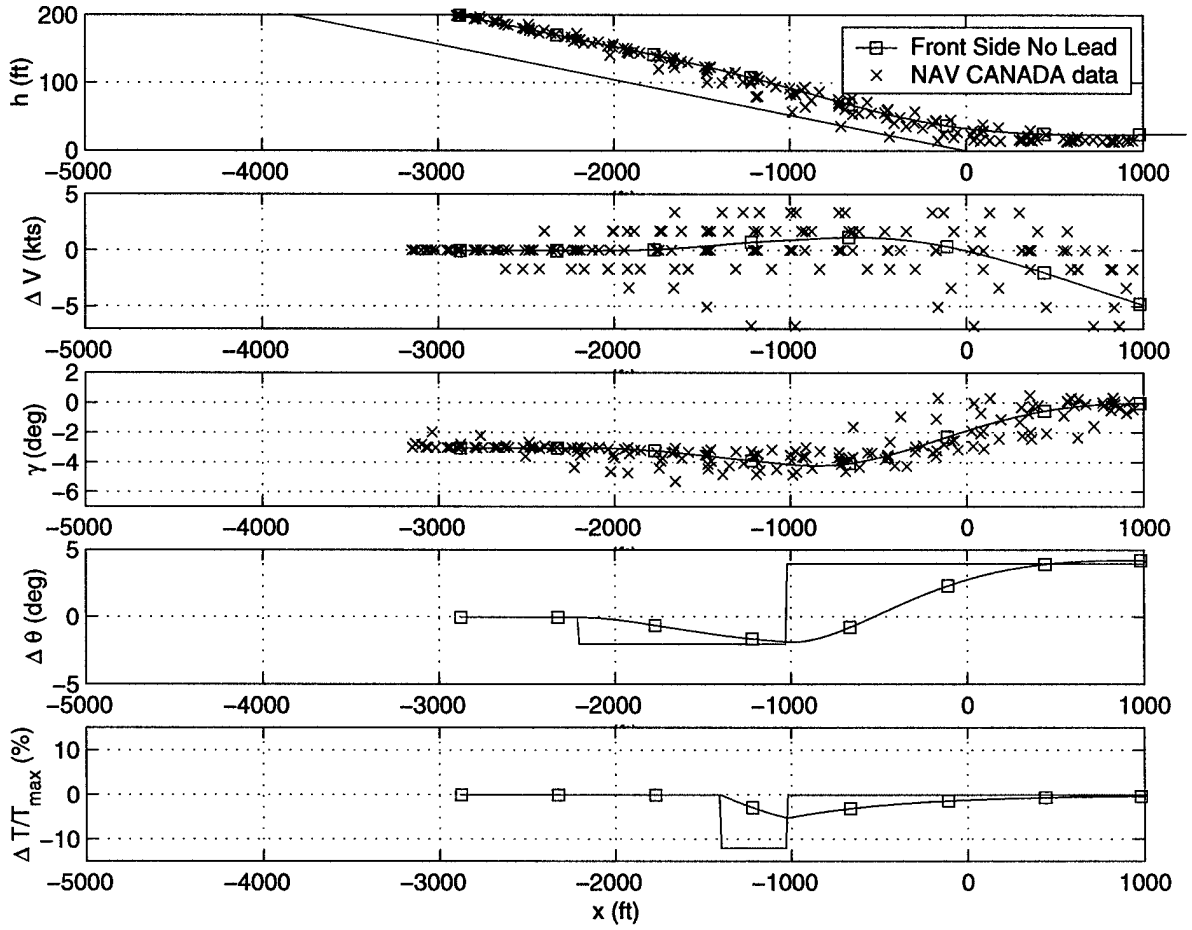

Figure 4.7: Long Initial Condition Response with No Lead

A similar analysis was conducted for the long initial condition of 2877 feet from the glide slope intercept point due to a vertical navigation error of +15 meters. Figure 4.7 illustrates the closed-loop system response of the front-side strategy with no glide slope deviation lead term ($k_d = 0$ seconds). After the three second decision time delay and the initial control inputs, the control activity is minimal. Two degrees nose down pitch attitude is commanded in an attempt to acquire the desired glide slope. Then at approximately 1000 feet from the glide slope runway intercept point, the flare is initiated.

Figure 4.8 illustrates the closed-loop system response of the front-side strategy with a glide

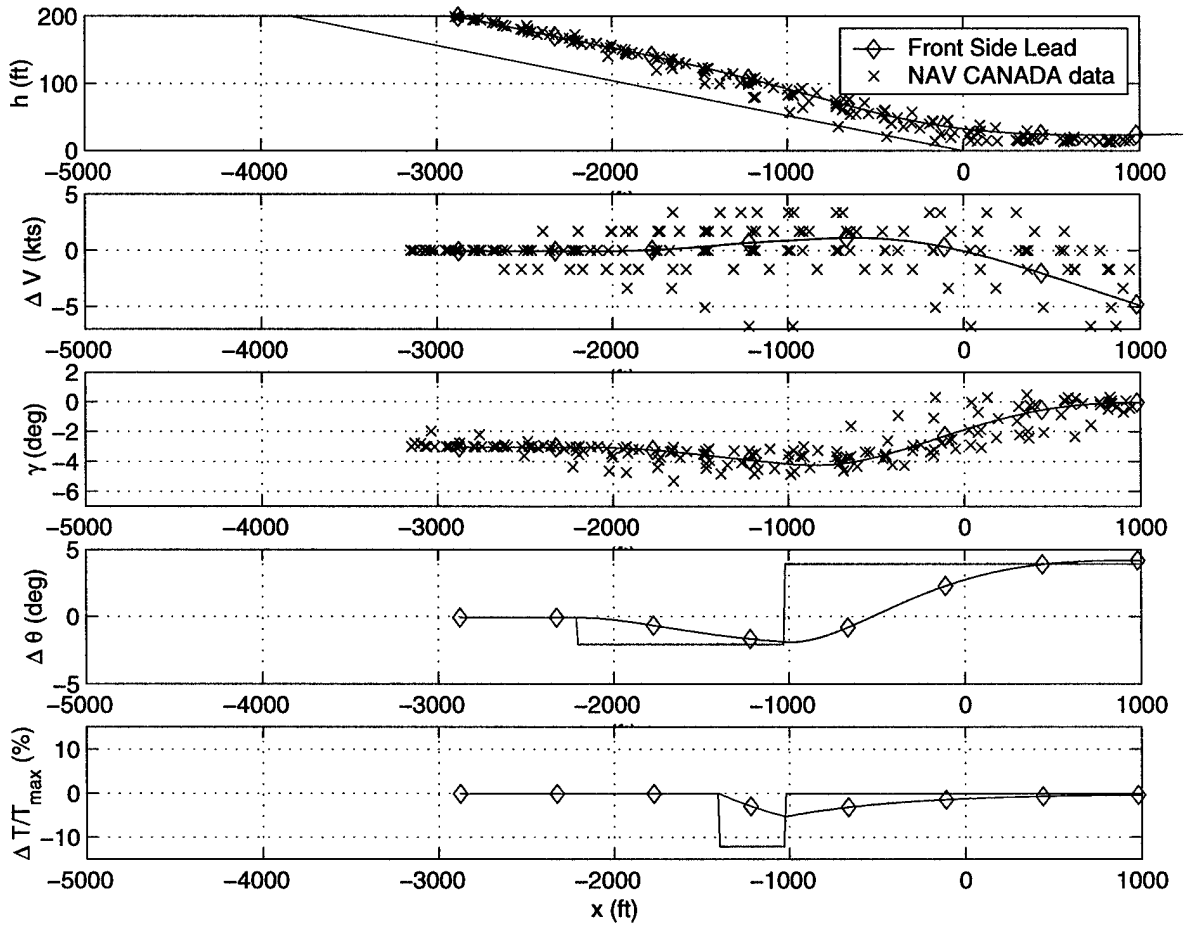

Figure 4.8: Long Initial Condition Response with Lead

slope deviation lead term of $k_{\dot{d}} = 6$ seconds. Figure 4.9 summarizes the trajectory response of the previous two of no lead and $k_{\dot{d}} = 6$ seconds. The two trajectories are nearly identical. Although the data set shows significantly more scatter than the simulation results, the simulation is successful in reproducing the trajectory of a typical if not slightly less aggressive pilot. It also highlights that for the long initial condition there is insufficient time or space to generate much of a trajectory response. As a result, the system response is dominated by aircraft performance, namely the maximum safe sink rate of approximately -1100 feet per minute.

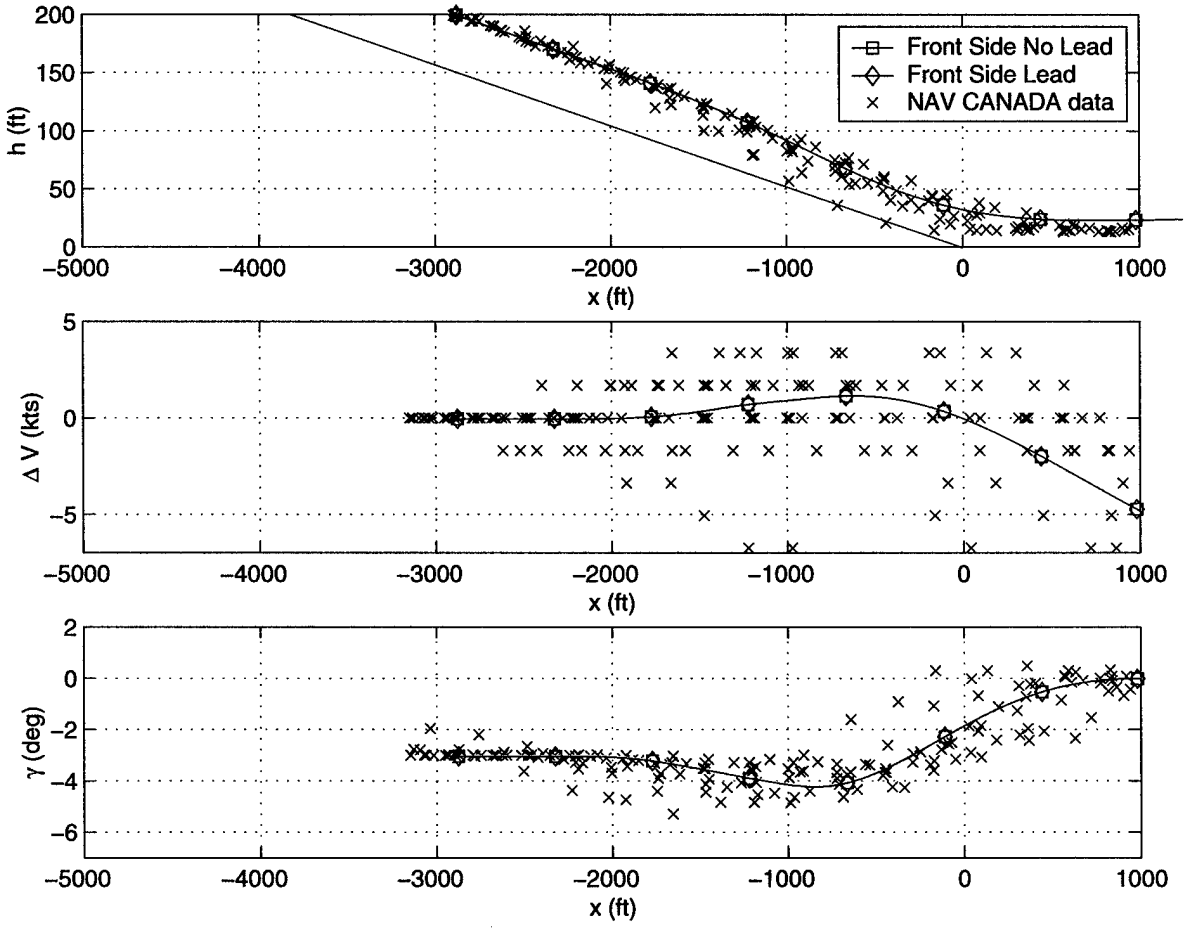

Figure 4.9: Summary Short Initial Condition Response

Applying the VSM methodology with a pilot strategy based on a literal interpretation of pilot training guidelines is successful in reproducing the trajectory responses observed in the NAV CANADA study. However, since no pilot command inputs and aircraft attitude measurements are in the data set, it can not be determined if the pilots are using a relay control law like the one in the model.

Chapter 5

Pilot Landing Strategies

In Chapter 4, the performance of a front-side landing strategy applied to an aircraft operating on the front side of the power curve was successfully compared to the NAV CANADA simulator data set. A back-side landing strategy could just as easily be implemented in the VSM. In the pilot community, the benefits of these two simple pilot training strategies are a continuing source of debate. In 1944, Langewiesche devoted a significant portion of his classic flying book *Stick and Rudder* to this debate and to the virtues of back-side flying techniques. [71] The debate is whether pilots should be taught to land an aircraft by front-side or back-side techniques. Conventional wisdom is that both front-side and back-side landing strategies can be employed on an aircraft operating on the front side of the power curve. But only back-side landing techniques are successful in controlling an aircraft operating on the back side of the power curve. [64]

This chapter explores this issue by applying both types of landing strategies to both types of aircraft dynamics. Since a representative front-side aircraft and landing strategy was developed in Chapter 4, this chapter begins by defining a suitable back-side aircraft dynamic model and landing strategy for the comparison. Next, each type of strategy is applied to each type of aircraft. This comparison confirms the conventional wisdom.

5.1 Model Details

Flying an aircraft at a speed on the front side of the power curve provides for stable open-loop dynamics in all modes. When an aircraft flies on the back side of the power curve it is typically done to achieve the lowest safe approach speed. However, at this speed, the open-loop aircraft's speed dynamics are unstable. The next example explores the effect of this unstable, open-loop plant on the pilot's acquisition strategy for the visual landing task.

5.1.1 Pilot Augmented Dynamics

The physical method for making an aircraft operate on the back side of the thrust required curve is to slow its speed. However, since a slower trim airspeed would allow more time to implement course corrections, it does not allow for an equal comparison of pilot control strategies for front-side and back-side aircraft dynamics. Instead, the stability derivative D_α is modified to generate the back-side aircraft dynamics at the same trim airspeed, angle of attack, lift, drag, and thrust. A value of

$$\left(\frac{\partial \gamma}{\partial u}\right)_{V=V_o} = 0.03^o/KTAS \tag{5.1}$$

puts the aircraft on the back side while maintaining the value of $\frac{\partial \gamma}{\partial u}$ within the bounds for Level 1 flying qualities as defined by MIL-STD-1797A. [65] Since

$$\left(\frac{\partial \gamma}{\partial u}\right)_{V=V_o} \approx \frac{T_V - D_V}{mg\cos\gamma_o - D_\alpha} \tag{5.2}$$

using (5.1) and the nominal values of T_V, D_V, m, V_o, and γ_o for the B-747 approach conditions gives a value of $D_\alpha = 1.47 \times 10^6$ lbs to model the desired back-side dynamic characteristics (verses the nominal front side value of $D_\alpha = 0.360 \times 10^6$ lbs). [67]

The basic functional form of the inner loop dynamics are the same as the previous chapter. The only difference is that $D_\alpha = 1.47 \times 10^6$ lbs. However, note this model no longer represents a B-747 but the dynamics of some fictional back side aircraft operating at the same trim

flight condition as the B-747 with the same inertial properties and thrust to weight as the B-747 model. The inner loop plant matrix is now

$$A = \begin{bmatrix} 0 & 221.3 & 0 & 0 & 0 & 0 \\ 0 & -0.4802 & 0.4728 & 0.001269 & 0.06079 & 0 \\ 0 & 0 & 0 & 0 & 1 & 0 \\ 0 & 51.43 & -83.60 & -0.04551 & 0 & 9.927 \\ 0 & 0 & -0.25 & 0 & -0.7 & 0 \\ 0 & 0 & 0 & 0 & 0 & -0.5 \end{bmatrix} \tag{5.3}$$

and the input matrix B remains the same as the front-side aircraft example of the previous chapter, see equation (4.14). The characteristic equation for this system is

$$\Delta_{il}(\lambda) = \lambda\left(\lambda^2 + 0.7\lambda + 0.25\right)(\lambda + 0.5)(\lambda - 0.0726)(\lambda + 0.5983) \tag{5.4}$$

with eigenvalues

$$\lambda_{il} = \{0, -0.35 \pm 0.3571i, -0.5, +0.0726, -0.5983\} \tag{5.5}$$

The most noticeable difference between these eigenvalues and the ones for the front-side aircraft (4.16) is the positive real roots at 0.0726. This root is associated with the unstable speed dynamics of an aircraft operating on the back side of the power curve.

5.1.2 Acquisition Control Law

The same outer loop control structure as in the transport aircraft example is used for the back-side aircraft, see equations (4.20) and (4.21).

5.1.3 Back-Side Landing Strategy

A simple mathematical representation of a back-side landing strategy as a decoupled switching strategy for the control law in equation (4.20) is

$$\begin{aligned} \sigma_\theta &= -\Delta V \\ \sigma_T &= d + k_d \frac{V_o}{\cos\gamma_o} \Delta\gamma \end{aligned} \tag{5.6}$$

A back-side switching surface (S_b) in terms of the state variables in equation (4.8) is

$$S_b = \begin{bmatrix} 0 & 0 & 0 & -1 & 0 & 0 \\ 1 & k_d \frac{V_o}{\cos\gamma_o} & 0 & 0 & 0 & 0 \end{bmatrix} \tag{5.7}$$

This control law would command a nose-up pitch command for fast airspeed deviations, nose-down for slow airspeed deviations, increased thrust for a low glide slope deviations, and decreased thrust for a high glide slope deviations.

5.1.4 Flare Control Law

A similar flare command is used with the same flare initiation altitude (4.26) except a thrust setting of +12% instead of 0% is used.

$$\begin{aligned} (\Delta\theta)_{\text{flare}} &= +4^o \\ \left(\frac{\Delta T}{T_{max}}\right)_{\text{flare}} &= 12\% \end{aligned} \tag{5.8}$$

5.2 Simulation and Analysis

To reduce the number of comparisons, both the front-side (4.23) and back-side (5.6) landing strategies are applied with a glide slope lead term of $k_d = 1$ second. Other values for the glide lead constant were explored, and the results for $k_d = 1$ second are representative of the trends in the other cases. Next each strategy is applied to each type of aircraft dynamic model for the long and short initial conditions studied in Chapter 4.

5.2.1 Front-Side Aircraft Dynamics

To simulate the front-side aircraft dynamics, the linear system described by equations (4.10), (4.13), and (4.14) was integrated with the pilot control law described by equation (4.20). Figure 5.1 illustrates the trajectory response of the closed-loop pilot/vehicle system for the short initial condition. The lines tagged with blue squares represent the system response using a front-side strategy, equations (4.20) and (4.23). The lines tagged with triangles squares represent the response using a back-side strategy, equations (4.20) and (5.6). Although the back-side strategy regulates the aircraft's velocity better than the front-side strategy, the two have similar trajectory responses.

Figure 5.2 illustrates the pitch response and command of the two strategies for the short initial condition. The upper graph is the aircraft's pitch attitude. The line tagged with squares is the response of the front-side strategy. The line tagged with triangles is the response of the back-side strategy. The middle graph (tagged with squares) is the pitch attitude command by the front-side strategy. The lower graph (tagged with triangles) is the pitch attitude command by the back side strategy. The back-side pitch commands are more active since they are performing essentially the regulating task of maintaining airspeed; whereas, the front-side pitch commands are less active performing the glide slope acquisition task. The front-side strategy initiates the flare maneuver at approximately 1100 feet from the desired glide slope runway intercept point. The back side strategy begins a flare at approximately 400 feet.

Figure 5.3 illustrates the thrust response and commands of the two strategies for the short initial condition. More differences between the two strategies input behavior are evident in this figure. Since in the back-side strategy the thrust is responsible for the acquisition of the glide slope, the back side thrust commands are much more active and aggressive than the front-side thrust commands. In the front-side strategy, the thrust is responsible only for regulating the aircraft's velocity. This thrust control of the glide path is also the reason the back-side strategy requires more thrust to flare the aircraft.

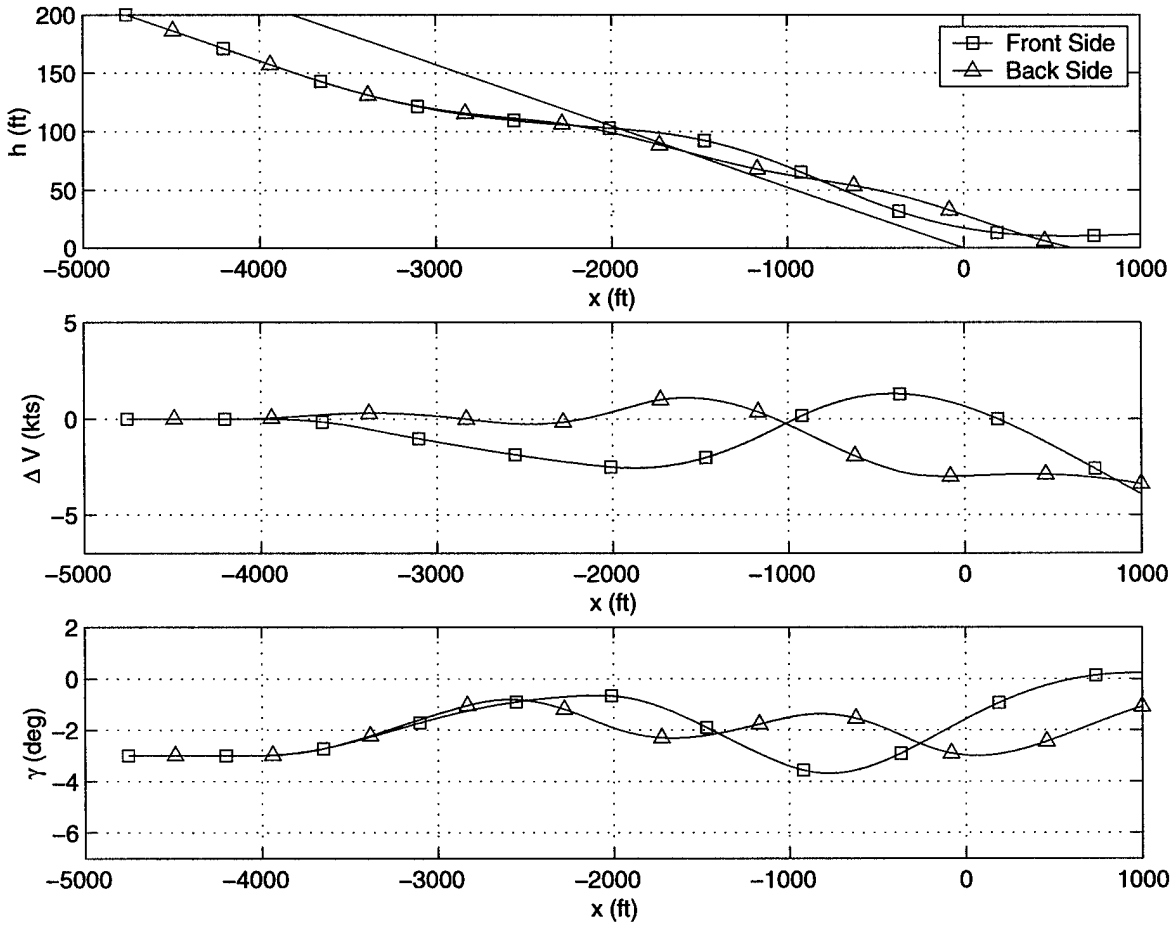

Figure 5.1: Front-Side Aircraft Response for Short Initial Condition

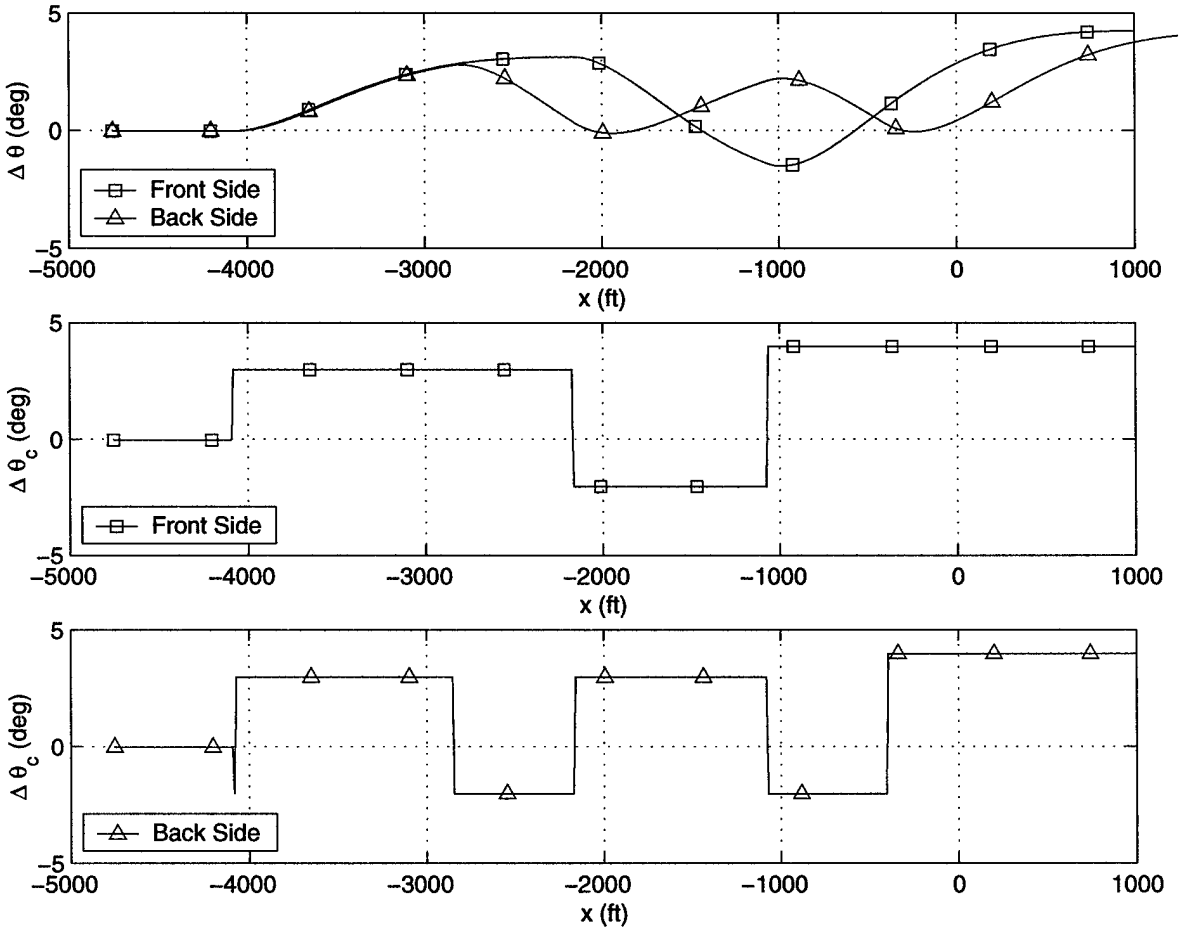

Figure 5.2: Front-Side-Aircraft Pitch Input for Short Initial Condition

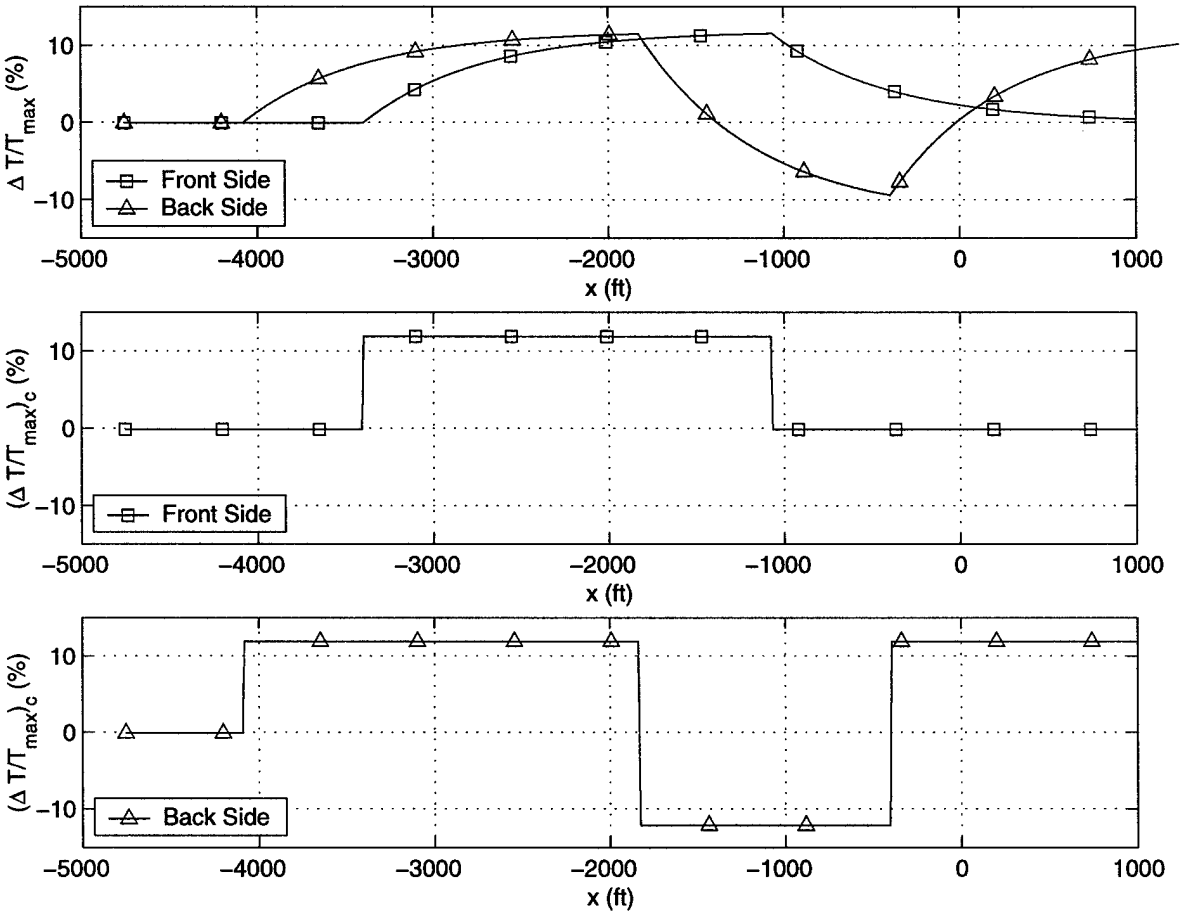

Figure 5.3: Front-Side-Aircraft Thrust Input for Short Initial Condition

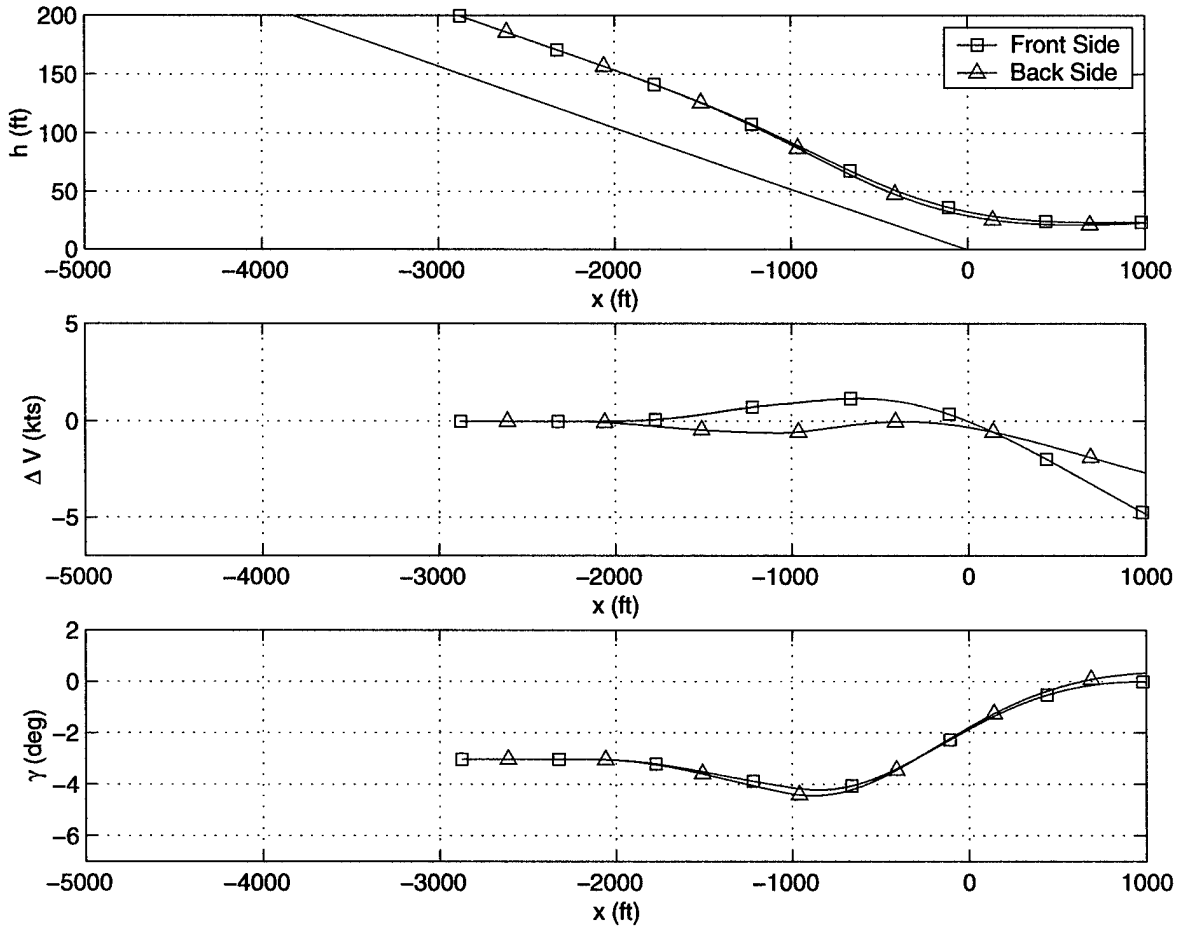

Figure 5.4: Front-Side-Aircraft Response for Long Initial Condition

Figure 5.4 illustrates the trajectory response of the closed-loop pilot/vehicle system for the long initial condition. The system responses of the front-side and back-side strategies are very similar. The pitch commands for the two strategies are also nearly identical with both beginning a flare at approximately 1000 feet from the desired glide slope runway intercept point. As for the short initial condition, the thrust inputs for the back-side strategy are more aggressive than the front side; however, due to the slow aircraft dynamics, instead of increasing the glide slope capture, it primarily generates a need for greater thrust in the flare. These responses illustrate that the long initial condition response of the closed-loop system is primarily performance limited. A difference in strategy has very little effect on the trajectory response.

Even though the two strategies employ different control inputs, the trajectory response of both for the front-side aircraft is similar. This was a common characteristic observed for various other initial conditions and values for the glide slope lead term ($k_{\dot{d}}$) explored. From a trajectory stand point, both strategies would appear to be successful in maneuvering an aircraft on the front side of the power curve.

5.2.2 Back-Side Aircraft Dynamics

To simulate the back-side aircraft dynamics, the linear system described by equations (4.10), (5.3), and (4.14) was integrated with the pilot control law described by equations (4.20), (4.23), and (5.6). Figure 5.5 illustrates the trajectory response for this closed-loop pilot/vehicle system for the short initial condition. Unlike the front-side aircraft response (Figure 5.1) this aircraft shows a dramatic difference between in the trajectory response due to the front-side and back-side strategies. The front side strategy is not sufficient to stabilize the airspeed dynamics.

Figures 5.6 and 5.7 illustrate the pitch and thrust commands, respectively, for each strategy. In general the back-side strategy is more aggressive in attempting to stabilize the airspeed dynamics. This result can be seen in the more active pitch commands (Figure 5.6) that the

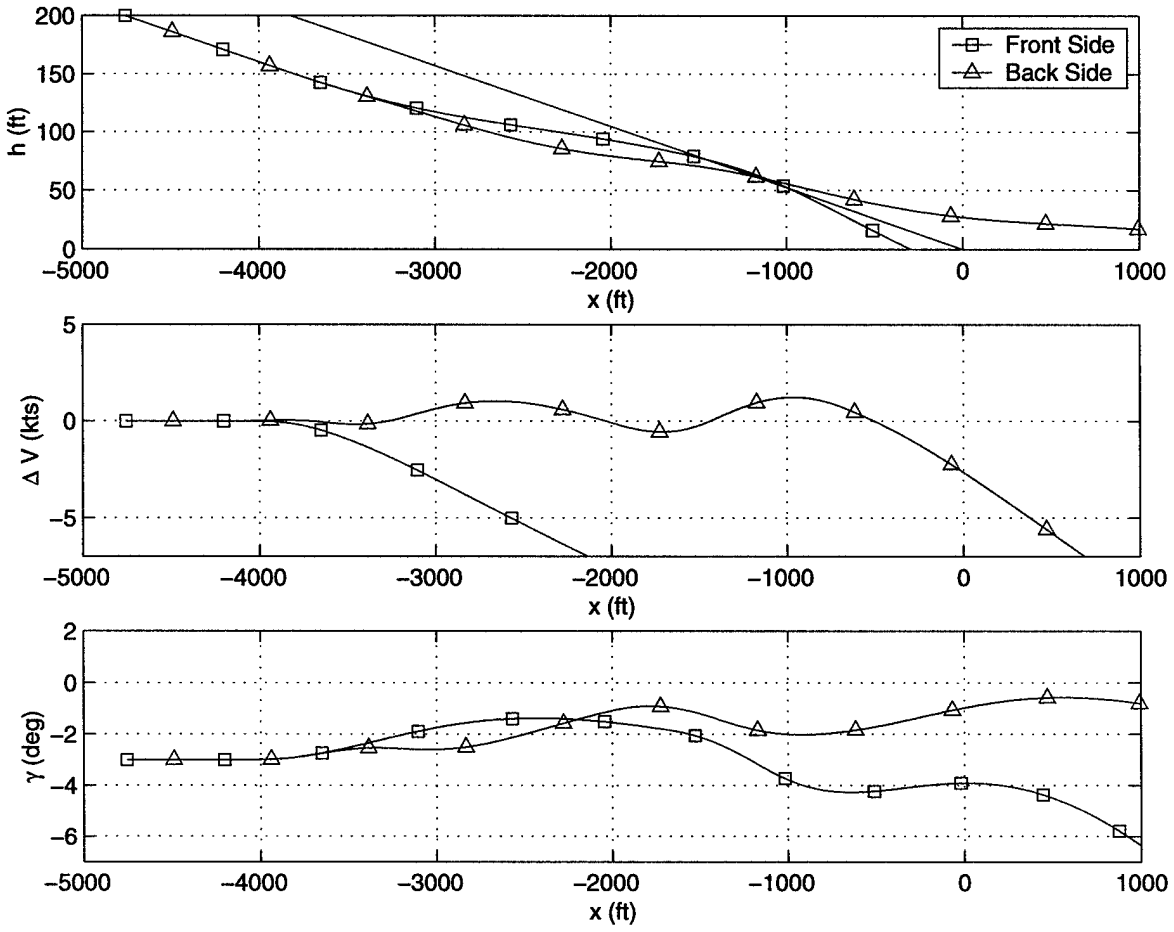

Figure 5.5: Back-Side-Aircraft Response for Short Initial Condition

backside strategy is using to control airspeed, and the earlier application of thrust (Figure 5.7) that the backside strategy is using for glide slope acquisition. Note from Figures 5.6 and 5.7 that the front-side strategy initiates the flare maneuver at approximately 1100 feet from the desired glide slope runway intercept point. Thus the flare initiation is well after the airspeed divergence in Figure 5.5 meaning this unstable behavior is due to the acquisition strategy and not the flare commands. Although greater values of glide slope lead (k_d) improve both strategies performance; in general, the front-side strategy is insufficient to stabilize the airspeed dynamics. Therefore, one can conclude that a back side landing strategy is required to land an aircraft flying on the back side of the power curve.

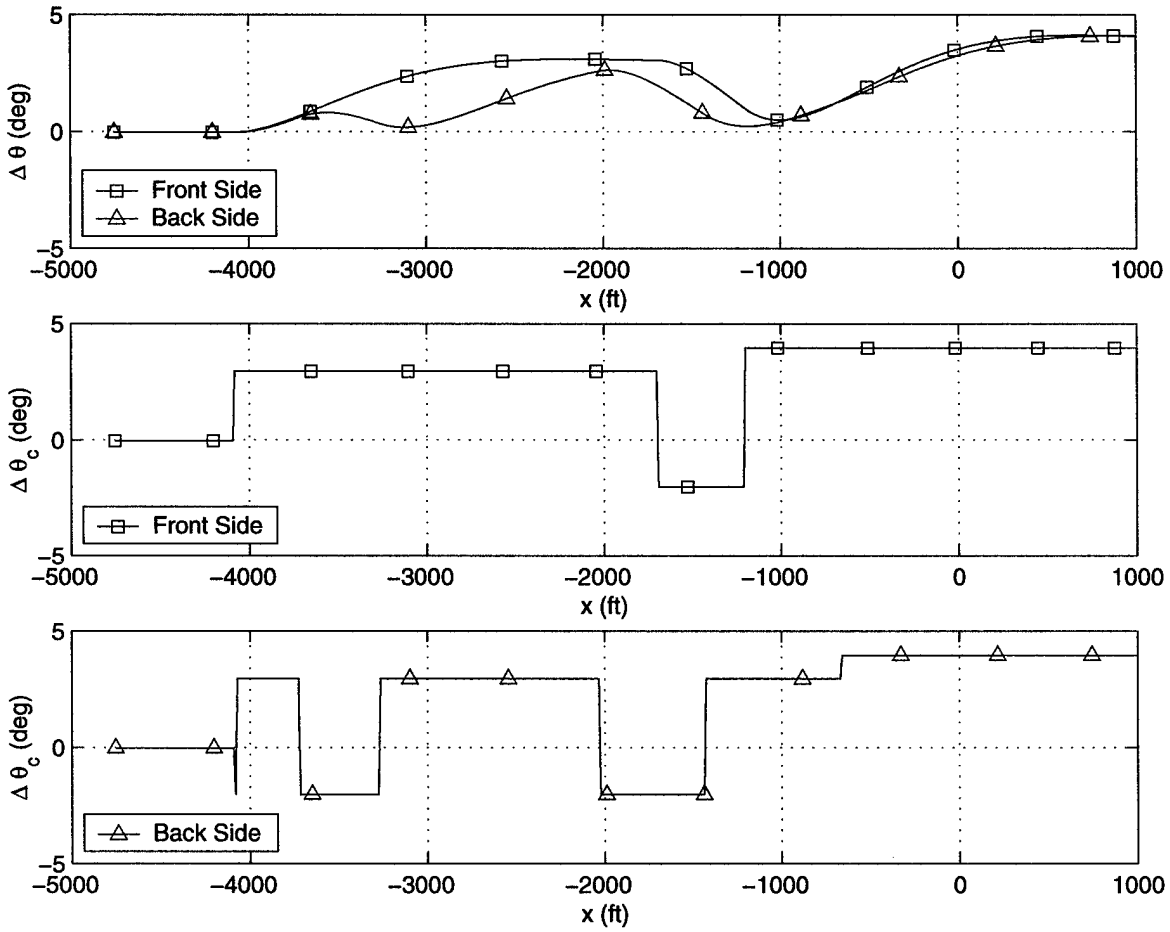

Figure 5.6: Back-Side-Aircraft Pitch Input for Short Initial Condition

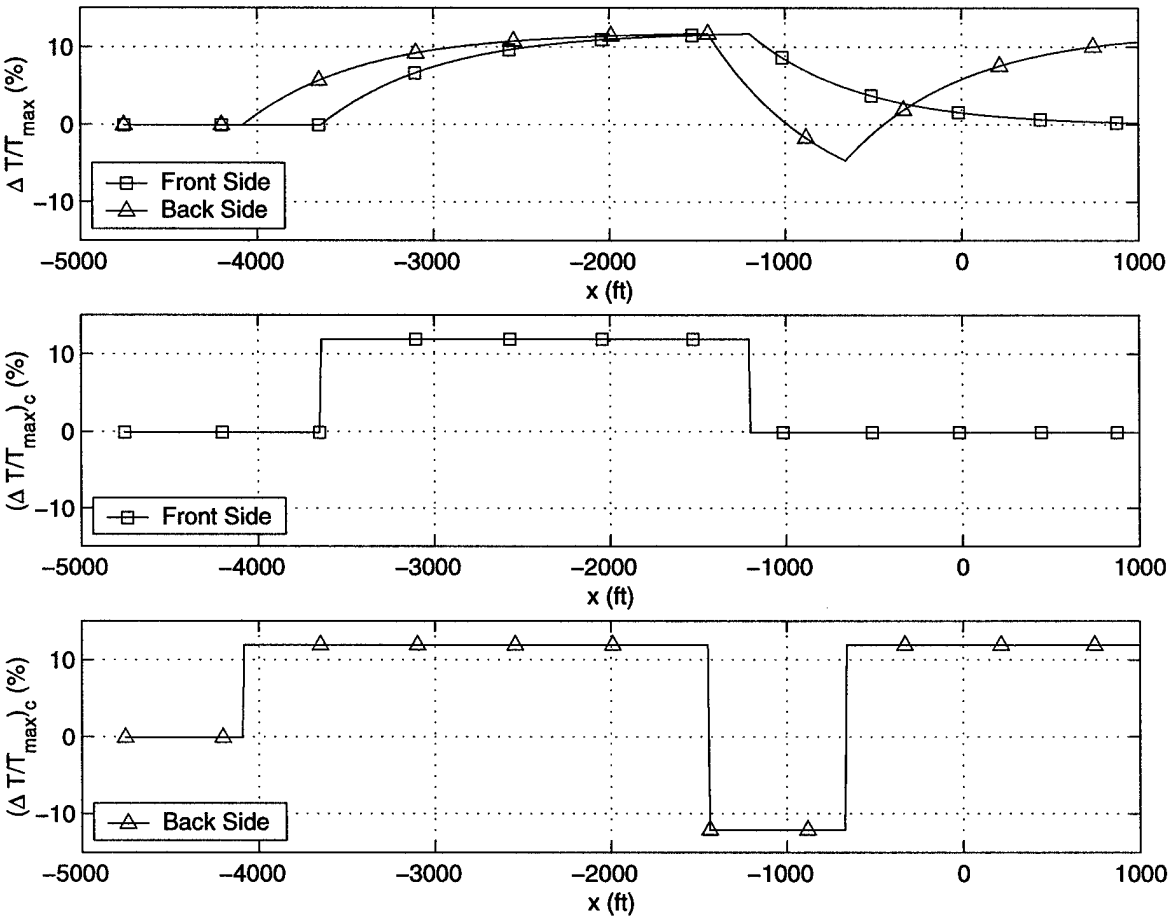

Figure 5.7: Back-Side-Aircraft Thrust Input for Short Initial Condition

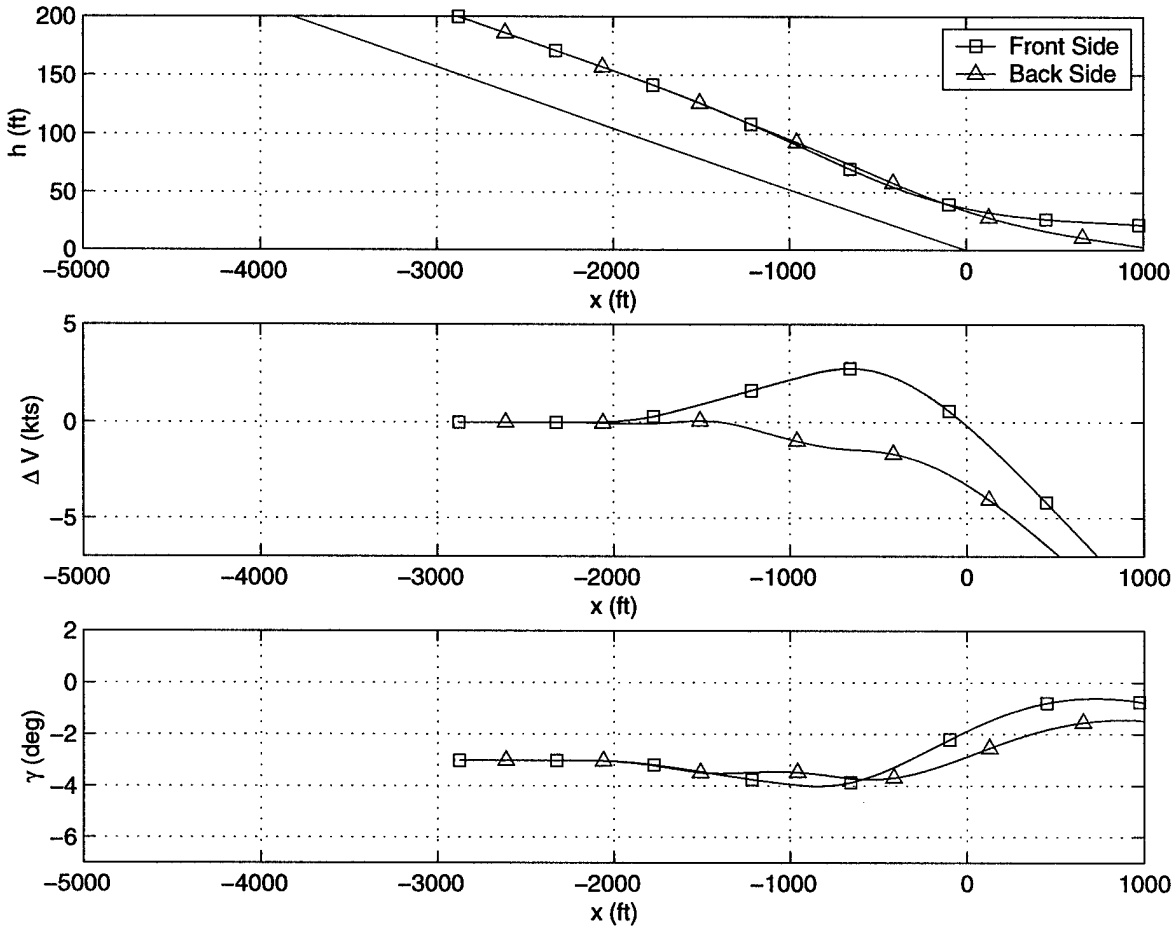

Figure 5.8: Back-Side-Aircraft Response for Long Initial Condition

Figure 5.8 illustrates the trajectory response of the two strategies from the long initial condition. The command responses of the for the two strategies are very similar, and both strategies begin the flare maneuver just inside of 1000 feet. For this initial condition, the back-side strategy does a slightly better job regulating the aircraft's airspeed during the landing segment than the front-side strategy. The excess speed loss of both strategies within 1000 feet is due to the flare command laws and the lack of ground effect modeling. Once again, the long initial condition response is limited more by aircraft performance than by piloting strategy.

Chapter 6

Refined Pilot Landing Strategies

Pilot training literature tends to describe multi-input tasks as multiple, decoupled single-input tasks. The previous chapters explored pilot landing strategies based on this concept and a literal interpretation of front-side and back-side landing techniques. These generic landing strategies were useful in bounding the pilots' performance in the NAV CANADA data set. However, an experienced pilot is expected to develop more refined strategies as experience in the aircraft and task is gained. This experience is reflected in a piloting strategy which reflects the dynamics of the particular aircraft being flown by introduction of cross-coupling terms in the strategy. These cross-coupling terms may be identified by experimental methods; however, detailed input/output data was not available in the NAV CANADA data set.

Instead, a more theoretical framework is proposed to identify candidate refined landing strategies. The basic methodology is to explore the concept that the switching surface is a mathematical representation of the pilot's strategy. In control terminology, by choosing a switching surface, the pilot is defining the placement of the open-loop transmission zeros and defining the null space or reduced-order system dynamics. [32, 72] If this is the case, a set of desired null space dynamics can be defined. Then an eigenstructure assignment method (section 2.1.1) can be used to define a switching surface to achieve the desired dynamics and

implement a refined pilot strategy.

This chapter uses the point mass characteristics of an aircraft to define the desired null space dynamics. These desired dynamics are applied to the front-side aircraft model of Chapter 4 and the back-side aircraft model of Chapter 5. This application illustrates how a pilot would achieve the desired dynamics with two different types of plant dynamics. Finally, an attempt is made to translate these switching surfaces back into a terminology that may be beneficial in communicating to a pilot learning to land these particular aircraft models.

6.1 Desired Null Space Dynamics

The range space dynamics of both the front and back side aircraft models are sixth ($n = 6$) order systems. Since both models use two controls ($m = 2$), the desired null space dynamics are fourth ($n - m = 4$) order systems. Therefore, four eigenvalues and portions of their associated mode shapes can be specified. Two of these modes can be determined from examining an ideal trajectory. The other two are based on the augmented pitch dynamics the pilot introduces into the inner loop stabilization of the aircraft.

Applying the front-side (4.24) and back-side (5.7) strategies as output matrices with a $k_d = 1$, to both the front-side (4.13) and back-side (5.3) plant and input matrices (4.14) creates the same set of open-loop transmission zeros. These transmission zeros are located at -1 and approximately -7.8. These values are used as two of the desired null space eigenvalues. However, since neither $(S_f B)^{-1}$ nor $(S_b B)^{-1}$ exist, the zero input directions of these transmission zeros cannot be associated with a null space eigenvector, as in (2.9) thru (2.11). Therefore, the mode shapes are determined by examining the dynamics of an ideal or generic aircraft landing trajectory.

A pilot may visualize an ideal aircraft trajectory as one free of the aircraft's pitch and thrust dynamics. Such a trajectory is modeled as a point mass representation of the aircraft. For

the visual landing task, consider the linear system

$$\begin{bmatrix} \dot{d} \\ \dot{\gamma} \\ \dot{V} \end{bmatrix} = \begin{bmatrix} 0 & \frac{V_o}{\cos\gamma_o} & 0 \\ 0 & -\left(\frac{L_\alpha + T_o - mg\sin\gamma_o}{mV_o + L_{\dot{\alpha}}}\right) & \left(\frac{L_V}{mV_o + L_{\dot{\alpha}}}\right) \\ 0 & \left(\frac{D_\alpha}{m} - g\cos\gamma_o\right) & \left(\frac{T_V - D_V}{m}\right) \end{bmatrix} \begin{bmatrix} d \\ \Delta\gamma \\ \Delta V \end{bmatrix} + \begin{bmatrix} 0 & 0 \\ \left(\frac{L_\alpha + T_o}{mV_o + L_{\dot{\alpha}}}\right) & 0 \\ -\frac{D_\alpha}{m} & \frac{T_{max}}{m} \end{bmatrix} \begin{bmatrix} \Delta\theta \\ \frac{\Delta T}{T_{max}} \end{bmatrix} \tag{6.1}$$

and ideal switching surfaces based on the pilot training literature of

$$S_{fi} = \begin{bmatrix} 1 & k_{\dot{d}}\frac{V_o}{\cos\gamma_o} & 0 \\ 0 & 0 & 1 \end{bmatrix} \tag{6.2}$$

$$S_{bi} = \begin{bmatrix} 0 & 0 & -1 \\ 1 & k_{\dot{d}}\frac{V_o}{\cos\gamma_o} & 0 \end{bmatrix} \tag{6.3}$$

Using the B-747 model parameters and $k_{\dot{d}} = 1$, these equations become

$$\begin{bmatrix} \dot{d} \\ \dot{\gamma} \\ \dot{V} \end{bmatrix} = \begin{bmatrix} 0 & 221.3 & 0 \\ 0 & -0.4802 & 0.0013 \\ 0 & -11.55 & -0.04551 \end{bmatrix} \begin{bmatrix} d \\ \Delta\gamma \\ \Delta V \end{bmatrix} + \begin{bmatrix} 0 & 0 \\ 0.4728 & 0 \\ -20.58 & 9.927 \end{bmatrix} \begin{bmatrix} \Delta\theta \\ \frac{\Delta T}{T_{max}} \end{bmatrix} \tag{6.4}$$

along with the switching surfaces of

$$S_{fi} = \begin{bmatrix} 1 & 221.3 & 0 \\ 0 & 0 & 1 \end{bmatrix} \tag{6.5}$$

$$S_{bi} = \begin{bmatrix} 0 & 0 & -1 \\ 1 & 221.3 & 0 \end{bmatrix} \tag{6.6}$$

Since the ideal, point mass model is a third order ($n = 3$) with two controls ($m = 2$), the reduced-order dynamic system is only a first order system ($n - m = 1$). The null space dynamics for both the front-side (6.5) and back-side (6.6) strategies is the first order system defined by the eigenpair

$$\lambda_n = -1 \quad , \quad v_n = \begin{pmatrix} -1 \\ 0 \\ 0 \end{pmatrix} \tag{6.7}$$

So the desired eigenvalue of -1 can be associated with glide slope deviation mode.

In the range space of the ideal point mass system, the dominate velocity of the front-side strategy is defined by the eigenpair

$$\lambda_r = -10 \quad , \quad v_r = \begin{pmatrix} 0 \\ 0 \\ 1 \end{pmatrix} \tag{6.8}$$

So the desired eigenvalue of -7.8 is associated with airspeed mode.

For the back-side aircraft dynamics, the point mass plant state space model is

$$\begin{bmatrix} \dot{d} \\ \dot{\gamma} \\ \dot{V} \end{bmatrix} = \begin{bmatrix} 0 & 221.3 & 0 \\ 0 & -0.4802 & 0.0013 \\ 0 & 51.43 & -0.04551 \end{bmatrix} \begin{bmatrix} d \\ \Delta\gamma \\ \Delta V \end{bmatrix} + \begin{bmatrix} 0 & 0 \\ 0.4728 & 0 \\ -83.60 & 9.927 \end{bmatrix} \begin{bmatrix} \Delta\theta \\ \frac{\Delta T}{T_{max}} \end{bmatrix} \tag{6.9}$$

Using the front-side (6.5) and back-side (6.6) switching surfaces, gives the same null space dynamics as (6.7). The dominate velocity mode of the range space dynamics using the back-side aircraft is a second order system with the real part of the eigenvalues equal to -10 or the same as that in equation (6.8).

The other two poles of the desired null space dynamics are assumed to be the complex conjugate poles that the pilot introduces into the inner loop dynamics,

$$\lambda_{il} = -0.35 \pm 0.3571i \tag{6.10}$$

This choice can be viewed as an attempt by the pilot to cancel out the aircraft's pitch dynamics.

Putting this information together gives the desired null space modes for both the front-side

and back-side aircraft as

$$\lambda_{d1} = -1 \qquad \lambda_{d2} = -7.8 \qquad \lambda_{d3,d4} = -0.35 \pm 0.3571i$$

$$v_{d1} = \begin{pmatrix} -1 \\ 0 \\ 0 \\ 0 \\ * \\ * \end{pmatrix} \quad v_{d2} = \begin{pmatrix} 0 \\ 0 \\ 0 \\ 1 \\ * \\ * \end{pmatrix} \quad v_{d3,d4} = \begin{pmatrix} * \\ * \\ * \\ * \\ * \\ * \end{pmatrix} \quad \text{where } v_{di} = \begin{pmatrix} v_d \\ v_\gamma \\ v_\theta \\ v_V \\ v_q \\ v_T \end{pmatrix} \tag{6.11}$$

Note the eigenvectors lie in the six dimensional state space of the aircraft state space models. Since only nm (or 12) degrees of freedom can be specified in the problem, the $*$'s denote portions of the dynamics that are not specified.

6.2 Front-Side Aircraft Dynamics

6.2.1 Eigenstructure Strategy

The eigenstructure assignment method outlined in section 2.1.1 was used for constructing a switching surface to achieve the desired null space dynamics specified in (6.11) with the front-side aircraft dynamic model given in (4.10), (4.13), and (4.14). This procedure resulted in a desired switching surface of

$$S_{df} = \begin{bmatrix} 0.0024 & 0.7474 & 1.1753 & -0.0110 & 1 & 0 \\ 0.0002 & -1.0980 & -2.1330 & 0.7811 & 0 & 1 \end{bmatrix} \tag{6.12}$$

This switching surface creates null space dynamics of

$$\lambda_1 = -1.0000 \qquad \lambda_2 = -7.8000 \qquad \lambda_{3,4} = -0.3500 \pm 003571i$$

$$v_1 = \begin{pmatrix} -0.9999 \\ 0.0045 \\ -0.0057 \\ -0.0007 \\ 0.0057 \\ -0.0065 \end{pmatrix} \quad v_2 = \begin{pmatrix} 0.0039 \\ -0.0001 \\ -0.0013 \\ 0.7866 \\ 0.0103 \\ -0.6174 \end{pmatrix} \quad v_{3,4} = \begin{pmatrix} 0.5593 \pm 0.8289i \\ -0.0022 \mp 0.0004i \\ -0.0004 \mp 0.0019i \\ 0.0000 \mp 0.0003i \\ 0.0008 \pm 0.0005i \\ -0.0034 \mp 0.0043i \end{pmatrix} \tag{6.13}$$

which closely approximates the desired dynamic modes in (6.11).

6.2.2 Refined Landing Strategy

The promising results of the switching surface S_{df} are used to develop a piloting technique for flying an aircraft represented by the front-side aircraft dynamics. To interpret the strategy S_{df} (6.12) consider a transformation into a set of variables more representative of the pilot's feed back structure, namely

$$y = \begin{bmatrix} d & \dot{d} & \Delta\theta & \dot{\theta} & \Delta V & \dot{V} \end{bmatrix}^T \tag{6.14}$$

This transformation is accomplished by the matrix C

$$C = \begin{bmatrix} 1 & 0 & 0 & 0 & 0 & 0 \\ 0 & \frac{V_o}{\cos\gamma_o} & 0 & 0 & 0 & 0 \\ 0 & 0 & 1 & 0 & 0 & 0 \\ 0 & 0 & 0 & 0 & 1 & 0 \\ 0 & 0 & 0 & 1 & 0 & 0 \\ 0 & \left(\frac{D_\alpha}{m} - g\cos\gamma_o\right) & -\frac{D_\alpha}{m} & \left(\frac{T_V - D_V}{m}\right) & 0 & \frac{T_{max}}{m} \end{bmatrix} \tag{6.15}$$

where $y = Cx$. The numerical values for the front-side aircraft are

$$C_f = \begin{bmatrix} 1 & 0 & 0 & 0 & 0 & 0 \\ 0 & 221.3 & 0 & 0 & 0 & 0 \\ 0 & 0 & 1 & 0 & 0 & 0 \\ 0 & 0 & 0 & 0 & 1 & 0 \\ 0 & 0 & 0 & 1 & 0 & 0 \\ 0 & -11.55 & -20.58 & -0.04551 & 0 & 9.9267 \end{bmatrix} \tag{6.16}$$

In these variables, the switching function is

$$\begin{bmatrix} \sigma_\theta \\ \sigma_T \end{bmatrix} = S_{df}x = S_{df}C_f^{-1}y \tag{6.17}$$

where

$$S_{df}C_f^{-1} = \begin{bmatrix} 0.0024 & 0.0034 & 1.1753 & 1 & -0.0110 & 0 \\ 0.0002 & 0.0003 & -0.0599 & 0 & 0.7857 & 0.1007 \end{bmatrix} \tag{6.18}$$

This strategy is simplified by constrained output feedback or eliminating those feedbacks which are less significant than others. [32] By examination, the pilot strategy in (6.18) can be approximated by

$$S_{df}C_f^{-1} \approx \begin{bmatrix} 0.002 & 0.002 & 1 & 1 & 0 & 0 \\ 0 & 0 & 0 & 0 & 1 & 0.13 \end{bmatrix} \equiv S_{P_f}C_f^{-1} \tag{6.19}$$

The pilot strategy in (6.19) could be interpreted as a front-side piloting strategy. Velocity control is solely the responsibility of thrust commands with a velocity lead gain of 0.13.

$$\sigma_T = \Delta V + 0.13\dot{V} \tag{6.20}$$

In the structure of (6.19), the velocity lead gain is primarily responsible for placing the null space velocity mode pole. The pitch command balances the glide slope task (with a deviation lead gain of 1) and the pitch stabilization (with a deviation lead gain of 1).

$$\sigma_\theta = 0.002\left(\Delta d + \dot{d}\right) + \left(\Delta\theta + \dot{\theta}\right) \tag{6.21}$$

The value 0.002 can be thought of as a relative weighting between these two tasks. In the structure of (6.19), this weight is responsible for placing the second-order, complex conjugate poles in the null space dynamics. It, combined with the pitch stabilization, could be considered a cross coupling in the strategy to improve performance given the aircraft's dynamic characteristics. This type of higher complexity is what is expected of an experienced pilot. Whereas the lead terms could be conveyed to a pilot in terms of rules of thumb, the task weighting would have to be developed by a pilot through experience in the aircraft and task.

Transforming equation (6.19) back into the state space representation of the linear model gives

$$S_{P_f} = \begin{bmatrix} 0.0020 & 0.4426 & 1.0000 & 0 & 1 & 0 \\ 0 & -1.5015 & -2.6753 & 0.9941 & 0 & 1.2905 \end{bmatrix} \tag{6.22}$$

The null space dynamics generated by S_{P_f} are still close to the desired null space dynamic modes in (6.11)

$$\lambda_1 = -1 \qquad \lambda_2 = -7.6923 \qquad \lambda_{3,4} = -0.2536 \pm 0.3808i$$

$$v_1 = \begin{pmatrix} -0.9999 \\ 0.0045 \\ -0.0057 \\ -0.0000 \\ 0.0057 \\ -0.0066 \end{pmatrix} \quad v_2 = \begin{pmatrix} 0.0040 \\ -0.0001 \\ -0.0000 \\ 0.7921 \\ 0.0001 \\ -0.6104 \end{pmatrix} \quad v_{3,4} = \begin{pmatrix} -0.4312 \pm 0.9023i \\ -0.0011 \mp 0.0018i \\ 0.0009 \mp 0.0018i \\ -0.0000 \pm 0.0000i \\ 0.0005 \pm 0.0008i \\ 0.0006 \mp 0.0058i \end{pmatrix} \tag{6.23}$$

The switching surface S_{P_f} in equation (6.22) was simulated with the front-side aircraft dynamics represented by (4.10), (4.13), and (4.14). Figure 6.1 illustrates the trajectory data of this strategy for a wide variety of longitudinal initial conditions representative of vertical navigation errors bounded by ± 15 meters. These trajectories possess many desirable characteristics. First, the trajectories illustrate that the aircraft is continually in a safe position to land. In addition, all glide slope corrections for the short initial conditions are completed

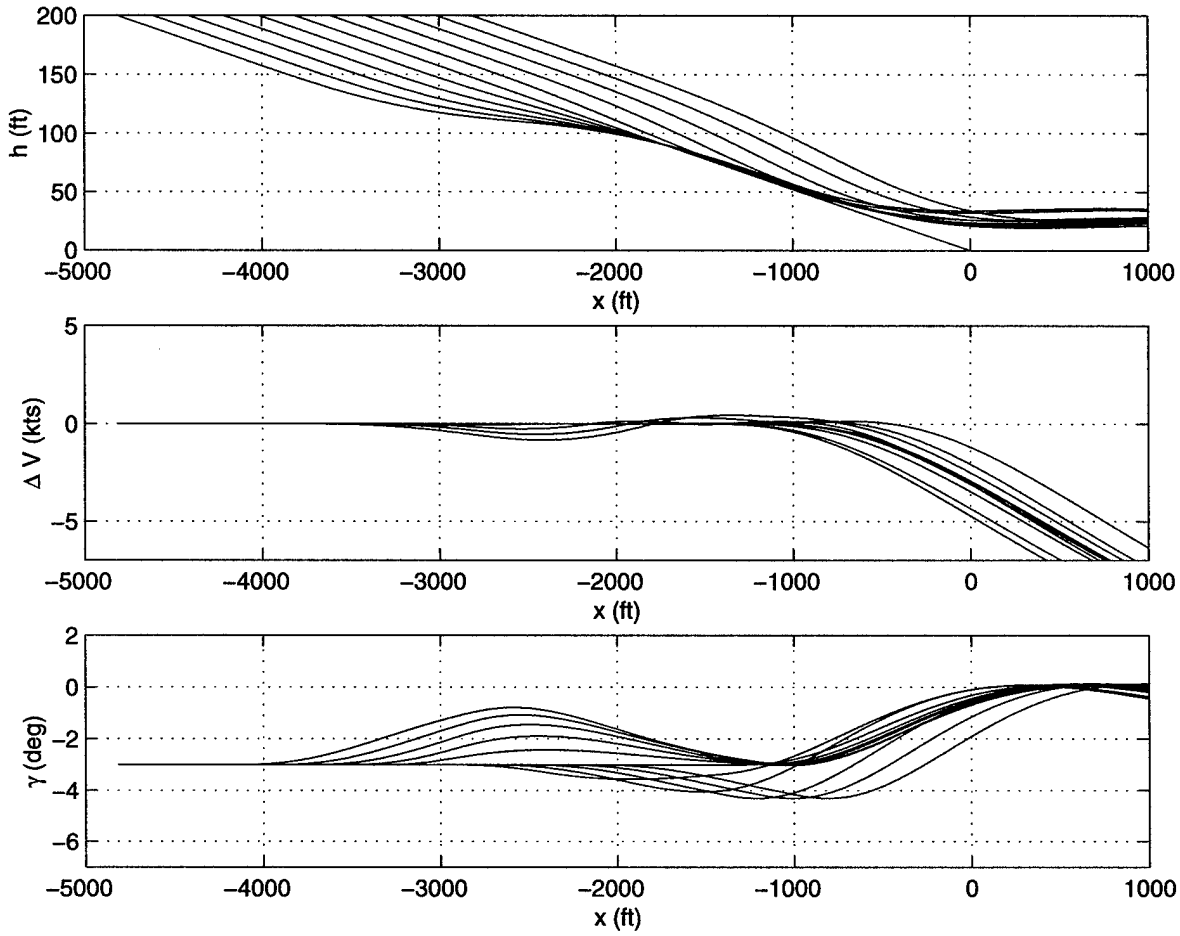

Figure 6.1: Front-Side Aircraft Refined Landing Strategy

by 100 feet above ground level. Second, the aircraft's airspeed is well regulated. The speed loss within 1000 feet of the desired glide slope runway intercept is over the runway and associated with the flare. Finally, the ground proximity warning system (GPWS) limit of approximately -1100 feet per minute (nominally -4.7^o flight path angle) is not exceeded.

Figure 6.2 illustrates the input/output system response for the short initial condition representative of the -15 meter vertical error of the NAV CANADA study. The chattering in the command time sequences is representative of the simple relay attempting to approximate a continuous tracking command. The refined strategy is a slightly more coupled response than

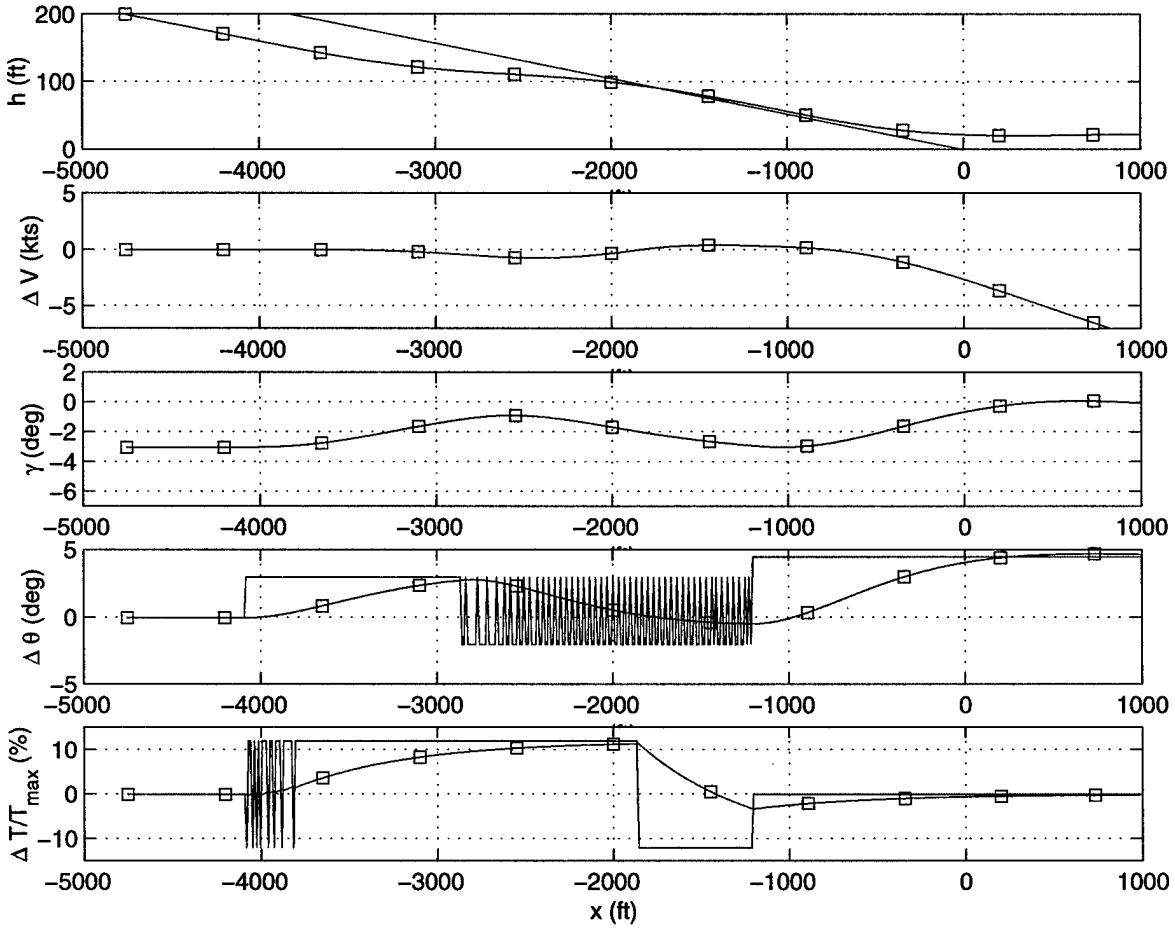

Figure 6.2: Front-Side Aircraft Refined Landing Strategy for Short Initial Condition

the literal front-side or back-side strategies. Initially, it commands nose-up pitch and throttle slowly up to attain a near level off while maintaining airspeed. Once the glide slope correction is near complete at approximately -2000 feet, it exhibits a front-side tracking strategy by using pitch only to maintain the desired glide slope. This is evident by the chattering pitch command from approximately -2000 feet to flare initiation at approximately -1200 feet.

Figure 6.3 illustrates the input/output system response for the long initial condition representative of the +15 meter vertical error of the NAV CANADA study. As in the short initial condition, slightly more coupling is evident in this strategy than the literal front-side or back-side strategies. Nose down pitch is commanded while throttle is slowly retarded to in-

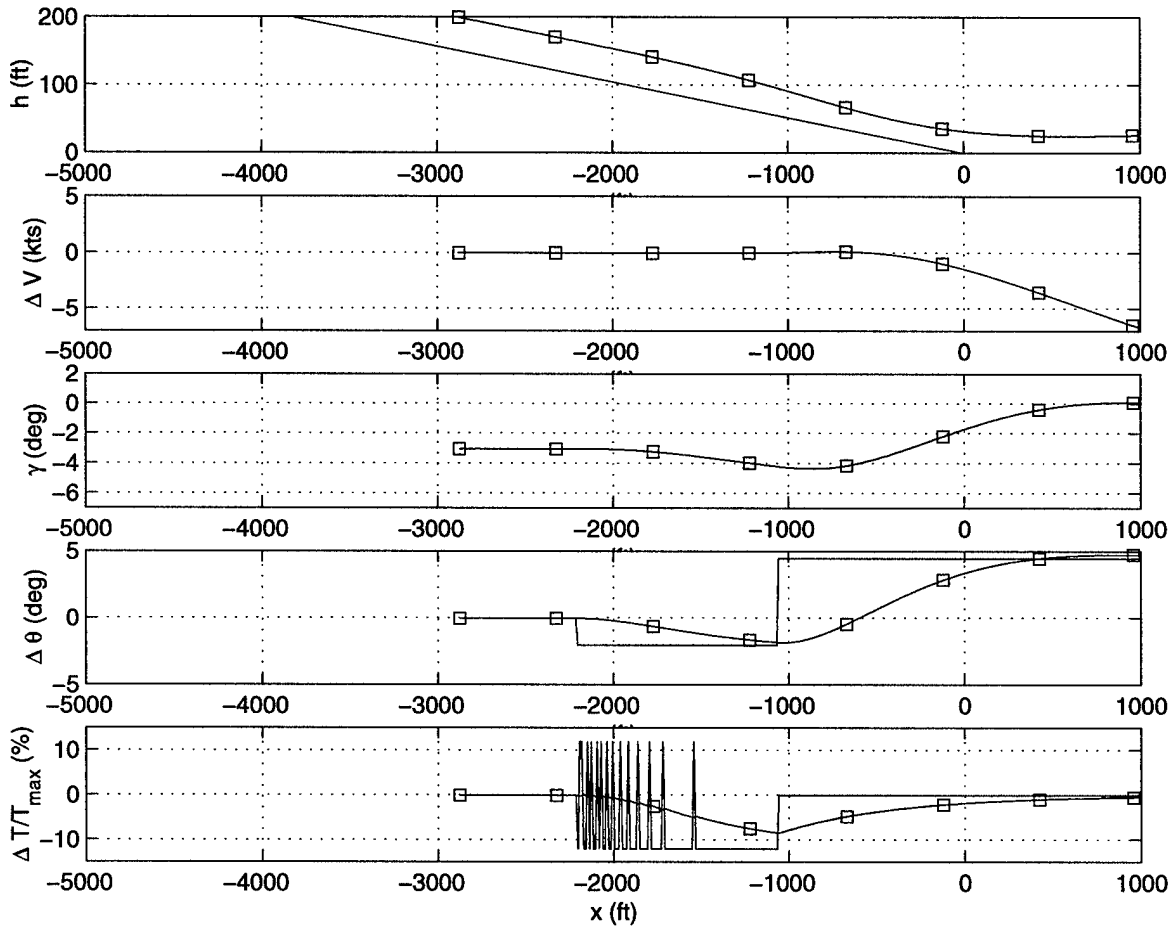

Figure 6.3: Front-Side Aircraft Refined Landing Strategy for Long Initial Condition

crease sink rate but maintain airspeed. As with the previous long initial condition examples, this example illustrates the performance limitations which govern the aircraft's response in accomplishing the task.

6.3 Back-Side Aircraft Dynamics

6.3.1 Eigenstructure Strategy

The same eigenstructure assignment procedure is used for constructing a switching surface to achieve the desired null space dynamics (6.11) with the back-side aircraft plant matrix (5.3). This procedure resulted in a desired switching surface of

$$S_{db} = \begin{bmatrix} 0.0019 & 0.7923 & 0.8888 & 0.2664 & 1 & 0 \\ -0.0012 & 5.3510 & -9.1597 & 0.8097 & 0 & 1 \end{bmatrix} \tag{6.24}$$

This switching surface creates null space dynamics of

$$\begin{aligned} &\lambda_1 = -1.0000 \qquad \lambda_2 = -7.8000 \qquad \lambda_{3,4} = -0.3500 \pm 003571i \\ &v_1 = \begin{pmatrix} -0.9975 \\ 0.0045 \\ -0.0057 \\ -0.0086 \\ 0.0057 \\ -0.0702 \end{pmatrix} \quad v_2 = \begin{pmatrix} 0.0041 \\ -0.0001 \\ 0.0038 \\ 0.8872 \\ -0.2637 \\ -0.3998 \end{pmatrix} \quad v_{3,4} = \begin{pmatrix} 0.6370 \pm 0.7707i \\ -0.0023 \mp 0.0002i \\ -0.0006 \mp 0.0018i \\ 0.0009 \mp 0.0005i \\ 0.0009 \pm 0.0004i \\ 0.0067 \mp 0.0142i \end{pmatrix} \end{aligned} \tag{6.25}$$

that closely approximates the desired null space dynamic modes in (6.11)

6.3.2 Refined Landing Strategy

As in the previous example, the results of the switching surface S_{db} to achieve the desired dynamics is used to develop a refined piloting strategy for flying the back-side aircraft represented by the plant dynamics in (5.3). To better interpret the acquisition strategy S_{db} in (6.24), the switching surface is transformed into the same feedback structure (6.14) as in the front-side example. The transformation matrix C_b (where $y = C_b x$) for the back-side plant

is

$$C_b = \begin{bmatrix} 1 & 0 & 0 & 0 & 0 & 0 \\ 0 & 221.3 & 0 & 0 & 0 & 0 \\ 0 & 0 & 1 & 0 & 0 & 0 \\ 0 & 0 & 0 & 0 & 1 & 0 \\ 0 & 0 & 0 & 1 & 0 & 0 \\ 0 & 51.43 & -83.60 & -0.04551 & 0 & 9.927 \end{bmatrix} \tag{6.26}$$

In these variables, the switching function is

$$S_{db}C_b^{-1} = \begin{bmatrix} 0.0019 & 0.0036 & 0.8888 & 1 & 0.2664 & 0 \\ -0.0012 & 0.0008 & -0.7386 & 0 & 0.8143 & 0.1007 \end{bmatrix} \tag{6.27}$$

Again this strategy is simplified by eliminating those feedbacks which are less significant than others. By examination, the pilot strategy in (6.27) can be approximated by

$$S_{db}C_b^{-1} \approx \begin{bmatrix} 0.002 & 0.002 & 1 & 1 & 0 & 0 \\ 0 & 0 & -1 & 0 & 1 & 0.13 \end{bmatrix} \equiv S_{P_b}C_b^{-1} \tag{6.28}$$

The primary difference between this strategy and the one for the front-side transport aircraft (6.19) is the addition of a pitch attitude feedback into the thrust command. This term can be interpreted as a cross-coupling term using pitch attitude to anticipate increases and decreases in drag. So the thrust switch is modified into

$$\sigma_T = \left(\Delta V + 0.13\dot{V}\right) - \Delta\theta \tag{6.29}$$

and the velocity command remains

$$\sigma_\theta = 0.002\left(\Delta d + \dot{d}\right) + \left(\Delta\theta + \dot{\theta}\right) \tag{6.30}$$

The pitch command balances the glide slope task (with a lead gain of 1) and the pitch stabilization (with a lead gain of 1). As before, this strategy for pitch could be thought of as primarily a front side piloting strategy.

Transforming equation (6.28) back into the state space representation of the linear model gives

$$S_{P_b} = \begin{bmatrix} 0.0020 & 0.4426 & 1 & 0 & 1 & 0 \\ 0 & 6.6865 & -11.8672 & 0.9941 & 0 & 1.2905 \end{bmatrix} \tag{6.31}$$

The null space dynamics generated by S_{P_b} are not only a stable tracking strategy, but also still closely approximate the desired dynamics (6.11)

$$\begin{aligned} \lambda_1 &= -1 & \lambda_2 &= -7.6924 & \lambda_{3,4} &= -0.2535 \pm 0.3815i \\ v_1 &= \begin{pmatrix} -0.9975 \\ 0.0045 \\ -0.0057 \\ -0.0065 \\ 0.0057 \\ -0.0704 \end{pmatrix} & v_2 &= \begin{pmatrix} 0.0040 \\ -0.0001 \\ -0.0000 \\ 0.7925 \\ 0.0001 \\ -0.6098 \end{pmatrix} & v_{3,4} &= \begin{pmatrix} 0.3673 \mp 0.9300i \\ 0.0012 \pm 0.0017i \\ -0.0007 \pm 0.0019i \\ -0.0007 \pm 0.0020i \\ -0.0005 \mp 0.0008i \\ -0.0124 \pm 0.0068i \end{pmatrix} \end{aligned} \tag{6.32}$$

The switching surface S_{P_b} in equation (6.31) was simulated with the back-side aircraft dynamics represented by (4.10), (5.3), and (4.14). Figure 6.4 illustrates the trajectory data of this strategy for a wide variety of longitudinal initial conditions. As in the front-side aircraft example (Figure 6.1), this strategy also has many desirable characteristics. The aircraft is continuously in a safe position to land although the glide slope corrections are slower than in the front-side aircraft. For the short initial conditions the -1100 feet per minute GPWS limits are not violated. The most noticeable difference is that it is more difficult to regulate the aircraft's airspeed during the short initial condition glide slope corrections due to the aircraft's unstable airspeed dynamics. However, the airspeed loss is less than 5 knots and may be acceptable depending upon the aircraft's stall speed. Once again the airspeed loss within 1000 feet of the desired glide slope runway intercept point is associated with the flare maneuver and not the landing strategy.

Figure 6.5 illustrates the input/output system response for the short initial condition representative of the -15 meter vertical error of the NAV CANADA study. The chattering in the

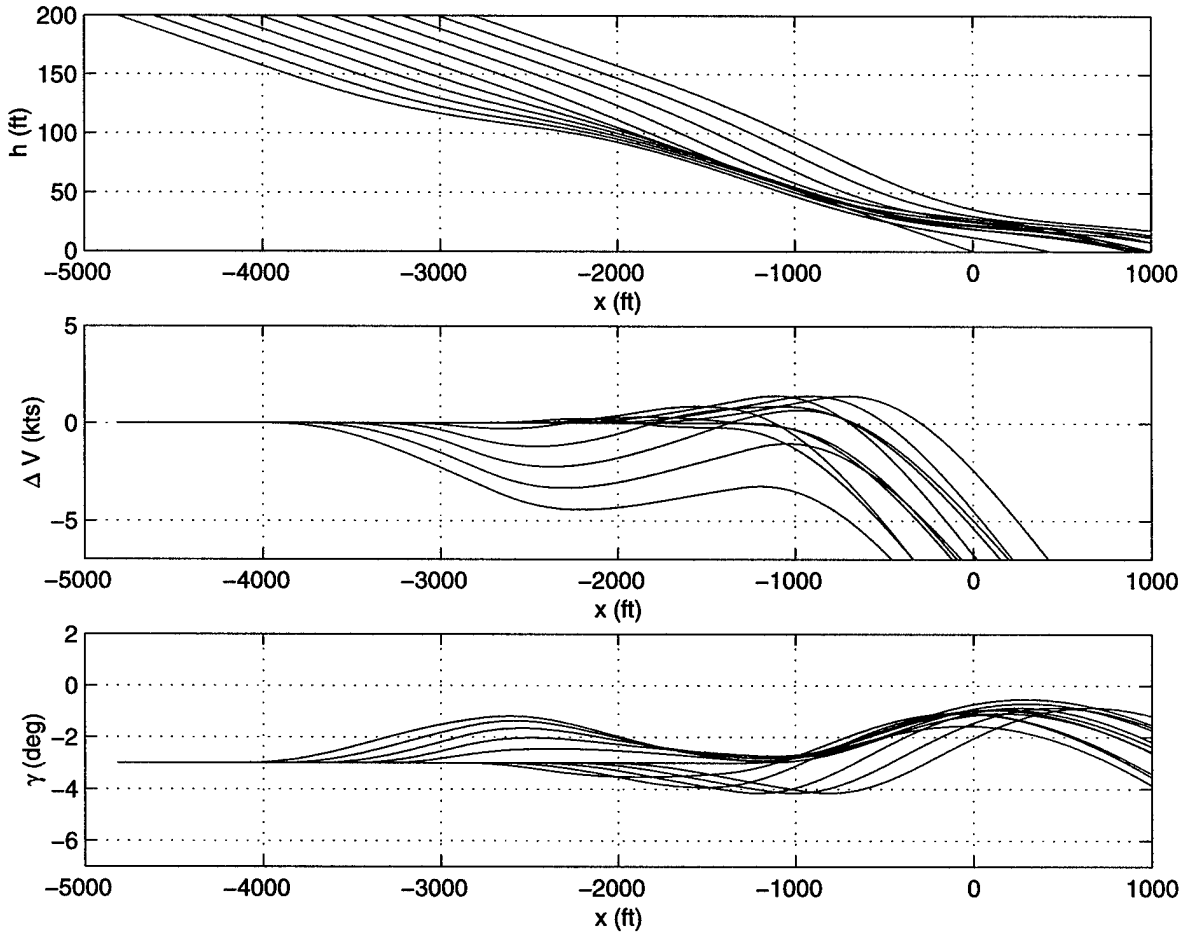

Figure 6.4: Back-Side Aircraft Refined Landing Strategy

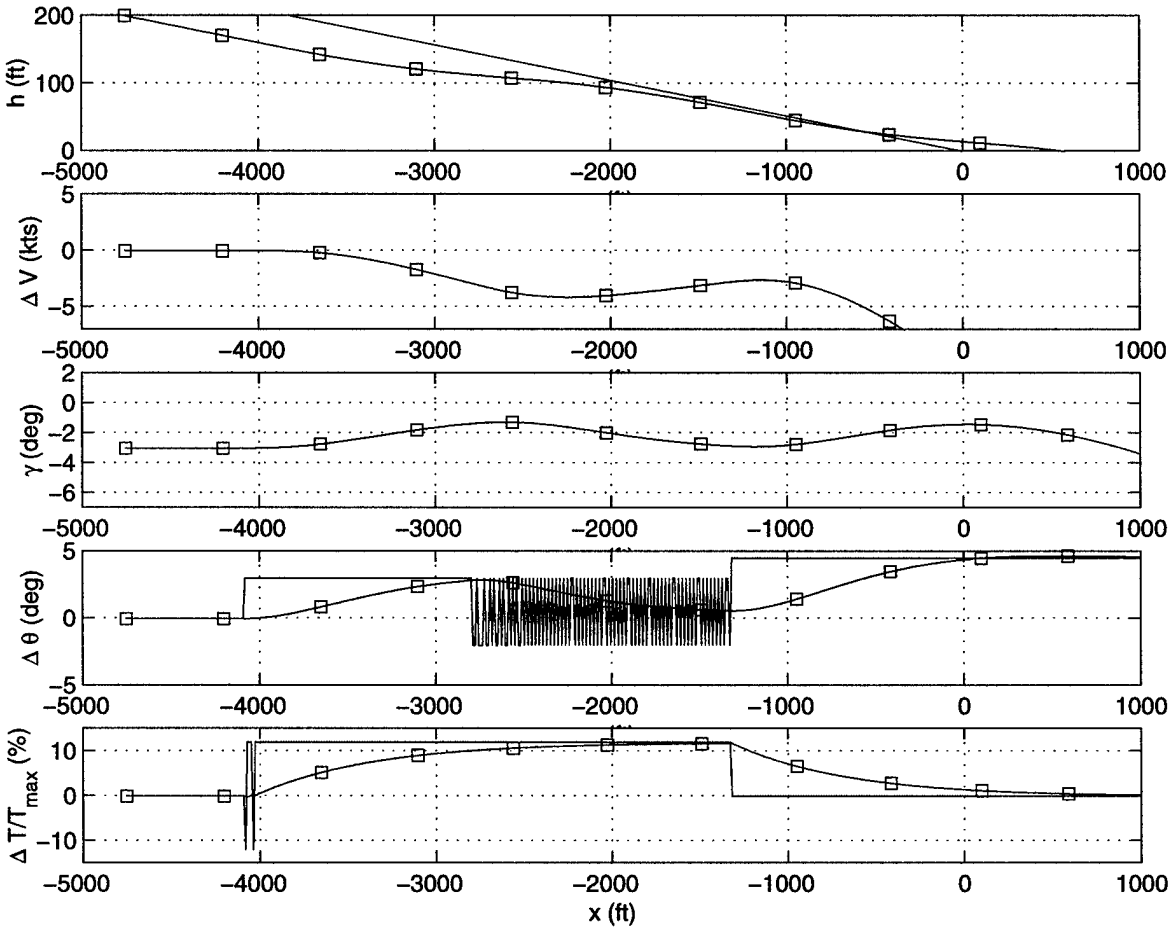

Figure 6.5: Back-Side Aircraft Refined Landing Strategy for Short Initial Condition

command time sequence is representative of the simple relay attempting to estimate a continuous tracking command. The input response is similar but perhaps more aggressive than the front side aircraft example in Figure 6.3. It surprisingly exhibits some front-side characteristics, leaving thrust up to regain the airspeed and using the chattering pitch command to track the desired glide slope.

Figure 6.6 illustrates the input/output system response for the long initial condition representative of the +15 meter vertical error of the NAV CANADA study. This strategy is also limited by the aircraft's performance. It basically commands nose down pitch and retard the throttles until flare initiation.

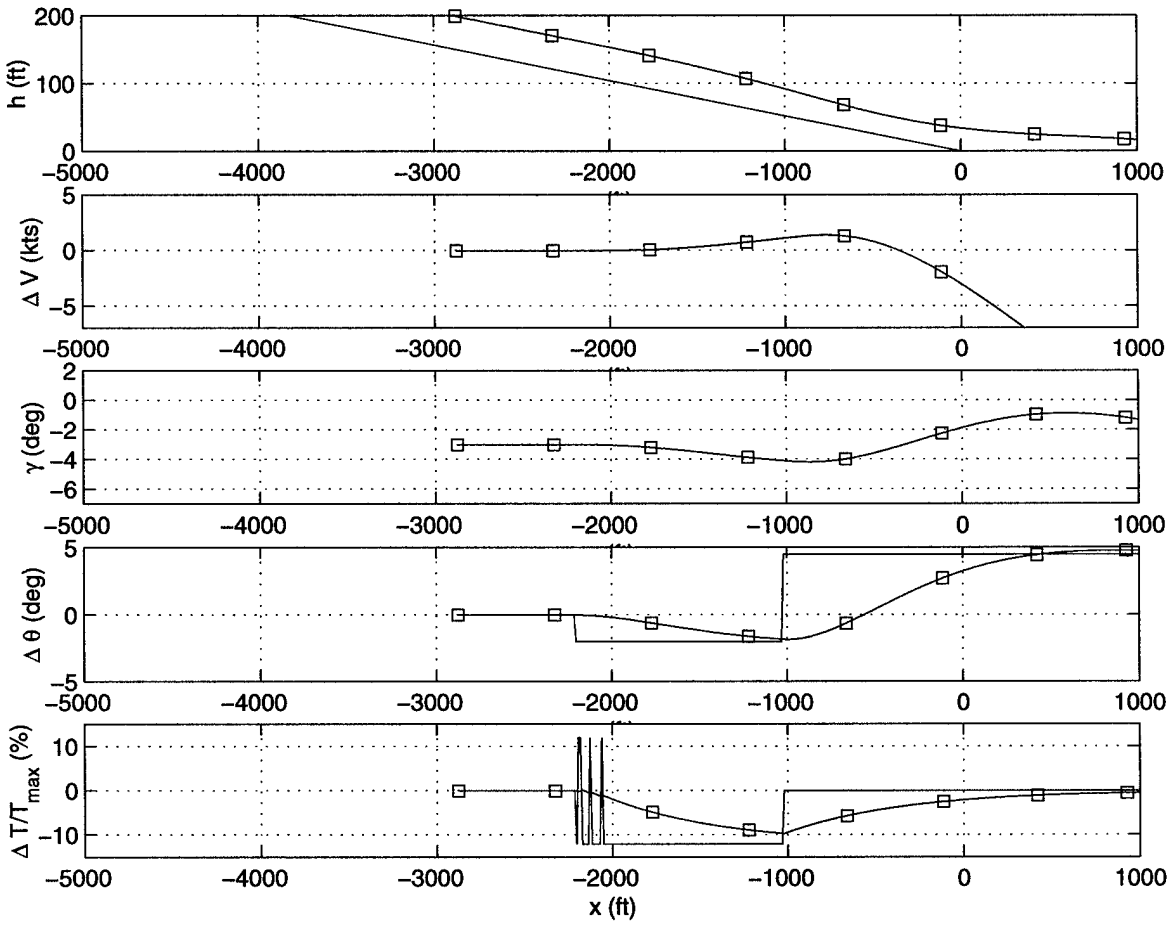

Figure 6.6: Back-Side Aircraft Refined Landing Strategy for Long Initial Condition

Chapter 7

Conclusions and Recommendations

The primary conclusion to be drawn from this research is that Variable Structure Control (VSC) techniques are useful in modeling human operators employing a discontinuous or "relay-like" control strategy. Human operators often employ this type of control strategy during large amplitude, acquisition tasks. The VSC switching surface formulation allows for easy mathematical representation of various piloting strategies based on pilot training literature. As a result, front-side and back-side flying techniques could be simulated for the visual-landing task. These strategies are sufficient to bound the limited NAV CANADA data set that is representative of well-trained pilots responding to a vertical navigation error.

In addition, the training literature strategies confirm the conventional wisdom that an aircraft flying on the front side of the power curve can be successfully landed with either a front or back-side piloting technique. Whereas, a front-side piloting technique is insufficient for controlling the unstable speed dynamics of an aircraft flying on the back side of the power curve.

A cross-coupled acquisition strategy is devised by analyzing the dynamics of an idealized point-mass aircraft trajectory. The null space or reduced-order system dynamics of this idealized system are reproduced by the sliding mode control technique of eigenstructure as-

signment. This technique includes parameters representative of the dynamics of the aircraft being controlled. As a result, an aircraft specific switching surface is developed and interpreted in term similar to the pilot training literature. For the front-side aircraft of interest, it results in a front-side technique with specified glide slope and velocity lead terms as well as a pitch stabilization task. For the back-side aircraft of interest, the addition of pitch feedback to the thrust command is recommended to anticipate the changes in drag by changes in pitch attitude.

Although the flight training literature strategies are sufficient for bounding the response characteristics of the limited NAV CANADA data set, there is insufficient data to ascertain whether the pilots implemented a sliding mode or bang-bang acquisition strategy. The NAV CANADA methodology of using a group of operational flight crews flying a simulator representative of their aircraft dynamics and cockpit environment is ideal for this study. However, more data (including pilot inputs, aircraft state variables, and rates of change) need to be successfully recorded at a sample rate of at least 20 hertz to shed more light on this distinction.

Further theoretical research could be conducted with the existing variable structure model to identify other desired dynamic responses the pilot may wish to emulate. These could be based on using the eigenstructure assignment method with different desired dynamics specified or using the quadratic minimization technique to devise an optimal control switching surface. The desired switching surfaces could then be interpreted in terms similar to the pilot training literature. This method could be employed to identify potential piloting techniques for specific aircraft and tasks.

Further research could also be conducted in refining the variable strategy model employed in this study. The importance of imprecise human observations and the human reaction time delay in the outer acquisition loop and their effects on stability needs be studied. This objective could be achieved by implementation of observation noise, indifference thresholds, a Padé time delays, and a Kalman filter as a predictor/estimator similar to the Modified

Optimal Control Model.

Additional details could also be added to the inner (pilot augmented) loop of the model. Instead of assuming a set of closed loop dynamics based on experimental observations, an inner loop control of the basic aircraft dynamics could be implemented. One method might be to employ a dynamic inversion methodology to determine when it is reasonable or not reasonable to assume the pilot can achieve the desired dynamics. Another method could be based on existing linear operator tracking models (such as the MOCM) to attempt to replicate the pilot's ability to achieve the desired inner loop dynamics. The MOCM methodology may tie in to the asymptotic properties of the Linear Quadratic Regulator (LQR) and the sliding mode controller.

Bibliography

[1] McRuer, D.T. and Jex, H.R. "A Review of Quasi-Linear Pilot Models," *IEEE Transactions on Human Factors in Electronics*, Vol. HFE-8, No. 3, 1967, pp. 231-249.

[2] McRuer, D.T. and Krendel E.S. "Mathematical Models of Human Pilot Behavior," North Atlantic Treaty Organization Advisory Group for Aerospace Research and Development, January 1974, AGARD-AG-188.

[3] Kleinman, D.L., Baron, S., and Levinson, W.H. "An Optimal Control Model of Human Response, Part I: Theory and Validation," *Automatica*, Vol. 6, No. 3, 1970, pp. 357-369.

[4] Sheridan, T.B. and Ferrell, W. *Man-Machine Systems: Information, Control, and Decision Models of Human Performance*, The MIT Press: Cambridge, MA, 1974. (ISBN 0-262-19118-0)

[5] Innocenti, M., Belluchi, A., and Balestrion, A., "New Results on Human Operator Modelling During Non-Linear Behavior in the Control Loop," *1997 American Control Conference, Albuquerque, NM, June 4-6 1997*, Vol. 4, American Automatic Control Council, Evanston, IL, 1997, p. 2567-2570.

[6] Innocenti, M., Petretti, A., and Vellutini, M., "Human Operator Modelling During Discontinuous Performance," *1998 AIAA Atmospheric Flight Mechanics Conference*, Boston, Massachusetts, August 1998, pp. 31-38. (AIAA Paper 98-4146)

[7] McRuer, D., Allen, W., and Weir, D. "The Man/Machine Control Interface - Precognitive and Pursuit Control," *Proceedings of the Joint Automatic Control Conference*, Vol. II, Philadelphia, Pennsylvania, October 1978, pp. 81-88.

[8] Young, L.R. and Meiry, J.L. "Bang-Bang Aspects of Manual Control in High-Order Systems," *IEEE Transactions on Automatic Control*, Vol. AC-10, July 1965, pp. 336-341.

[9] Pew, R.W. "Performance of Human Operators in a Three-State Relay Control System with Velocity-Augmented Displays," *IEEE Transactions on Human Factors*, Vol. HFE-7, No. 2, 1966, pp. 77-83.

[10] Diamantides, N.D. "A Pilot Analog for Aircraft Pitch Control," *Journal of Aeronautical Sciences*, Vol. 25, 1958, pp. 361-371.

[11] Costello, R.G. "The Surge model of the Well-Trained Human Operator in Simple Manual Control," *IEEE Transactions on Man-Machine Systems*, Vol. MMS-9, No. 1, 1968, pp. 2-9.

[12] Hess, R.A. "A Rational for Human Operator Pulsive Control Behavior," *Journal of Guidance, Control, and Dynamics*, Vol. 2, No. 3, 1979, pp. 221-227.

[13] Phatak, A.V. and Bekey, G.A. "Model of the Adaptive Behavior of the Human Operator in Response to a Sudden Change in the Control Situation," *IEEE Transactions on Man-Machine Systems*, Vol. MMS-10, No. 3, 1969, pp. 72-80.

[14] Pitkin, E.T. "A Non-Linear Feedback Model for Tracking Studies," *Proceedings of the Eight Annual Conference on Manual Control*, University of Michigan, Ann Arbor, Michigan, May 1972, pp. 11-22. (AFFDL-TR-72-92)

[15] Meritt, M.J. and Bekey, G.A. "An Asynchronous Pulse-Amplitude Pulse-Width Model of the Human Operator, " *Third Annual NASA-University Conference on Manual Control*, March 1967, pp. 225-239. (NASA SP-144)

[16] Johannsen, G. "Development and Optimization of a Nonlinear Multiparameter Human Operator Model," *IEEE Transactions on Systems, Man, and Cybernetics*, Vol. 2, No. 4, 1972, pp. 494-504.

[17] Angel, E.S. and Bekey, G.A. "Adaptive Finite-State Models of Manual Control Systems," *IEEE Transactions on Man-Machine Systems*, Vol. 9, No. 1, 1968, pp. 15-20.

[18] Costello, R. and Higgins. "An Inclusive Classified Bibliography Pertaining to Modeling the Human Operator as an Element in an Automatic Control System," *IEEE Transactions on Human Factors in Electronics*, Vol. HFE-7, No. 4, 1966, pp. 174-181.

[19] Andrisani, D. and Gau, C.F. "A Nonlinear Pilot Model for Hover," *Journal of Guidance, Control, and Dynamics*, Vol. 8, No. 3, 1985, pp. 332-339.

[20] Heffley, R. "Pilot Models for Discrete Maneuvers," *1982 AIAA Guidance, Navigation, and Control Conference Proceedings*, San Diego, CA, August 1982, pp. 132-142. (AIAA Paper 82-1519)

[21] Hess, R.A. "Structural Model of the Adaptive Human Pilot," *Journal of Guidance, Control, and Dynamics*, Vol. 3, No. 5, 1980, pp. 416-423.

[22] Moorehouse, D. "Modelling a Distracted Pilot for Flying Qualities Applications," *1995 AIAA Atmospheric Flight Mechanics Conference*, Baltimore, Maryland, August 1995, pp. 14-24. (AIAA Paper 95-3426-CP)

[23] Edwards, C.E. and Spurgeon, S.K. *Sliding Mode Control: Theory and Application.* Taylor and Francis, Ltd.: London, 1998. (ISBN 0-7484-0601-8)

[24] Utkin, V.I. "Variable Structure Systems with Sliding Modes," *IEEE Transactions on Automatic Control*, Vol. AC-22, No. 2, April 1977, pp. 212-222.

[25] DeCarlo, R.A., Stanislaw, H.Z., and Matthews, G.P. "Variable Structure Control of Nonlinear Multivariable Systems: A Tutorial," *Proceedings of the IEEE*, Vol. 76, No. 3, March 1988. pp. 212-232.

[26] Rosenbrock, H.H. *State Space and Multivariable Theory*, Thomas Nelson and Sons, LTD: London, Great Britain, 1970.

[27] MacFarlane, A.G.J. and Karcanis, N. "Poles and Zeros of Linear Multivariable Systems: A Survey of the Algebraic, Geometric, and Complex-Variable Theory," *International Journal of Control*, Vol. 24, No. 1, 1976. pp. 33-74.

[28] El-Ghezawi, O.M.E., Billings, S.A., and Zinober, A.S.I. "Variable Structure Systems and System Zeros," *IEE Proceedings, Part D: Control Theory and Applications*, Vol. 130, No. 1, January 1983. pp. 1-5.

[29] Utkin, V.I. *Sliding Modes in Control and Optimization*, Springer-Verlag: New York, 1992. (ISBN 0-387-53516-0)

[30] Zinober, A.S.I. and Dorling, C.M. "Hyperplane Design and CAD of Variable Structure Control Systems," *Deterministic Control of Uncertain Systems*, A.S.I. Zinober (ed.), Peter Peregrinus Ltd.: London, 1990, pp. 52-79. (ISBN 0-86341-170-3)

[31] Brogan, W.L. *Modern Control Theory*, Prentice Hall: Englewood Cliffs, NJ, 1991. (ISBN 0-13-589763-7)

[32] Andry, A.N., Shapiro, E.Y., and Chung, J.C. "Eigenstructure Assignment for Linear Systems," *IEEE Transactions on Aerospace and Electronic Systems*, Vol. AES-19, No. 5, September 1983, pp. 711-729.

[33] Wonham, W.M. and Morse, A.S. "Decoupling and Pole Assignment in Linear Multivariable Systems: A Geometric Approach," *SIAM Journal of Control*, Vol. 8, No. 1, Feburary 1970. pp. 1-18.

[34] Morse, A.S. and Wonham, W.M. "Decoupling and Pole Assignment by Dynamic Compensation," *SIAM Journal of Control*, Vol. 8, No. 3, August 1970. pp. 317-337.

[35] Morse, A.S. and Wonham, W.M. "Status of Noninteracting Control," *IEEE Transactions of Automatic Control*, Vol. AC-16, No. 6, December 1971, pp. 568-581.

[36] Wonham, W.M. *Linear Multivariable Control: A Geometric Approach*, Springer-Verlag: New York, New York, 1985.

[37] Gao, W. and Hung, J. "Variable Structure Control of Nonlinear Systems: A New Approach," *IEEE Transactions on Industrial Electronics*, Vol. 40, No. 1, February 1993. pp. 45-55.

[38] Drazenovic, B. "The Invariance Conditions in Variable Structure Systems," *Automatica*, Vol. 5, 1969. pp. 287-295.

[39] Buffington, J.M. and Shtessel, Y.B. "Saturation Protection for Feedback Linearizable Systems using Sliding Mode Theory," *Proceedings of the American Control Conference*, Philadelphia, Pennsylvania, June 1998, pp. 1028-1032.

[40] Lewis, F.L. *Optimal Control*, John Wiley & Sons, Inc.: New York, NY, 1986. (ISBN 0-471-81240-4)

[41] Harvey, C. and Stein, G. "Quadratic Weights for Asymptotic Regulator Properties," *IEEE Transactions on Automatic Control*, Vol. AC-23, No. 3, 1978, pp. 378-387.

[42] Stein, G. "Generalized Quadratic Weights for Asymptotic Regulator Properties," *IEEE Transactions on Automatic Control*, Vol. AC-24, No. 4, 1979, pp. 559-566.

[43] Anderson, B. and Moore, J. *Optimal Control Linear Quadratic Methods*, Prentice Hall: Englewood Cliffs, NJ, 1990. (ISBN 0-13-638560-5).

[44] Kwakernaak, H. and Sivan, R. *Linear Optimal Control Systems*, John Wiley & Sons, Inc: New York, NY, 1972. (ISBN 0-471-51110-2).

[45] Kwakernaak, H. and Sivan, R. "The Maximally Achievable Accuracy of Linear Optimal Regulators and Linear Optimal Filters," *IEEE Transactions on Automatic Control*, Vol. AC-17, No. 1, 1972, pp. 79-86.

[46] Guralnik, D.B. (ed). *Webster's New World Dictionary,* The World Publishing Co: New York, New York, 1972.

[47] Rasmussen, J. "Skills, Rules, and Knowledge; Signals, Signs, and Symbols, and Other Distinctions in Human Performance Models," *IEEE Transactions on Systems, Man, and Cybernetics*, Vol. SMC-13, No. 3, May/June 1983, pp. 257-266.

[48] Stengel, R.F. "Toward Intelligent Flight Control," *IEEE Transactions on Systems, Man, and Cybernetics*, Vol. 23, No. 6, November/December 1993, pp. 1699-1717.

[49] Anderson, M.R., Clark, C., and Dungan, G. "Flight Test Maneuver Design Using a Skill- and Rule Based Pilot Model," *IEEE International Conference on Systems, Man, and Cybernetics*, Vancouver, British Columbia, October 1995.

[50] Anon. *Flying Operations: Instrument Flight Procedures*, Department of the Air Force, AFMAN 11-217, Vol. 1, 1 April 1996.

[51] Anon. *FAA - Instrument Flying Handbook*, Department of Transportation, Federal Aviation Administration, AC 61-27C, 1980.

[52] Heffley, R. "Derivation of Human Pilot Control Laws based on Literal Interpretation of Pilot Training Literature," *1981 AIAA Guidance, Navigation, and Control Conference Proceedings*, Albuquerque, NM, August 1981, pp. 513-519. (AIAA Paper 81-1822)

[53] Davidson, J.B. and Schmidt, D.K. "Modified Optimal Control Pilot Model for Computer-Aided Design and Analysis," NASA-TM-4384, 1992.

[54] Hess, R.A., and Yousefpor, M. "Analyzing the Flared Landing Task with Pitch-Rate Flight Control Systems, *Journal of Guidance, Control, and Dynamics,* Vol. 15, No. 3, May-June 1992. (AIAA Paper 90-3483)

[55] Anderson, M.R. "Inner and Outer Loop Manual Control of Carrier Aircraftr Landing," *AIAA Guidance, Navigation and Control Conference*, San Diego, California, July 1996. (AIAA Paper 96-3877)

[56] Heffley, R., Schulman, T., and Clement, W. "An Analysis of Airline Landing Flare Data Based on Flight and Training Simulator Measurements," NASA-CR-166404, August 1982. (N83-10047)

[57] Scalera, K.R. and Durham, W.C. "Modification of a Surplus Navy 2F122A A-6E OFT for Flight Dynamics Research and Instruction," *AIAA Modeling and Simulation Technologies Conference and Exhibit*, Boston, Massachusetts, August 1998, pp. 163-167. (AIAA Paper 98-4180)

[58] Phillips, J.M. and Anderson, M.R. "A Variable Strategy Pilot Model," *2000 AIAA Atmospheric Flight Mechanics Conference*, August 2000, Denver, Colorado. (AIAA Paper 2000-3983)

[59] Anon. *Criteria For Approval of Category I and Category II Weather Minima for Approach,* FAA Advisory Circular AC 120-29, Chg. 3, December 1974.

[60] Anon. *Federal Air Regulation Part 91 General Operating and Flight Rules,* FAR 91, 26 August 1994.

[61] Johnson, W.A. and Hoh, R.H. "Determination of ILS Category II Decision Height Window Requirements," NASA-CR-2024, May 1972.

[62] Anon. *Wide Area Augmentation System Glide Path Bias Investigation Canadian Airlines Boeing 767 Simulator*, NAV CANADA, Satellite Navigation Program Office, Ottawa, Ontario, Canada, K1A 0N8, February 8, 1998.

[63] Neal, T.P. and Smith, R.E. "An In-Flight Investigation to Develop Control System Design Criteria for Fighter Aircraft," AFFDL-TR-70-74, Vol. I, December 1970.

[64] Hodgkinson, J. *Aircraft Handling Qualities*, AIAA Education Series, Blackwell Science, Ltd: Oxford, United Kingdom, 1999. (ISBN 0-632-03816-0)

[65] Annon. *Flying Qualities of Piloted Aircraft, Appendix A*, Department of the Air Force, MIL-STD-1797A, Notice 1, Appendix A, 28 June 1995.

[66] Weingarten, N.C. and Chalk, C.R. "In-Flight Investigation of Large Airplane Flying Qualities for Approach and Landing," *Journal of Guidance, Control, and Dynamics*, Vol. 7, No. 1, 1984, pp. 92-98.

[67] Roskam, J. *Airplane Flight Dynamics and Automatic Flight Controls, Part I*, Roskam Aviation and Engineering Corporation, Lawrence, Kansas, 1994.

[68] Heffley, R. "Terminal Control Factors for the Carrier Landing Task," *1986 AIAA Guidance, Navigation, and Control Conference*, Williamsburg, Virginia, August 1986, pp. 867-874. (AIAA Paper 86-2251)

[69] Anon. *Aircraft Accident Report: Descent Below Visual Glidepath and Collision with Terrain, Delta Air Lines Flight 554, McDonnell Douglas MD-88, N914DL, Laguardia Airport, New York, October 19, 1996*, National Transportation Safety Board, Washington DC, August 25, 1996. (NTSB/AAR-97/03)

[70] Johnson, E.W., Cormack, D.L., and Hadley, L.M. "Psychological and Procedural Aspects Related to ILS Approaches and Landings in Visibility less than 1200 feet," *Aircraft Landing Systems,* AGARD-CP-59-70, 20-23 May 1969.

[71] Langewiesche, L. *Stick and Rudder,* The McGraw-Hill Book Comapany, Inc: New York, NY, 1944.

[72] Patel, R.V. and Misra, P. "Transmission Zero Assignment in Linear Multivariable Systems," *1992 American Control Conference, Chicago, Illinois, June 24-26 1992*, Vol. 4, American Automatic Control Council, Evanston, IL, 1992, p. 644-648.

[73] Davison, E.J. and Wang, S.H. "Properties and Calculation of Transmission Zeros of Linear Multivariable Systems," *Automatica*, Vol. 10, 1974, pp. 643-658.

Appendix A

Reduced-Order System Eigenvalues and Transmission Zeros

A.1 Proposition

If the state space representation of the dynamic system is a minimal representation the transmission zeros are not elements of the spectrum of the plant matrix A. In addition, if $(SB)^{-1}$ exists, z_j is a transmission zero of the open-loop system represented by the matrix triple (S, A, B) iff it is an eigenvalue (λ_j) of the reduced-order system dynamics (representing the dynamic modes of the constrained system to $Sx = 0$).[1]

[1]Edwards and Spurgeon [23] present an alternative form for this proof using the Rosenbrock [26] system matrix. El-Ghezawi et al [28] proposed using this relationship as a meanings of calculating the transmission zeros of any linear, time-invariant system.

A.2 Given

A minimal (least order) representation [26] of the linear time invariant dynamic system

$$\begin{aligned} \dot{x} &= Ax + Bu \\ \sigma &= Sx \end{aligned} \tag{A.1}$$

where $A \in \Re^{n\times n}$, $B \in \Re^{n\times m}$, $S \in \Re^{m\times n}$, $x \in \Re^n$, $u \in \Re^m$ and $\sigma \in \Re^m$. A minimal system representation such as this is fully controllable and fully observable. [26] The transmission zeros [27] ($z_j \in \mathcal{C}^1$) are given by the roots of

$$\det\left[S\left(z_j I_n - A\right)^{-1} B\right] = 0 \tag{A.2}$$

Since the state space system defined by equation (A.1) is square ($\dim(\sigma) = \dim(u) = m$) and the Rank$(SB) = m$, there will be $n - m$ transmission zeros [27, 73] of the open-loop system represented by the system in equation (A.1). Since the state space system defined by equation (A.1) is a minimal representation, none of the transmission zeros ($z_j \in \mathcal{C}^1, j = 1, \cdots, n-m$) are elements of the spectrum of A [26]; so $(z_j I_n - A)^{-1}$ exists.

Now consider the output of this system as constrained to zero.

$$0 = Sx \tag{A.3}$$

So $x \in \ker(S)$. The eigenvalues ($\lambda_i \in \mathcal{C}^1, i = 1, \cdots, n$) of the constrained system are given by the roots of

$$\det\left[\lambda_i I_n - \left(I_n - B(SB)^{-1}S\right)A\right] = 0 \tag{A.4}$$

where $n - m$ of these roots represent the constrained dynamic modes of the system and m of these roots are zero as a result of enforcing the constraint. [23]

$$\lambda_i = \begin{cases} \lambda_i \equiv \lambda_j & i = 1, 2, \cdots, n-m = j \\ \lambda_i = 0 & i = n-m+1, \cdots, n \end{cases} \tag{A.5}$$

A.3 Proof

A.3.1 Conjecture: $z_j \Rightarrow \lambda_j$

Transmission zeros (z_j) of the open-loop system are the eigenvalues of the reduced-order system (λ_j) .

Proof

Reposing the definition of the open-loop transmission zeros defined in equation (A.2) as a vector equation gives

$$S\left(z_j I_n - A\right)^{-1} Bw = 0 \tag{A.6}$$

where $S \in \Re^{m\times n}$, $A \in \Re^{n\times n}$, $B \in \Re^{n\times m}$,$w \in \Re^m$, $w \neq \{0\}$, $z_j \in \mathcal{C}^1 \neq 0$, and $j = 1, \cdots, n-m$. Since the system in equation (A.1) is a minimal representation, z_j is not an eigenvalue of A [26], and $\left(z_j I_n - A\right)^{-1}$ exists. Equation (A.6) can be interpreted as

$$\left(z_j I_n - A\right)^{-1} Bw \in \ker(S) \tag{A.7}$$

Since $x \in \ker(S)$, let

$$x = \left(z_j I_n - A\right)^{-1} Bw \tag{A.8}$$

Using equation (A.8) to find w in terms of x

$$\begin{aligned} \left(z_j I_n - A\right) x &= Bw \\ z_j x - Ax &= Bw \\ z_j Sx - SAx &= SBw \\ 0 - SAx &= SBw \end{aligned}$$

gives

$$w = -\left(SB\right)^{-1} SAx \tag{A.9}$$

Substituting equation (A.9) into equation (A.8) gives

$$\begin{aligned} x &= -\left(z_j I_n - A\right)^{-1} B \left(SB\right)^{-1} SAx \\ \left(z_j I_n - A\right) x &= -B \left(SB\right)^{-1} SAx \\ \left[z_j I_n - \left(I_n - B \left(SB\right)^{-1} S\right) A\right] x &= 0 \end{aligned}$$

So z_j is an eigenvalue of the reduced-order system and x is its associated eigenvector (v_j). Also note $v_j \in \ker(S)$. Since $x \neq \{0\}$

$$\det\left[z_j I_n - \left(I_n - B \left(SB\right)^{-1} S\right) A\right] = 0 \tag{A.10}$$

Meaning the transmission zeros (z_j) of the open-loop system defined by the matrix triple (S, A, B) and equation (A.2) are the eigenvalues of the reduced-order system defined by equation (A.4).

$$\{z_j\} \Rightarrow \{\lambda_j\} \tag{A.11}$$

A.3.2 Conjecture: $\lambda_j \Rightarrow z_j$

Eigenvalues of the reduced-order system (λ_j) are the transmission zeros (z_j) of the open-loop system

Proof

Reposing the definition of the eigenvalues given in equation (A.4) as an eigenvector problem gives

$$\left(I_n - B(SB)^{-1}S\right) Av = \lambda_i v \tag{A.12}$$

where $S \in \Re^{m \times n}$, $A \in \Re^{n \times n}$, $B \in \Re^{n \times m}$, the eigenvector $v \in \Re^n$, $v \neq \{0\}$, and

$$\lambda = \begin{cases} \lambda_i \in \mathcal{C}^1 & \text{for } i = 1, \cdots, n-m \\ \lambda_i = 0 & \text{for } i = n-m+1, \cdots, n \end{cases} \tag{A.13}$$

Rearranging gives equation (A.12) gives,

$$\begin{aligned} Av - B(SB)^{-1}SAv &= \lambda_i v \\ -B(SB)^{-1}SAv &= (\lambda_i I_n - A)\, v \end{aligned}$$

If the eigenvalues of the reduced-order system λ_i are not eigenvalues of the original system matrix A, then $(\lambda_i I_n - A)^{-1}$ exists, and

$$-(\lambda_i I_n - A)^{-1} B(SB)^{-1}SAv = v \tag{A.14}$$

Define $w \in \Re^m$ as

$$w \equiv -(SB)^{-1}SAv \tag{A.15}$$

So equation (A.14) becomes

$$(\lambda_i I_n - A)^{-1} Bw = v \tag{A.16}$$

Note since $v \neq \{0\}$, $w \neq \{0\}$. Multiplying equation (A.16) by S gives

$$-S(\lambda_i I_n - A)^{-1} Bw = Sv \tag{A.17}$$

From equation (A.12) it can be shown that for $\lambda_i \neq 0 \equiv \lambda_j$,

$$\begin{aligned} S(I_n - B(SB)^{-1}S)\, Av &= \lambda_j Sv \\ (S - SB(SB)^{-1}S)\, Av &= \lambda_j Sv \\ (S - S)\, Av &= \lambda_j Sv \\ 0 &= Sv \end{aligned}$$

So

$$v \in \ker(S) \tag{A.18}$$

Equation (A.17) becomes

$$S(\lambda_j I_n - A)^{-1} Bw = 0$$

and since $w \neq 0$

$$\det\left[S(\lambda_j I_n - A)^{-1} B\right] = 0 \tag{A.19}$$

where $\lambda_j \neq 0$ and λ_j is not an eigenvalue of A that are the conditions on the definition of the transmission zeros. So the eigenvalues of the reduced-order system (λ_j) defined by equations (A.4) and (A.5) are the transmission zeros (z_j) of the open loop system defined by the matrix triple (S, A, B) and equation (A.2).

$$\{\lambda_j\} \Rightarrow \{z_j\} \tag{A.20}$$

A.3.3 Conclusion

If the state space representation of the dynamic system is a minimal representation and if $(SB)^{-1}$ exists, z_j is a transmission zero of the open-loop system represented by the matrix triple (S, A, B) iff it is an eigenvalue (λ_j) of the reduced-order system dynamics (representing the dynamic modes of the constrained system to $Sx = 0$).

$$\{\lambda_j\} = \{z_j\} \tag{A.21}$$

Vita

John Michael Phillips was born 20 November 1962 to Arlene and Johnnie Phillips of Portsmouth, Virginia. At the age of three, his family moved to Chesapeake, Virginia where he spent the next 15 years of his life. He graduated from E.W. Chittum Elementary, Western Branch Jr. and Sr. High Schools. In 1981, he accepted a four year US Air Force ROTC scholarship to the Massachusetts Institute of Technology. In 1985 he graduated with a S.B. of Aeronautics and Astronautics and was commissioned a 2LT in the US Air Force. The Air Force allowed him to stay at MIT and receive a S.M. of Aeronautics and Astronautics in 1987. After graduation, he was assigned to the USAF Foreign Technology Division at Wright-Patterson AFB, Ohio for 5 years. During this time he married Elizabeth Ann Campbell of Chesapeake, Virginia. In 1992, Captain Phillips was selected to attend the US Air Force Test Pilot School. Upon graduation from the flight test engineering curriculum, he was assigned to the C-17 Developmental Flight Test Program at Edwards AFB, California. At 1:00AM 21 November 1995, the most momentous event in his life occurred; his daughter, Meghan Phillips, was born. Major Phillips' career continued, becoming Chief of the Flight Test Engineering section for the C-17. In 1995 he became a Performance Flight Test Instructor at the Test Pilot School. In 1997, the Air Force Institute of Technology selected him for the Civilian Institution Program to attend Virginia Tech. Upon graduation, he will return to the Test Pilot School. Since his family fell in love with beautiful, green Blacksburg, they will unwillingly accompany him back to California's high desert.